Development of a 3D Collagen Model for the *In Vitro* Evaluation of Magnetic Stimulation on Osteogenesis

Rebecca, Zhiyu Yuan

Department of Mechanical Engineering

University College London

A thesis submitted for the degree of

Doctor of Philosophy

September, 2017

Declaration

I, Rebecca Zhiyu Yuan, confirm that the work presented in this thesis is my own. Where information has been derived from other sources, I confirm that this has been indicated in the thesis.

Signature:

Date:

I would like to dedicate this thesis to my families and friends ...

Acknowledgements

I would like to express my deepest gratitude to my supervisors, **Dr Jie Huang**, **Prof Robert A Brown** and **Prof Rob P Allaker** for their excellent guidance, patience and providing me with this opportunity to work on this project. In my three year's postgraduate studies, they have always been constantly offering encouragement, support and aspirations.

I would like to acknowledge Dr Sally Day and Dr James Phillips for them being the examiners for my upgrade viva, they offered massive valuable suggestions for me to accomplish my study. It is only appropriate to thank Dr Kaveh Memarzadeh, Dr Abish S Stephen, Dr Jian Ping Fan, Dr Josephine Wong and Dr Peng Wang, who patiently helped me with professional techniques and have always been resourceful and supportive. I would also like to thank Mr Kevin Reeves, Mr Mark Turmaine and Mr Innes Clatworthy, for their great assistance on imaging techniques.

My sincere thanks goes to Dr Alvin P Blackie, who acted as my undergraduate project supervisor, has provided me with the necessary

foundation and encouragement for pursuing this PhD.

Last but not least, I would like to thank my family and friends for their love and support throughout these years.

To Robert: You will always be remembered. R.I.P.

Things won are done; joy's soul lies in the doing.

William Shakespeare (1564 - 1616)

Publications and Conference Presentations

Conference Publications

Yuan R, Memarzadeh K, Brown RA and Huang J (2016). Magnetic nanocomposites for tissue regeneration therapies. Front. Bioeng. Biotechnol. Conference Abstract: 10th World Biomaterials Congress.

Conference Presentations

Rebecca Zhiyu Yuan, Kaveh Memarzadeh, Robert Brown and Jie Huang, "Magnetic Nanocomposites for Tissue Regeneration Therapies". Oral presentation at World Biomaterials Congress (WBC), Montreal, Canada, May 2016.

Rebecca Zhiyu Yuan, Robert Brown and Jie Huang, "Smart Nanocomposites Scaffolds for Tissue Regeneration Therapies". Poster presentation accepted at European Society of Biomaterials (ESB), Liverpool, UK, August 2014.

Journal Publications

Yuan, Z.Y., Memarzadeh, K., Stephen, A.S., Allaker, R.P., and Huang, J. "Development of a 3D Collagen Model for the *In Vitro* Evaluation of Magnetic Stimulation on Osteogenesis." 2017. Ready for submission.

Yuan, Z.Y., Memarzadeh, K., Stephen, A.S., Allaker, R.P., and Huang, J. "Cellular and Molecular Evaluation of Magnetic Stimulation on Osteogenesis *In Vitro*." 2017. In Preparation.

Yuan, Z.Y., Memarzadeh, K., and Huang, J. "Development of a Magnetic Bio-reactor for Bone Fracture Healing Applications." 2017. In Preparation.

Abstract

Magnetic stimulation has been applied to bone regeneration and fracture non-union treatments, however, the cellular and molecular mechanisms of repair still require better understanding. In this study, a three-dimensional (3D) collagen model has been developed using plastic compression (PC), which produces dense, cellular, and mechanically strong native collagen structures. Osteoblast cells (MG-63, UMR-106, MC3T3-E1), bioactive nano-hydroxyapatite (nHA) and magnetic iron oxide nanoparticles (IONPs), were incorporated into the collagen gels to produce a range of cell-laden models. A magnetic bio-reactor to support cell growth under static magnetic fields (SMFs) was designed and fabricated by 3D printing. The influences of SMFs on cell proliferation, differentiation, extracellular matrix production, mineralisation and gene expression were evaluated. Results demonstrated that SMFs and IONPs stimulated the proliferation, alkaline phosphatase (ALP) production and level of mineralisation of MG-63 cells *in vitro*. Transmission Electron Microscopy (TEM) examination showed some changes in microstructure of collagen fibres subjected to SMFs. Real-time polymerase chain reaction (PCR) investigation further determined the effects of SMFs on the expression of Runt-related transcription factor 2 (Runx2), osteonectin (ON), and bone

morphogenic protein 2 and 4 (BMP-2 and BMP-4). The stimulating effects were identified as the combination of SMFs and IONPs, which can enhance the osteogenesis process *in vitro*. The results indicated that the magnetic stimulation influences the matrix/cell interactions, and is capable of encouraging gene expression. Therefore, the collagen model developed in this study not only offers a novel 3D bone model to better understand the effects of magnetic stimulation on osteogenesis, but also paves the way for further applications in tissue engineering and regenerative medicine.

Impact statement

This is the first study on investigating the mechanisms of static magnetic fields and magnetic nanoparticles on bone regeneration applications. This study provides an insight understanding how magnetic fields affect the osteoblasts at molecular levels, the osteogenesis, and hence the regeneration process.

The key outcomes of this study are described as below.

1. A magnetic bio-reactor with moderate intensity was designed and used for *in vitro* studies.

2. A 3D collagen based bone model was developed, which offers the possibility of incorporating various biofactors and supports cell growth.

3. With the incorporation of iron oxide nanoparticles, the proliferation, differentiation and mineralisation of osteoblasts in 3D collagen scaffolds have been stimulated under static magnetic fields.

4. The stimulation of the osteogenesis process of osteoblasts in 3D collagen model can be contributed to the complex interactions between nanoparticles, extracellular matrix and cells, hence the up-regulation of several key genes in osteoblasts.

In vitro 3D tissue models bridge the gap between *in vitro* 2D and *in vivo* models. It not only overcomes the limitations of current 2D model system, but also reduces the uses of animal models. The 3D model developed in the current study can be served as a platform for testing varies of techniques, cells and biofactors *in vitro*, as it mimics the structure of bone extracellular matrix, as well as being biocompatible and biodegradable. Collagen plastic compression is a simple but reliable technique, which can be reproduced for large scale. The plastic compressed collagen model can be further synthesised into multi-layer with varies cells and biofactors to better mimic the real tissue structure.

Therefore, the collagen model developed in this study offers not only a novel 3D platform to better understand magnetic stimulation on osteogenesis, but also paves the way for further applications in tissue engineering and regenerative medicine.

Contents

Contents **xii**

List of Figures **xviii**

List of Tables **xxi**

Nomenclature **xxiv**

1 Introduction and Literature Review **1**

1.1 Introduction 1

1.2 Bone Physiology 5

1.2.1 Collagen Matrix 6

1.2.2 Bone Cells 11

1.2.3 Cell/Matrix Interactions 20

1.3 Three-dimensional Bone Tissue Models 22

1.3.1 Two-dimensional towards Three-dimensional Tissue Models 22

1.3.2 Types of Three-dimensional Tissue Models 24

1.4 Collagen Plastic Compression 28

1.4.1 Collagen Hydrogels 28

1.4.2 Plastic Compression 30
1.4.3 Cell Response within PC Models 32
1.4.3.1 Proliferation 32
1.4.3.2 Differentiation 33
1.4.3.3 Mineralisation 34
1.4.4 Further Engineering in Plastic Compression 34
1.5 Bone Regeneration 38
1.5.1 Bone Fracture 38
1.5.2 Bone Regenration 38
1.5.3 Fracture Non-union 41
1.6 Stimulation Techniques for Bone Regeneration 44
1.6.1 Biological Stimulations 44
1.6.1.1 Osteoinductive Factors 44
1.6.1.2 Osteoconductive Materials 47
1.6.2 Physical Stimulations 49
1.6.2.1 Mechanical Stimulations 49
1.6.2.2 Magnetic Stimulations 51
1.7 Magnetic Stimulation 53
1.7.1 Static Magnetic Fields 53
1.7.2 Magnetic Nanoparticles 59
1.8 Thesis Objective and Structure 65
1.8.1 Objectives 65
1.8.2 Structure 65

2 Development of the Experimental Techniques 67

2.1 Overview 67
2.2 Materials 68
2.3 Methods 69
2.3.1 Computational Simulation of Magnetic Field Strength . . . 69
2.3.2 Magnetic Field Strength Validation by Tesla Meter 71
2.3.3 Permanent Magnets Selection 73
2.3.4 3D Printing 73
2.3.5 Synthesis and Preparations of Iron Oxide Nanoparticles . . 74
2.3.6 Synthesis and Preparations of Nano-hydroxylapatite and Nano-zinc oxide 77
2.3.7 Formation of Collagen Gel 78
2.3.8 Plastic Compression 79
2.4 Characterisations 82
2.4.1 Transmission Electron Microscopy (TEM) 82
2.4.2 Scanning Electron Microscopy (SEM) 83
2.5 *In vitro* Study 84
2.5.1 Cell Lines 84
2.5.2 Subculture of Adherent Cell Lines 84
2.5.3 AlamarBlue Assay 85
2.5.4 Alkaline Phosphatase Quantification 86
2.5.5 Alizarin Red S Staining 87
2.5.6 Histology 88
2.5.7 Gene Expression 89
2.5.7.1 RNA Extraction 89

2.5.7.2 Reverse Transcription with Elimination of Genomic DNA for Quantitative, Real-Time PCR 90
2.5.8 Statistical Analysis 92
2.6 Summary 92

3 Development of a Magnetic Bio-reactor for Magnetic Stimulation 95
3.1 Overview 95
3.2 Development of a Magnetic Bio-reactor 96
3.2.1 Computational Simulation of Magnetic Fields 96
3.2.2 Designing of the Magnetic Bio-reactor 103
3.2.3 Final Validation of the Magnetic Bio-reactor 106
3.3 Discussion 109
3.4 Summary 112

4 Development of a 3D Collagen Model for the *In Vitro* Evaluation of Magnetic Stimulation on Osteogenesis 113
4.1 Overview 113
4.2 Effects of SMFs on Cell Cultures 115
4.3 Effects of SMFs on 2D/3D Models 115
4.4 Effects of SMFs on 3D Collagen Model with Various Bio-factors . 117
4.4.1 IONPs Incorporated Collagen Models 117
4.4.2 nHA Incorporated Collagen Models 119
4.4.3 nZnO Incorporated Collagen Models 121
4.5 Discussion 123
4.5.1 Effects of SMFs on Various Cell Lines 123

4.5.2 Effects of SMFs on 2D/3D Models 126
4.5.3 Effects of SMFs on 3D Collagen Model with Various Bio-factors 127
4.6 Summary 130

5 Cellular and Molecular Evaluation of the 3D Collagen Model under Static Magnetic Fields 132

5.1 Overview 132
5.2 Cell Proliferation 134
5.3 Cell Differentiation 136
5.4 Cell Mineralisation 137
5.5 RNA Extraction 140
5.6 Gene Expression : Real-time Polymerase Chain Reaction 141
5.7 Cellular Responses 145
5.8 Microstructure of the Cell-Seeded Magnetic Collagen Scaffolds . . 146
5.9 Discussion 153
5.9.1 Effects of SMFs on Cell Proliferation 153
5.9.2 Effects of SMFs on Cell Differentiation 158
5.9.3 Effects of SMFs on Cell Mineralisation 159
5.9.4 Effects of SMFs on Gene Expression 160
5.9.5 Effects of SMFs on Cell/matrix Interactions 162
5.9.6 Effects of SMFs on Cell Membrane 165
5.10 Summary 167

6 Conclusions and Future work 169

6.1 General Discussion and Conclusion 169

6.2 Future Work 175

7 Appendix A: Characterisation of Iron Oxide Nanoparticles 178

References 181

List of Figures

1.1 The structure of bone. 7

1.2 A schematic diagram illustrating the organisation of collagen fibrils. 10

1.3 Microstructure of collagen fibres under strong magnetic field. . . . 12

1.4 A sketch of an osteoblast. 14

1.5 An illustration of osteogenic lineage. 15

1.6 Temporal changes in expression of osteoblast cell genes. 16

1.7 Illustration of cells seeded on electrospun fibre meshes. 27

1.8 Illustration of cells incorporated within collagen hydrogels. 30

1.9 Schematic view of plastic compression (PC) process. 32

1.10 Schematic diagram and summary of secondary fracture healing process. 42

2.1 Illustration of the tesla metre. 72

2.2 Illustration of the tested points in the magnetic fields. 72

2.3 Illustration of downward flow plastic compression (PC) process. . 80

2.4 Illustration of upward flow collagen plastic compression (PC) process. 81

2.5 Illustration of the rolling process. 81

3.1 Illustrations of the variables used in the stimulation. 97

3.2 Computational simulation of SMFs with NdFeB30 and NdFeB35 magnets. 99
3.3 Computational simulation of SMFs with SmCo24 and SmCo28 magnets. 100
3.4 Computational simulation of SMFs with 2 cm separation. 101
3.5 Computational simulation of SMFs with 4 cm separation. 102
3.6 Computational simulation of SMFs with 8 cm separation. 104
3.7 Initial design of the magnets holder. 105
3.8 Illustrations of the magnetic bio-reactor 107
3.9 Computational simulation of the magnetic bio-reactor. 108
3.10 Experimental measurement of the magnetic fields. 108

4.1 Comparisons of cell monolayer proliferation. 116
4.2 Comparisons of cell proliferation of MG-63 on collagen models. . . 118
4.3 A comparison of cell proliferation of MG-63 cell line when in contact with IONPs. 120
4.4 A comparison of cell proliferation of MG-63 cell line when in contact with nHA. 122
4.5 A comparison of cell proliferation of MG-63 cell lines when in contact with nZnO. 124

5.1 A comparison of cell proliferation under SMFs. 135
5.2 A comparison of cell differentiation under SMFs. 136
5.3 A comparison of cell mineralisation under SMFs. 138
5.4 A comparison of cell mineralisation with IONPs. 139
5.5 Quantification of the level of mineralisation. 140

5.6 RNA isolation. 141
5.7 Relative expression of Runx2. 142
5.8 Relative expression of Osteonectin. 143
5.9 Relative expression of BMP-2. 144
5.10 Relative expression of BMP-4. 145
5.11 The effects of SMFs on cellular responses by histology. 147
5.12 The effects of IONPs on cellular responses by histology. 148
5.13 Quantification of cell viability from histology. 149
5.14 Microstructure of cell loaded collagen scaffolds examined under TEM at day 1. 150
5.15 Microstructure of cell loaded collagen scaffolds with IONPs examined under TEM at day 1. 151
5.16 Microstructure of cell loaded collagen scaffolds examined under TEM at day 7. 152
5.17 Microstructure of cell loaded collagen scaffolds examined under TEM at day 14. 154
5.18 Microstructure of collagen matrix examined under TEM at day 14. 155
5.19 Microstructure of collagen fibres. 156

7.1 X-Ray Diffraction patterns of IONPs nanoparticles. 179
7.2 Microstructure of fabricated IONPs. 179

List of Tables

1.1 Summary of various cell type, density and additional materials used in PC 36
1.2 Summary of major effects of moderate intensity SMFs on cells. . . 58
1.3 Summary of toxicity of IONPs with and without biocompatible coatings. 64

2.1 Magnetic properties of NdFeB30, NdFeB35, SmCo24 and SmCo28. 73
2.2 Summary of synthetic methods for iron oxides 75
2.3 Primers designed and used for PCR studies. 93

3.1 Summary of the simulation results from different designs. 103

Nomenclature

Roman Symbols

2D	Two-dimensional
3D	Three-dimensional

Acronyms

ALP	Alkaline Phosphate
BMPs	Bone Morphologenetic Proteins
BSP	Bone Sialoprotein
DNA	Deoxyribonucleic Acid
ECM	Extracellular Matrix
FGF	Fibroblast Growth Factor
GDFs	Growth and Differentiation Factors
HA	Hydroxyapatite
HLF	Human Ligament Fibroblast

Nomenclature

IGF	Insulinlike Growth Factor
MNPs	Magnetic Nanoparticles
mRNA	Messenger Ribonucleic Acid
MSCs	Mesenchymal Stem Cells
OC	Osteocalcin
ON	Osteonectin
OP	Osteopontin
PC	Plastic Compression
PCL	Polycaprolactone
PCR	Polymerase chain reaction
PDGF	Platelet-derived Growth Factor
PEMFs	Pulsed Electromagnetic Fields
PEO	Poly(ethylene oxide)
PLGA	Poly(lactic-co-glycolic acid)
PLLA	Poly(l-lactic acid)
PS	Polystyrene
PVA	Poly (vinylalcohol)
PVP	Poly (vinylpyrrolidone)

Nomenclature

RGD	Arg-Gly-Asp
Runx2	Runt-related Transcription Factor 2
SEM	Scanning Electron Microscopy
SMFs	Static Magnetic Fields
TEM	Transmission Electron Microscopy
TGF-β	Transforming Growth Factor β
TNF-α	Tumor Nerosis Factor α
VEGF	Vascular Endothelial Growth Factor
XRD	X-Ray Diffraction

Chapter 1

Introduction and Literature Review

1.1 Introduction

Every year, approximately 850,000 patients suffer from bone fracture in the UK. The rate of non-union is suggested to be 5-10%, and the cost to the National Health Service (NHS) of treating non-union has been reported to range between £7,000 and £79,000 per person [Mills & Simpson, 2013]. Moreover, it also has been estimated that 10 % of the 7.9 million annual fracture patients in the US experiences non-union and/or delayed unions, which have a substantial economic and quality of life impact [Kwong & Harris, 2008]. Bone regeneration is a physiologic process that replaces the injured bone with new bone thereby renewing the biological and mechanical properties to the injured site. It is a complicated metabolic process, which requires the interaction of many factors, including growth and differentiation factors, hormones, cytokines, and extracellular components. If these factors are inadequate or interrupted, healing will be delayed or impaired, resulting in a non-union of the bone.

For more than a century, investigators have been developing alternative treatments that aim at resolving the bone fracture healing process, by physical or biological methods. The physical strategy includes the use of mechanical stimulation [Chao *et al.*, 1998; Claes *et al.*, 1998; Kenwright & Goodship, 1989], electrical stimulation [Brighton *et al.*, 1985; Haddad *et al.*, 2007; Mollon *et al.*, 2008], electromagnetic and static magnetic stimulation [Aaron *et al.*, 2004; Ryaby, 1998; Trock, 2000], and low-intensity ultrasound stimulation [Busse *et al.*, 2002; Duarte, 1983]. The biological approach involves the use of osteoconductive biomaterials, such as tricalcium phosphate, hydroxyapatite and bioactive glasses [Jones *et al.*, 2006; Ohgushi *et al.*, 1992] and growth factors (platelet derived growth factor (PDGF), fibroblast growth factor (FGF), insulin-like growth factor 1 (IGF-1) and the transforming growth factor-beta (TGF-β) super-family) [Hollinger & Wong, 1996; Lind, 1998].

Magnetic stimulation has been applied on bone regeneration applications through the mechanism of mechanotransduction. It has been proposed that static magnetic fields (SMFs) are capable of stimulating the osteogenesis of osteoblasts, by influencing their proliferation, differentiation, extracellular matrix production and mineralisation [Cai *et al.*, 2015; Chiu *et al.*, 2007; Meng *et al.*, 2013; Rosen, 2003]. Despite the success of SMFs stimulations in several *in vivo* and *in vitro* studies, there remains two major concerns. Firstly, it is believed that bone responds to dynamic rather than static loading, and the stimulation is related to the peak strain magnitude and the loading frequency [Rubin & Lanyon, 1985]. Therefore in some of the cases, SMFs failed to demonstrate a positive effect on cell

proliferation, differentiation and other factors. Secondly, for the situations where SMFs successfully stimulate the osteogenesis process, the molecular mechanisms of this phenomenon are not well understood.

Tissue models can be used to evaluate the effect of magnetic stimulation on osteogenesis. There are various types of three-dimensional (3D) tissue models used in laboratory studies, such as porous tissue scaffolds (sponge or foam), fibrous scaffolds (electrospun fibres) and custom scaffolds made by computer-aided design (CAD). For these types of scaffolds/models, cells are normally being seeded on the surfaces of the substrates. On the other hand, hydrogels have an established track record as potential 3D models for tissue regeneration applications, with the ability of incorporating cells/bio-factors directly inside the 3D construct, providing a more extracellular matrix (ECM)-like environment.

Collagen hydrogels have a long track record as potential 3D scaffolds for tissue regeneration applications. Collagen molecules can interact with each other as well as with other ECM molecules to provide a huge range of structures and functions, however, the conventional hydrogels are weak in mechanical stabilities. Plastic compression [Brown *et al.*, 2005] has been used to increase the collagen hydrogels density, hence increase the physiology relevance of the hydrogels for local cells. The plastic compressed collagen gels offer several advantages compared to the conventional collagen hydrogels. First of all, by applying the load on top of the collagen gel, the aqueous component can be removed from the gel, leading to an increase in mechanical strength and collagen density of the compressed scaffolds. Besides, the compression has minimal impacts on the viability of pre-seeded cells,

which maintains over 90% after compression [Brown *et al.*, 2005]. Furthermore, the plastic compressed collagen gels have thickness of 100-200 μm, providing the possibility to produce multi-layer scaffolds. In addition, the fabrication process is extremely rapid and non-reversible, upon the removal of the loads, the water does not return to the collagen fibre, therefore known as the term "plastic". Furthermore, cells incorporated within this dense structure have also been demonstrated to have better proliferation [Ghezzi *et al.*, 2011b], differentiation [Buxton *et al.*, 2008] and mineralisation ability [Marelli *et al.*, 2011].

The aim of this study was to develop a reliable 3D collagen model to investigate the effects of SMFs on osteogenesis *in vitro*. There are three main objectives:

1. To design a magnetic bio-reactor with moderate intensity to support cell growth under SMFs *in vitro*.

2. To develop a 3D bio-mimetic collagen based bone model with the ability to incorporate various cells and bio-factors.

3. To study the effects of SMFs and IONPs on the osteogenesis process of cells incorporated within the 3D collagen model, as well as the mechanisms at molecular levels.

1.2 Bone Physiology

Bone is a highly specialised connective tissue which forms the basis of the skeleton. It is a dense composite consisting of a soft organic matrix together with complex mineral. Bone is also a highly vascular dynamic tissue which undergoes constant remodelling and chemical exchange with the rest of the body. It is therefore subject to continual changes in its structure and composition, due to both cellular and external mechanical activities.

Bone has many different complex functions. First of all, it constitutes the rigid skeleton of the body. Secondly, it protects the internal organs from physical damage, including the brain, lungs and heart. Besides, the skeleton provides physical support and related movement. It also acts as a reservoir of inorganic ions that are recruited by physiological systems.

According to the hierarchical levels of organisation, bone can be categorised into 5 main levels (shown in Figure 1.1):

1. The subnanostructure (below a few hundred nanometers), composed of mineral, collagen, and non-collagenous organic proteins.
2. The nanostructure (from a few hundred nanometers to 1 μm), includes fibrillar collagen and embedded mineral.
3. The sub-microstructure(1 - 10 μm): lamellae.
4. The microstructure (from 10 to 500 μm), which includes the haversian systems, osteons and single trabeculae.

5. The macrostructure: cancellous and cortical bone.

1.2.1 Collagen Matrix

Collagen is a family of proteins with 29 types having been identified to date [Domb & Kumar, 2011; Gordon & Hahn, 2010]. For most soft and hard connective tissues, collagen fibrils and their networks play a dominant role in maintaining the biologic and structural integrity of ECM, as well as being highly dynamic and undergoing constant remodelling [Cen *et al.*, 2008]. The differences in density, packing and orientation results in distinctively varying mechanical properties in tissues such as bone, skin, tendon and cartilage [Cheema *et al.*, 2011; Domb & Kumar, 2011; Gordon & Hahn, 2010]. There are several groups of collagens found in human body, which have been categorised by different functions:

1. The most abundant group within the collagen family is the fibril forming collagens (types I, II, III, V, and XI). They can be assembled into highly organised supra molecular fibrils. For example, type I collagen has been found in bone, tendon and the cornea. In bone, type I collagen can associate with HA crystals and provides rigid and shock-resistant tissues with high Young's modulus. While in tendon, it behaves with low rigidity and high deformation to rupture. Besides, type I collagen shows optical properties in cornea [Cen *et al.*, 2008]. Collagen type II is the most commonly form found in cartilage tissue.

2. Network-forming collagens, such as type IV, is commonly acting as the principal component of basement membranes. Other examples include type

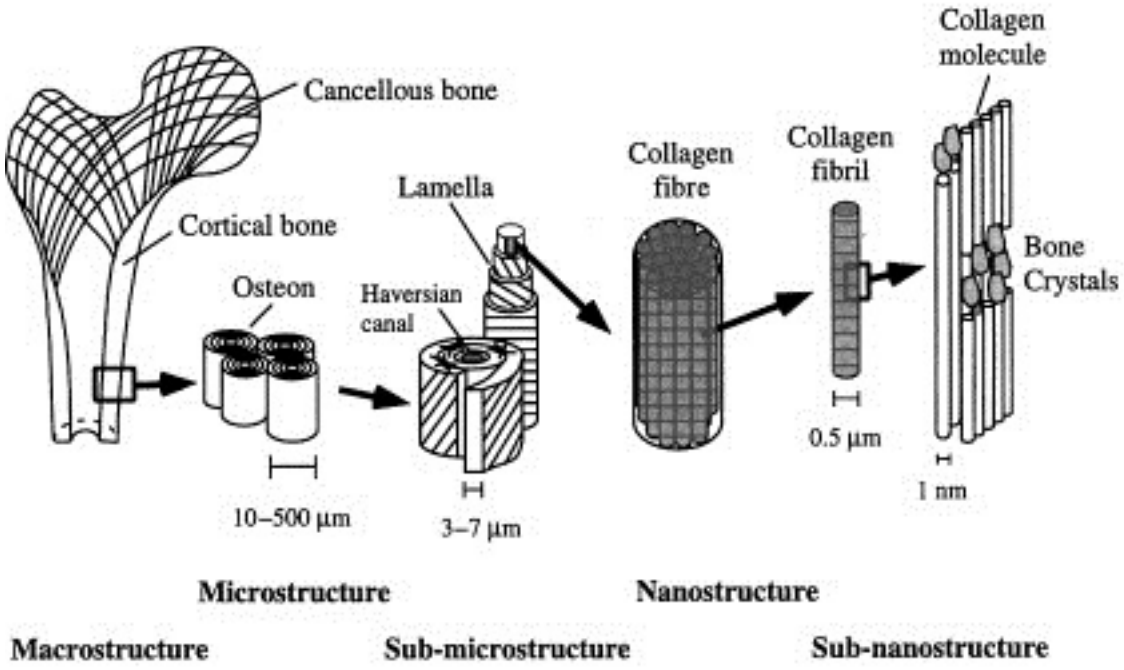

Figure 1.1: The structure of bone. The sub-nanostructure composed of three main materials, includes crystals, collagens, and non- collagenous organic proteins. The mineralised collagen fibril is the basic building block of bone, at the nanostructure, collagen fibres are in the size range of 100 nm to 1 mm. At the sub-microstructure, collagen fibrils are ordered into arrays to form bone lamellae with 3 - 7 μm thick. The formation of osteons can be observed at the microstructure. At the macrostructure level, bone is separated into the cortical and cancellous types. Figure reproduced with permission from Ritchie *et al.* [2005].

VIII (subendothelium of vascular walls) and type X (endochondrial growth plates).

3. There are also fibril associated collagens, like type IX, XII, XIV, XVI, XIX and XX. These types of collagen tend to be located on the surface of collagen fibrils in a tissue specific manner.

4. Type VI is a micro fibrillar collagens that forms a distinct network of fine filaments throughout most connective tissues, while the short chain collagen (types X and VIII) forms hexagonal networks [Kielty & Grant, 2003].

Type I collagen is the most abundant protein found in bone. It contains two $\alpha 1$ chains and one $\alpha 2$ chain which forms a triple helix. Each α chain contains over 1050 amino acids with a molecular weight of approximately 95,000 g/mol, and consisting of an amino acid sequence with a repeating structure (Gly-X-Y). Glycine (Gly) is found at every third residue along the chain, which is important for an undistorted structure. X is usually a proline (Pro), and Y is often a hydroxyproline (Hyp) [Viguet-Carrin *et al.*, 2006]. This composition leads to the stability of the collagen triple helix [Kar *et al.*, 2006]. Collagen has the ability of organising into a hierarchy of fibrils with diameters up to several hundred nanometers and complex fibrillar, liquid crystal-like architectures [Hulmes, 2002; Kirkwood & Fuller, 2009].

Hodge & Petruska [1963] studied stained natural and synthetic collagen fibrillar structures under TEM, and proposed a structural model that represents the basis of all current concepts of collagen structure. They proposed that the triple helical molecules are arranged in a staggered array such that a gap exists between the NH2-terminus of one triple helical molecule and the COOH-terminus of the next. In two dimensions this results in a zone of densely packed molecules (overlap zone) and a zone of less densely packed molecules (gap zone) due to the presence of the gaps (as illustrated in Figure 1.2). The characteristic D (65 - 67 nm) periodicity provides resistance to tensile stress.

Collagen exists with controlled orientations in bone. Woven bone consists of randomly oriented collagen fibrils, and lamellar bone composed with highly orientated collagen fibres [Kini & Nandeesh, 2012]. The mechanisms which guide the spatial arrangement of collagen fibres have not been fully understood yet. In 1975, Jones *et al.* [1975] attempted to investigate this phenomenon. They observed that collagen fibres were oriented in the same direction as osteoblasts. However, they have not been able to identify whether the cells controlled the orientation of the collagen fibres or vice versa. Kadler *et al.* [2008] proposed that collagen fibres were formed at the nano-scale by self-assembly. While, on a macro scale, Martinez *et al.* [1999] provided clear evidence that collagen fibres orientate following external loading patterns. As a result, many researchers still focus on determining the mechanisms which regulate collagen fibril assembly, and whether cells influence this process.

It has been reported that the spatial arrangement of collagen fibres can be

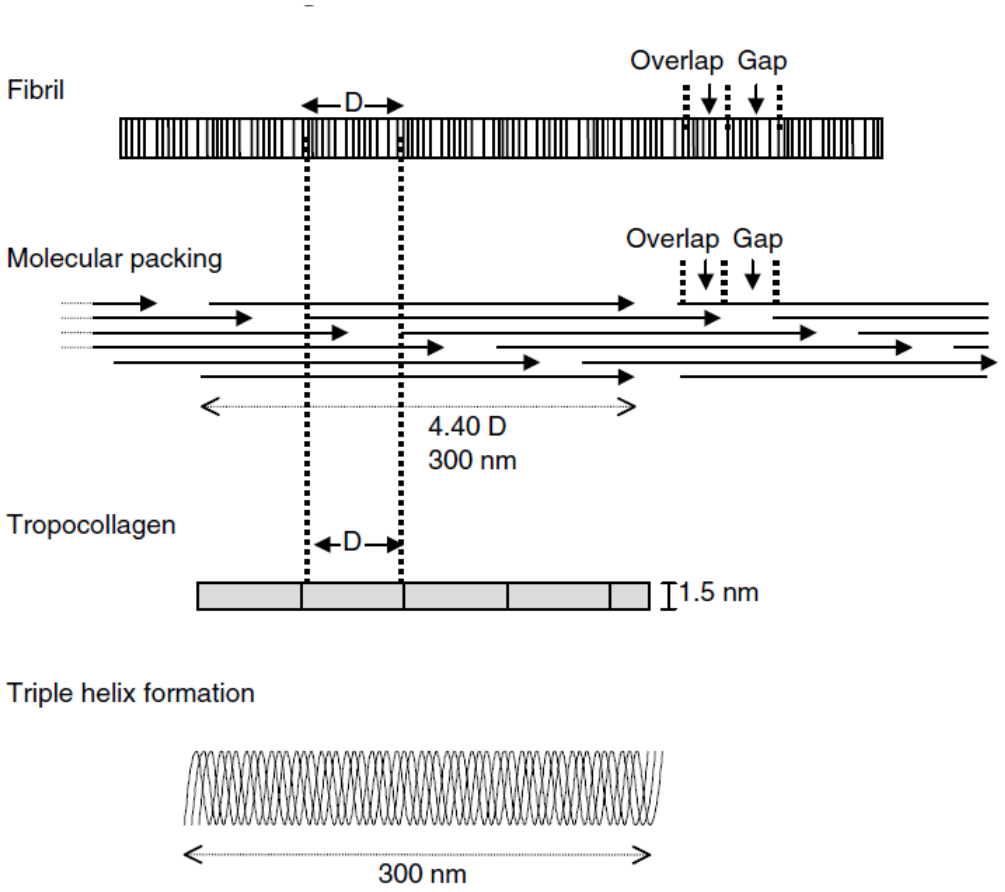

Figure 1.2: A schematic diagram illustrating the organisation of collagen fibrils. From bottom to top: the triple helix structure which contains three polypeptide chains; the tropocollagen molecule which are long rods comprising three polypeptide chains; the packing of tropocollagen molecules; collagen fibrils with its characteristic cross-striated (banding) fibrillar structure. Figure reproduced with permission from Vaughan [1970].

regulated by several *in vivo* and *in vitro* factors. Procollagen molecules have recently been shown to undergo liquid crystalline ordering in solution, prior to fibril assembly [Kirkwood & Fuller, 2009]. This may provide an explanation for the liquid crystal-like architectures of different connective tissues [Hulmes, 2002]. One of the characteristic features of liquid crystals is that they can be ordered in electric and magnetic fields [Brown *et al.*, 1971]. The earliest investigation on the *in vitro* alignment of collagen systems was conducted by using an electrical gradient [Benjamin *et al.*, 1964]. Later on, several groups developed ways to align collagen fibres by using varies techniques. The most common studies among these techniques involves exposing collagen solution to a strong static magnetic field with strength higher than 1T during gelation [Dubey *et al.*, 2001; Guido & Tranquillo, 1993; Kotani *et al.*, 2000; Torbet & Ronziere, 1984]. Here, the fibrils formed in a direction of perpendicular to the field (shown in Figure 1.3a and 1.3b). Possible explanations of this phenomenon have been investigated. In the study of Worcester [1978] and Pauling [1979], they proposed that each collagen molecule has a small negative diamagnetic susceptibility, in which peptide bonds and aromatic residues are the main potential sources of anisotropy. The regular organisation of such molecules leads to a large enough negative diamagnetic susceptibility along the fibres to affect such alignment under magnetic field [Torbet & Ronziere, 1984].

1.2.2 Bone Cells

There are three main type of cells in bone, namely osteoblasts, osteocytes, and osteoclasts. They are responsible for the bone production, maintenance and mod-

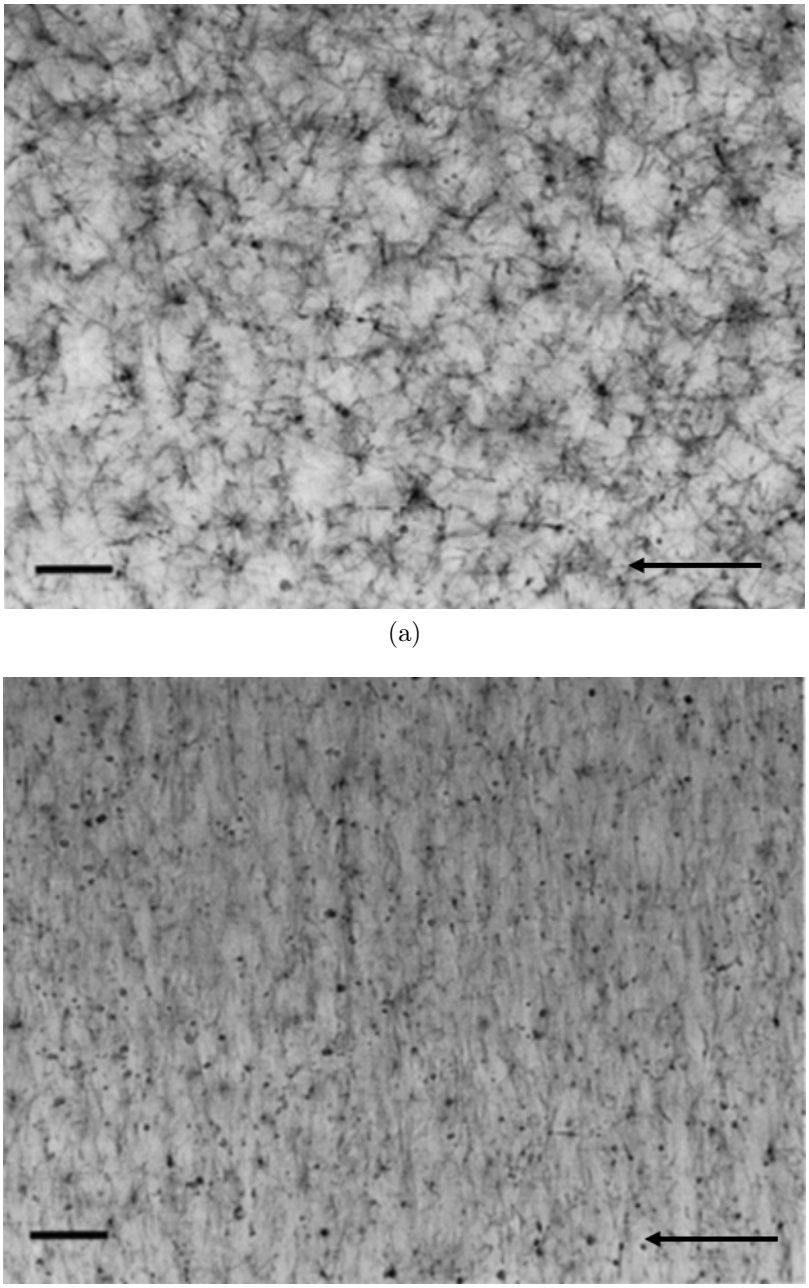

(a)

(b)

Figure 1.3: Microstructure of collagen fibres (a) with 0T and (b) with 8T exterior SMFs. The arrow indicates the direction of the magnetic field. Scale bar = 250 um. Figure reproduced with permission from Kotani *et al.* [2000].

elling, respectively. Osteoblasts are the major cellular component of bone, with the responsibility of forming and replacing new bone matrix [Pritchard, 1972]. They deposit collagen matrix and release minerals that combine to make the bone mineral. Once osteoblasts create the new bone around themselves, they are trapped inside of the bone matrix and can no longer move or form bone, this is how osteocytes are created. The responsibility of osteocytes is to maintain bone density by sensing mechanical strains and damage [Pritchard, 1972]. Osteoclasts are located at the bone surface and responsible for the absorption of bone matrix. Their main function is to degrade small pieces of bone tissue, resorbing bone via two distinct processes, including the acidification and the secretion of various proteases, and the breaking up of both inorganic and organic parts of the bone [Kini & Nandeesh, 2012]. In healthy adult humans, the rate of bone formation, which is accomplished by the osteoblasts, should be equal to the rate of bone absorption, by the osteoclasts, resulting in a renewal of 5 - 10 % of the bone volume per year [Hernandez-Gil *et al.*, 2006].

Osteoblasts are large cells (20-30 μm), with a basophilic cytoplasm, large nucleus, a substantial rough and large endoplasmic reticulum (as they synthesise large quantities of proteins), golgi apparatus, mitochondrial and lysosomes scattered throughout the cytoplasm (as shown in Figure 1.4) [Hernandez-Gil *et al.*, 2006].

There are several functions of osteoblasts. First of all, osteoblasts synthesise the organic matrix or osteoid materials at a rate of 2 to 3 μm per day, and mineralise at a rate of 1 to 2 μm per day. Osteoblasts also secrete a complex

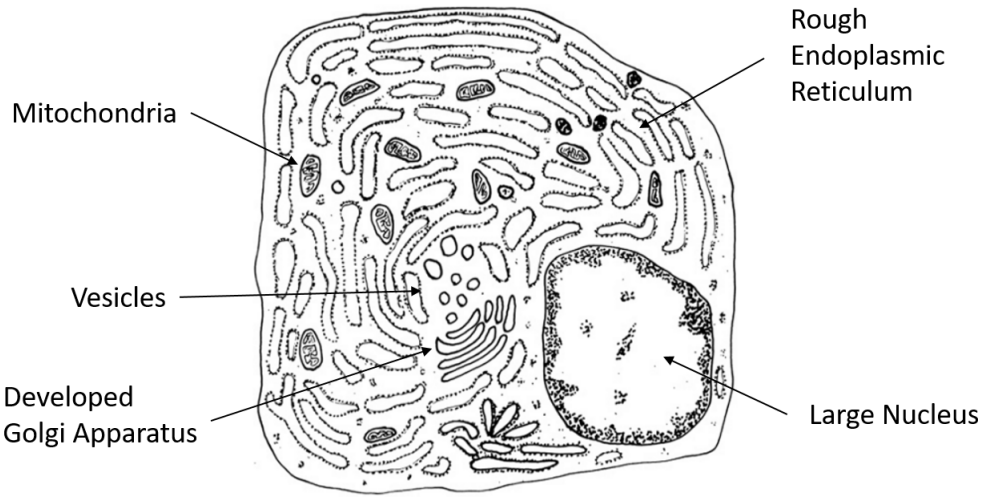

Figure 1.4: A sketch of an osteoblast. The nucleus of the cell is placed characteristically to one side of the cell. the cell contains a developed Golgi apparatus, mitochondria, ribosome and rough endoplasmic reticulum. Figure reproduced with permission from Revell [2012].

ECM containing collagenous and non-collagenous proteins, bone morphogenetic protein (BMPs), and growth factors. Besides, osteoblasts synthesise the bone matrix due to their location, morphology and histochemistry. By taking up of amino acids, glucose and sulphate groups through the cytoplasmic process, osteoblasts can also produce collagen matrix, proteins and glycoproteins to form the osteoid [Pritchard, 1972]. Moreover, osteoblasts also have several roles in calcification. They can act as the origin of matrix vesicles, store calcium in their mitochondria and pass this to the matrix, and transport calcium ions in and out of bone fluid. The presence of a relatively high concentration of calcium in osteoblasts suggests that these cells transport calcium from the blood stream to calcifying matrix. Furthermore, they can direct the arrangement of extracellular matrix fibrils as well as synthesise growth factors [Hernandez-Gil *et al.*, 2006].

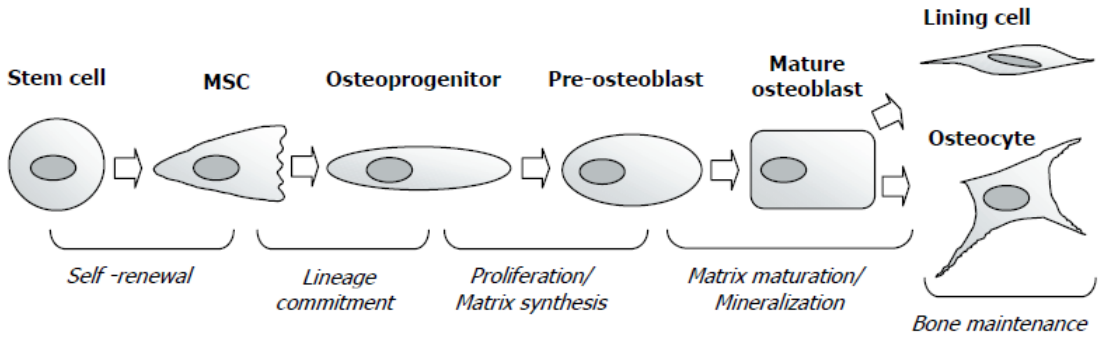

Figure 1.5: Osteogenic lineage, originating from mesenchymal stem cells (MSCs) in a sequence of steps controlled by transcription factors, growth factors, ECMs proteins and the parallel expression of specific genes and proteins. Figure reproduced with permission from [Epstein *et al.*, 1995].

Osteoblasts undergo a complex differentiation process in a sequence progressing from mesenchymal stem cells (MSCs), osteoprogenitor, preosteoblasts to differentiated osteoblasts (mature osteoblasts) (shown in Figure 1.5) [Webster *et al.*, 2007]. There are three phases in the differentiation process, as identified by Lian & Stein [1992] (shown in Figure 1.6). They differentiate through a characterised temporal sequence of expression osteoblastic markers.

In the initial phase, three genes have been identified to control the rate of proliferation, known as c-fos (a proto-oncogene of the retroviral oncogene v-fos), c-myc (a regulator gene that codes for a transcription factor, which plays a role in cell cycle progression, apoptosis and cellular transformation) and c-jun (a protein encoded by the JUN gene). They are up-regulated together with the transcription factor core-binding factor a1, (Cbfa1, also known as Runt-related transcription factor 2 or Runx2) and osterix [Lian & Stein, 1992]. Runx2 is a multifunctional transcription factor that controls skeletal development by regulating the differ-

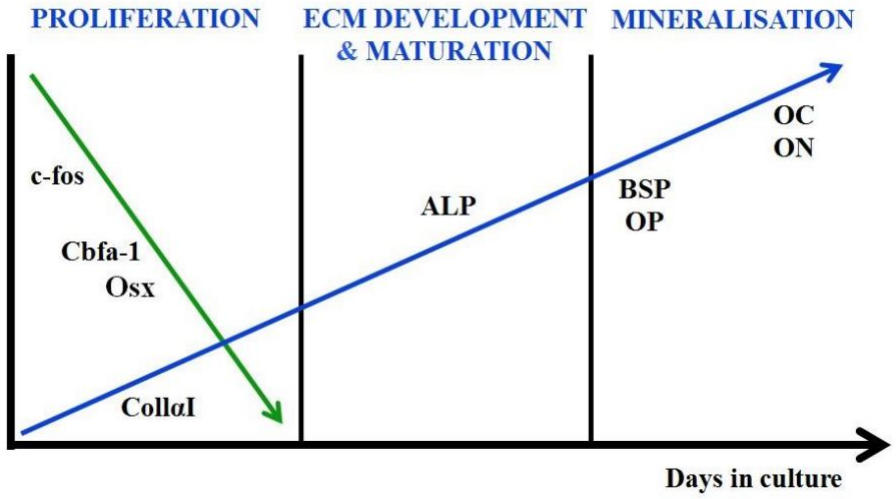

Figure 1.6: Temporal changes in expression of osteoblast cell genes. Cell cycle-regulated genes (green) include Runx2 and Osterix, and osteoblast phenotype differentiation genes (blue) include Collagen type I, ALP, BSC, OC, ON, OP. Adapted from Lian & Stein [1992]. Figure reproduced with permission from Lian & Stein [1992].

entiation of osteoblasts and the expression of many extracellular matrix protein genes during osteoblast differentiation. As the expression precursor cells differentiate, they express proteins specific to their function in the cellular membrane. The expression of Runx2 is the first indication of osteogenic differentiation [Grant & Ralston, 1997]. Interestingly, maintained expression of Runx2 produces a reduction in cortical bone mass and increased trabecular bone mass mineralisation [Maruyama *et al.*, 2007], indicating that while this factor is essential for osteoblast lineage specificity, its prolonged expression actually hinders subsequent osteoblast differentiation. At the end of this stage, the expression of osterix, type I collagen and growth factors, such as transforming growth factor β (TGF - β) and fibroblast growth factor (FGF), are actively synthesised [Aubin & Triffitt, 2002]).

Other than providing a scaffold for mineral deposition, type I collagen is essential for osteoblast functionality based on the fact that dysfunctional fibril formation impairs the subsequent stages of osteoblast phenotypic development. Through the interaction with $\alpha 2\beta 1$ integrin, collagen influences the activation of the osteocalcin promoter within the nucleus [Xiao *et al.*, 1998], while also activates the mitogen-activated protein kinase (MAPK) signalling pathway, leading to phosphorylation of Runx2.

Alkaline phosphatase (ALP) has an important role in the matrix development stage, and its expression coincides with the synthesis of type I collagen. ALP acts locally to increase the phosphate concentration via hydrolysis of mono-phosphate esters (inorganic phyrophophate) at high pH, which together with calcium ions form the substrate for hydroxyapatite formation [Harris, 1990].

Finally, during the mineralisation stage, proteins such as bone sialoprotein (BSP), osteonectin (ON), osteopontin (OP) and osteocalcin (OC) reach a maximal level. BSP and ON belong to the Small Integrin Binding Ligand N-linked Glycoprotein (SIBLING) gene family, which contain Arg-Gly-Asp (RGD) motifs in their structure. They can bind to various matrix constituents and cell types. Studies showed that BSP acts as a nucleation factor for hydroxyapatite formation and deposition [Hunter & Goldberg, 1993]. ON is a promoter of hydroxyapatite crystal formation, only when it is connected to the collagen by binding to its discrete fibrillar sites [Roach, 1994]. OP is another glycoprotein with a RGD sequence. OP is secreted in mineralising and non-mineralising tissues, and in both normal and pathological states. Conversely to BSP and ON, OP is believed to

act as an inhibitor of mineralisation as it hinders hydroxyapatite nucleation, by preventing premature precipitation of calcium phosphate crystals [Roach, 1994]. Additionally, owing to a RGD sequence in peptide structure, OP serves as a cell-matrix/matrix-mineral mediator. Another non-collagenous protein, OC can interact with calcium and hydroxyapatite by regulating the process of mineralisation and bone remodelling [Roach, 1994]. In the study of Owen *et al.* [1990], OC have been considered as a marker of late osteoblastic differentiation.

Since the first attempt of isolation and *in vitro* culture of osteoblast cells from the adult human bone as conducted by Bard *et al.* [1972], a significant improvement in the knowledge of osteoblastic cell culture has been made. A variety of cell culture systems have been successfully used to study the biological behaviour of osteoblasts. Each system can provide unique advantages of increasing the understanding of bone development, differentiation, gene expression and responses to local and synthetic factors. Laboratory investigations commonly based on the employment of primary cultures of osteoblastic cells derived from fetal calvaria or subperiosteal fetal long bones, established clonal cell lines from cells isolated from bone tumours (typically osteosarcoma, ROS 17/2.8 or UMR-106; human MG-63) and non-transformed cell lines (MC3T3-E1 or UMR-201 cell lines).

The primary cell cultures undergo changes which mimic osteoblastic differentiation *in vivo*, thus providing insights into the stage-wise regulation of gene expression in osteoblastic cells. However, it is noticeable that depending on the cell system and culture conditions, temporal aspects of the osteoblast differentiation varies dramatically. One of the problems of using primary cultures is

that they contain a heterogeneous mixture of osteoblastic cells at different stages of differentiation and cells of other lineages (including fibroblastic cells) [Aubin *et al.*, 1993]. Thus the uses of primary cells have been limited. Furthermore, it is also important to note that the source and the age of the bone, the medium, culture system, and the isolation system all affect the sensitivity of the cells [Stern & Krieger, 1983]. For example, cells obtained through the enzymatic isolation proliferate faster than cells from outgrowth cultures, but the ALP activity is comparable in cells from both isolation types [Voegele *et al.*, 1999]. Contradictory results in terms of ALP activity were found in another study where the enzyme level was higher in cells obtained from outgrowth culture [Jonsson *et al.*, 1999].

Osteosarcomas are malignant bone tumours consisting of cells with abnormal cellular functions. Osteosarcoma cell lines refer to the cells derived from bone tumours. These cells share some osteoblastic features, therefore they have been widely used *in vitro* as osteoblastic cell models. The most commonly used osteosarcoma cell lines include UMR-106, MG-63, ROS 17/2 and ROS 17/2.8. UMR-106 is a cell line derived from a transplantable rat P-induced malignant osteogenic sarcoma. This cell line has been extensively characterised with properties of enrichment in ALP activity, type I collagen production and the ability to mineralise. On the other hand, MG-63 cell lines, which were derived from a human osteosarcoma, revealed an immature osteoblast phenotype and undergo temporal development in long term culture [Billiau *et al.*, 1977]. This cell line display rapid cell growth without exhibiting contact inhibition [Heremans *et al.*, 1978]. MG-63 cell lines have been used as an experimental model to study a variety of different osteoblastic functions such as adhesion [Heino *et al.*, 1989], ECM

synthesis [Franceschi *et al.*, 1988], alkaline phosphatase activity [Boyan *et al.*, 1989; Franceschi *et al.*, 1985] and osteocalcin production [Lajeunesse *et al.*, 1990]. Moreover, due to their immature phenotype, MG-63 cells can be considered as a suitable cell model to investigate the differentiation process into a mature osteoblast phenotype. However, inconsistency exists in the literature regarding the mineralisation capabilities of MG-63 cells in monolayer. For example, Clover & Gowen [1994] and Pierschbacher *et al.* [1988] indicated that MG-63 cells do not mineralise over the cultured period. This may limit the use of osteosarcoma cells as models for matrix mineralisation.

MC3T3-E1 is a clonal non-transformed cell line established from mouse calvaria. This cell line exhibits high ALP activity and is capable of synthesising collagen matrix. In addition, this cell line was shown to undergo temporal changes from proliferation to nodule formation and mineralisation in a similar manner as in intramembranous osteogenesis *in vivo* [Sudo *et al.*, 1983]. Although MC3T3-E1 cells experience a similar proliferation stage as human primary cells, the gene expression differs significantly from each other. This is due to species-specific differences in gene regulation [Quarles *et al.*, 1992; Wang *et al.*, 1999].

1.2.3 Cell/Matrix Interactions

The ECM normally provides more than just a structural support, it also provide cells with chemical and physical cues, to allow cell attachment and migration, to deliver and retain cells and biochemical cues, to enable diffusion of vital cell nu-

trients and expressed products, and to exert mechanical and biological influences to induce certain cell behaviour. Potentially, by providing ECM with different chemical cues (such as growth factors, biocompatible nanoparticles) and physical conditions (such as matrix stiffness, topography), the cell behaviour can be altered. Cellular responses to mechanical signals include differentiation, migration, proliferation, and alterations in cell-cell and cell-matrix adhesion [Mason *et al.*, 2012].

Cells communicate with their ECM through integrins. Intergrins are a family of cell surface receptors that associate with both internal and external environment of the cell, among which, $\alpha 1\beta 1$, $\alpha 2\beta 1$, $\alpha 10\beta 1$ and $\alpha 11\beta 1$ can interact with collagen molecules [White *et al.*, 2004]. For example, $\alpha 2\beta 1$ integrin has been found to be essential in the organisation and deposition of fibrillar collagen. Following ligand binding, the cytoplasmic domains of integrins connect to the cytoskeleton of the cell and trigger the assembly of signalling complexes. Conversely, the binding of intracellular cytoplasmic components influences cell adhesiveness by altering integrin conformation. Thus, a large variety of complex signalling events can be transduced by integrins in a bidirectional manner across the cell membrane. These events serve to modulate and coordinate many aspects of cell behaviour, such as proliferation, shape, polarity, motility, gene expression, and differentiation [Askari & Humphries, 2004]. In this way, cell can sense the changes in the ECM, such as change in stiffness [Mason *et al.*, 2012], fibril diameter and alignment [Muthusubramaniam *et al.*, 2012]. For example, when matrix stiffness increases, the cell-substrate adhesion increases. In the study of Muthusubramaniam *et al.* [2012], it has been found that larger fibril diameter

lead to the up-regulation of several gene expressions and markers.

1.3 Three-dimensional Bone Tissue Models

1.3.1 Two-dimensional towards Three-dimensional Tissue Models

The commonly used tissue models include *in vivo* (animal) and *in vitro* models. *In vivo* models often refer to the processes performed within a living organism. In biological research, it often refers to animal models to study the biological behaviours within a complete and intact system. *In vivo* models provide the advantages that the implanted biomaterials will be subjected to the real physiological environment. However, the *in vivo* models are normally complex and have limited access, as well as having ethical, costs and time issues. Because of the inherent difficulties encountered during *in vivo* evaluations, the majority of research has been conducted using *in vitro* models. *In vitro* models provide a simpler way for the analysis of tissue components away from the intact living organism. When compared to the *in vivo* models, *in vitro* models are easy to access, they can help to reduce the cost/waste of animal models, and can also be incorporated/synthesised with different test variables. The *in vitro* models can be further categorised into two types, two-dimensional (2D) or three-dimensional (3D), distinct by whether the cells have been seeded on or within a cell adherent material.

2D tissue models normally refer to the system where cell monolayers are cultured on a stiff or flat surface. Conventional 2D *in vitro* tests can be performed in tissue culture plastics, which provide the advantages of low cost and high speed. 2D models can serve as simple and easy systems to assess the effects of materials on cultured cells, however, they still differ from the natural tissue in several ways. First of all, the 2D models lack cell/matrix interactions and cell/cell attachments when compared to the natural tissue. Cells in most natural tissue environments are embedded within the ECM. This matrix supports cells within a structured scaffold and exhibits environmental cues to interstitial cells. However, the 2D models cannot provide the function of a natural ECM. Secondly, the substrate stiffness is different in 2D and natural matrix. The cells seeded on 2D models normally attach to the surface of the model in one plane only, therefore they receive high resistance from the attached plane not the others. While in the real tissue environment, the cells are interacting with the surrounding environment and experiencing physiological forces from all dimensions. Thirdly, the concentration of essential nutrients available to cells in 2D and real tissue environment differ from each other due to the variance in density. In 2D models, the culture medium with nutrients are not available to the cell surfaces that attached to the model surface. While in the real 3D environment, nutrients delivered to the cells have to diffuse through the dense matrix, resulting in a concentration gradient. This concentration gradient can favour the biological behaviours of the cultured cells. Therefore, the 2D model may not fully represent the real situation in natural tissue. These limitations have motivated researchers to develop *in vitro* 3D models for laboratory biological studies.

Culturing cells in a 3D environment has attracted a lot of interest. It is evident that many cells behave differently when cultured in 3D, and often adopt more *in vivo*-like morphologies. Culturing cells in 3D radically alters the mechanical signals from those provided in 2D, thus affecting cell-receptor ligation, intercellular signalling and critical cell behaviours such as cellular migration. The 3D environment also influences the diffusion and adhesion of proteins, growth factors, and enzymes, which ensures cell viability and can influence cell functions [Nisbet *et al.*, 2008]. Maintaining cells in 3D systems, such as spheroids, micromass and pellets, promotes progression in osteoblastic differentiation leading to osteoblast cell maturation [Jahn *et al.*, 2010; Kale *et al.*, 2000]. For instance, osteoblast cell phenotype progression was observed for human osteoblast cells in pellet and spheroids cultures compared to monolayer cultures. Human bone precursor or osteoblast cells in spheroids, formed by induction with TGF-β1, had increased osteonectin and alkaline phosphatase gene expression and collagen synthesis compared to monolayer cells [Kale *et al.*, 2000].

1.3.2 Types of Three-dimensional Tissue Models

There are various types of 3D tissue models used in laboratory studies, such as porous tissue scaffolds (sponge or foam), fibrous scaffolds (electrospun fibres) and custom scaffolds made by computer-aided design (CAD). Porous tissue scaffolds/models, possess high porosity, interconnected structure and are easy to manufacture, however, they usually employ highly toxic solvents, experience low pore interconnectivity and sometimes weak mechanical properties (due to highly

porous structures). Fibrous scaffolds produce large surface area-volume ratio and high inter-fibre distances for nutrition and gas exchange, however, they may lack mechanical integrity and experience limited cell infiltration due to small pore size. As for the customised models using CAD techniques, they have the advantages of controlled matrix architecture such as size, shape, interconnectivity, geometry and orientation, as well as the required pore size, mechanical properties and degradation kinetics. However, the technique is highly dependent on the equipment, and the choices of materials are restricted.

Fibrous structure tissue models have been widely applied in tissue engineering applications. Fibrous structures have advantages of large specific surface area, small pore size, flexibility in surface functionalities, and high mechanical performance [Huang *et al.*, 2003]. Among a lot of techniques for fabricating fibrous models, electrospinning has attracted great attention own to the ease of operation, feasibility with various polymers and the resemblance to the ECM nanostructure. Electrospun fibres provide more bonding site to the cells, they can enhance cell adhesion [Jiang *et al.*, 2012; Stevens, 2008], cell proliferation as well as differentiation [Yoshimoto *et al.*, 2003]. There is a wide range of biodegradable and biocompatible synthetic or natural polymers that can be used for producing electrospun nanofibres. Synthetic polymers can be categorised into hydrophilic and hydrophobic. Hydrophilic polymers include poly (vinylpyrrolidone) (PVP) [Xiao *et al.*, 2014], poly (vinylalcohol) (PVA) [Wang *et al.*, 2004], poly (ethylene oxide) (PEO) [Lu *et al.*, 2006], and hydrophobic polymers include poly(l-lactic acid) (PLLA) [Yin *et al.*, 2010], polycaprolactone (PCL) [Chakrapani *et al.*, 2012], polystyrene (PS) [Huang *et al.*, 2012] and poly(lactic-co-glycolic acid) (PLGA)

[Katti *et al.*, 2004]. There are also several natural polymers derived for electrospinning, such as type I collagen [Matthews *et al.*, 2002], gelatin [Mo *et al.*, 2000] and chitosan [Bhattarai *et al.*, 2005].

One problem associated with electrospun fibres is that cells cultured on these scaffolds often adhere to the surface of the scaffold with minimum penetration, as illustrated in Figure 1.7. It is evident that electrospun fibres usually promote the assembly of thin tissues on their surface and do not allow proper infiltration of the cells to the core of the matrix [Dvir *et al.*, 2011; Goh *et al.*, 2013]. However, it is worth noting that the electrospun fibre scaffolds are still uniquely different from 2D models, as the cells seeded on fibres receive nutrients and growth cues three-dimensionally [Nisbet *et al.*, 2008]. Besides, the diameters of the electrospun fibres are usually produced at the upper limits of the 50 - 500 nm range seen in natural ECM (human bone ECM, for example, have an average diameter of 20 nm) [Dvir *et al.*, 2011], which is not favourable for cell attachment and growth. In addition, the most common materials for electrospun fibres are synthetic polymers. Many polymers are only soluble in scarce and expensive solvents at high temperature (above 60 °C) [Matthews *et al.*, 2002]. This limits the use of these polymers in fibre production. Besides, a variety of solvents used in electrospinning systems are fire and explosion hazards, which is another important drawback of solution technology [Malakhov *et al.*, 2009].

To emulate natural ECM better in terms of structural and functional properties, as well as to promote cell/matrix interaction at the molecular level, 3D scaffolds were created by molecular self-assembly by using natural or synthetic poly-

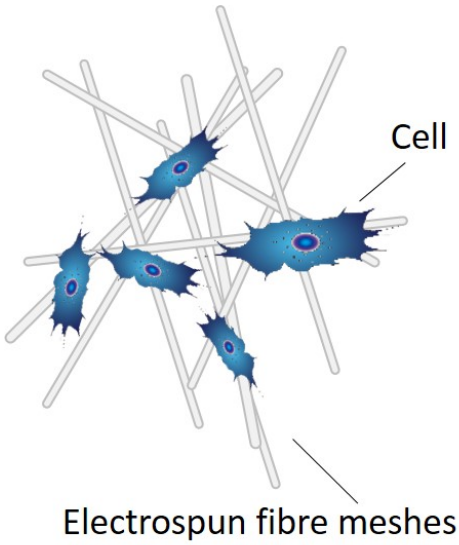

Figure 1.7: Illustration of cells seeded on electrospun fibre meshes.

mers. Natural polymers include alginate [Rowley *et al.*, 1999], gelatin [Yamamoto *et al.*, 2001], chitosan [Berger *et al.*, 2004], fibrinogen [Ahmed *et al.*, 2008], hyaluronic acid [Gurski *et al.*, 2009] and collagen [Cen *et al.*, 2008]. Synthetic materials include poly(ethylene oxide) (PEO) [Patel & Amiji, 1996], poly(vinyl alcohol) (PVA) [Yoshii *et al.*, 1999] and polypeptides [Markland *et al.*, 1999]. Synthetic polymers can be reproducibly produced with specific molecular weights, block structures, degradable linkages, and cross-linking modes [Drury & Mooney, 2003]. They are generally cost-efficient and have good availability. However, there always remains a concern about the degradation product of these materials after implantation. On the other hand, hydrogels formed by natural derived materials are more frequently used. This is due to the fact that they are either components of or have macromolecular properties similar to the natural ECM. These materials are naturally recognised by cells, and more likely to stimulate physiological responses in cells. For example, collagen is the most abundant protein

found in bone and some other of mammalian tissue ECM, it plays a dominant role in maintaining the biologic and structural integrity of bone ECM [Cen *et al.*, 2008]. Natural proteins such as type-I collagen contains binding sites recognised by cell membrane integrin. Particularly, $\alpha 1\beta 1$ and $\alpha 2\beta 1$ play important roles in dictating cell behaviours. The presence of collagen molecules in the tissue model increases the biological relevance of the construct, and encourages cells to behave as they would in their native ECM environment.

The advantages and disadvantages of using hydrogels as a 3D tissue model/scaffold are listed as below. First of all, they can be designed to be highly biocompatible and biodegradable. Secondly, they contain pores large enough to accommodate living cells, allowing good transport of nutrient to and from the cells. However, a significant disadvantage of hydrogels is their relatively weak mechanical strength. They posses difficulties in handling, sterilising and stabilising.

1.4 Collagen Plastic Compression

1.4.1 Collagen Hydrogels

In order to better mimic the ECMs and accommodate cells in such a 3D structure, further understanding of how to control the assembly of this bio-mimetic structure is required. Native type I collagen can be extracted into acid solutions; the solubilised collagen monomers are known to spontaneously self-assemble *in vitro* at neutral pH and room temperature to form native type fibrils [Yuan & Veis,

1973]. Most tissues can be simplified and defined by its predominant features (such as matrix stiffness, cell density, biocompatible factors and growth factor). By incorporating these features into collagen based scaffolds, tissue specific models can be produced.

Collagen hydrogels have an established track record as potential scaffolds for tissue modelling and regeneration applications. One of the main advantages of collagen as a scaffold material is its ability of incorporating cells directly inside its 3D environment (as shown in Figure 1.8). In addition, during tissue or organ development and repair processes, collagen can interact directly with cells to influence several cellular activities, including adhesion, growth, differentiation, mineralisation of ECM, as well as the expression of growth factors and cytokines. This provides the desired properties as a ECM-like scaffold, including water retention capacity, nano/micro-porosity to allow cells to grow and arrange in 3D, biodegradability, and pore inter-connectivity to allow free flow of oxygen and nutrients [Dutta & Dutta, 2009; Tomasek *et al.*, 2002]. Due to these advantages, a large number of applications of collagen gels can be seen, such as nerve guide tube for peripheral nerves [Phillips *et al.*, 2005] and scaffolds for connective tissues [Brown, 2013].

However, some properties of collagen hydrogels may limit their application. For example, collagen density in those gels is only measured as approximate 0.2 to 0.5 % of wet weight, with large excess of fluid (>98%). This results in poor mechanical properties, the lack of orientated architecture, and limited direct cell contact [Brown *et al.*, 2005]. When cells being seeded within collagen hydrogels,

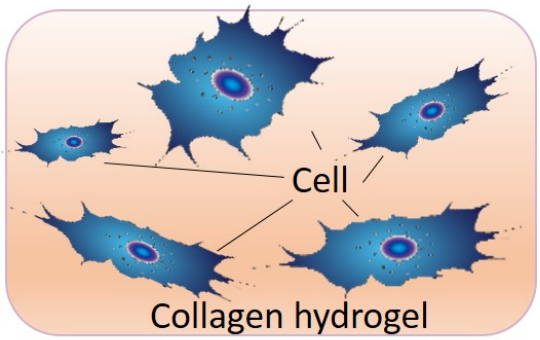

Figure 1.8: Illustration of cells incorporated within PC collagen hydrogels.

they can expel some of this excess fluid and increase the collagen density [Bell *et al.*, 1979]. However, this process can take several days, and only gives a modest increase in mechanical strength with limited precision and control. Therefore the direct use of collagen hydrogels scaffolds remains an imperfect solution.

1.4.2 Plastic Compression

In order to construct a mechanically strong collagen based scaffold, as well as maintain all the properties, a novel approach known as plastic compression (PC) has been developed by Brown *et al.* [2005]. Many studies have demonstrated the suitability of PC collagen scaffolds in tissue engineering applications, such as skin [Hu *et al.*, 2010], bone [Buxton *et al.*, 2008] and cornea [Mi *et al.*, 2010]. The PC process can be achieved by compressing conventional collagen gels, leading to the controlled expulsion of interstitial liquid. Figure 1.9 represents the schematic view of plastic compression process.

PC allows for the fabrication of dense collagen constructs, which mimic the ECM fibrillary density, microstructure, and biological properties. For example, a conventional collagen hydrogels is made from a collagen solution with a density of 2 mg/ml, and the resultant hydrogel contains 0.2 % collagen and 99.8 % water. With a single plastic compression system, collagen density in the resultant model can increase to 11 - 18 % [Brown *et al.*, 2005]. Furthermore, this construct has been tested to persist for at least 5 weeks *in vivo* [Mudera *et al.*, 2007]. Within this dense tissue, cells can migrate through the construct while maintaining the overall dimension and the shape of the model. The migration of cells within the PC collagen construct are related to the oxygen concentration gradients (Cells migrate from lower to higher partial pressure of oxygen) [Ardakani *et al.*, 2014] as well as substrate stiffness (towards stiffer regions) [Hadjipanayi *et al.*, 2009b].

The plastic compressed collagen gels offer several advantages compared to the conventional collagen hydrogel. First of all, by applying the load on top of the collagen gel, the aqueous component can be removed from the gel, leading to an increase in mechanical strength and collagen density of the compressed scaffolds. Besides, the compression does not affect the viability of pre-seeded cells, with over 90 % viability after compression [Brown *et al.*, 2005]. This can be contribute to the controlled compression of the sample and the high permeability of the construct to the cell essential molecules. Furthermore, the plastic compressed collagen gels have a thickness of100-200 μm, providing the possibility to produce multi-layer scaffolds. In addition, the fabrication process is extremely rapid and non-reversible, upon the removal of the loads, the water does not return to the collagen fibre, therefore known as the term "plastic".

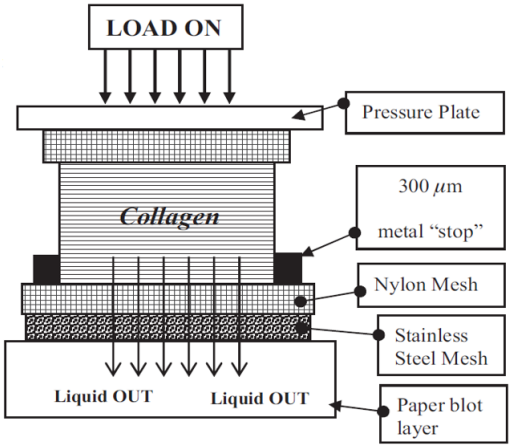

Figure 1.9: Schematic view of plastic compression (PC) process. Diagram shows the conventional assembly of PC of pre-formed collagen gels. The liquid in the collagen hydrogel was expelled by application of compressive mechanical loads. Figure reproduced with permission from Brown *et al.* [2005].

1.4.3 Cell Response within PC Models

By culturing cells inside PC collagen hydrogels with dense structure, their cell behaviour can be influence, particularly the cell proliferation, differentiation and mineralisation. Below are some highlighted findings.

1.4.3.1 Proliferation

Plastic compression produces dense collagen structures by compression, the load applied does not affect the viability of the cells seeded within the model. Generally, the cell viability was found to be more than 90 % after compression (for human dermal fibroblasts (HDFs)), with even higher percentage by using differ-

ent cell types [Brown *et al.*, 2005]. Since the cells can survive in the construct, they start to proliferate naturally. The proliferation can be affected by several factors. First of all, the initial cell seeding density can affect proliferation ability. Bitar *et al.* [2007] studied the relationship between cell density and proliferation by seeding 1×10^5 - 1×10^8 /ml cells. They found that low cell density (1×10^5 /ml) results in higher proliferation rate. Hadjipanayi *et al.* [2009a] studied the relationship between seeding 1×10^6 - 20×10^6 /ml cells, and they proved that higher cell density led to a lower proliferation rate. Given a same size of scaffold, large cell number would reach sufficient cell density quickly, hence inducing contact inhibition. Secondly, the cell proliferation is also directly regulated by the stiffness of the matrix. Hadjipanayi *et al.* [2009a] found increased cell proliferation with increasing collagen density, and the collagen density is also proportional to matrix stiffness. In gels of 0.7% collagen, there was an 87% increase in cell number (within 48 h), this was reduced to 25% in gels of 0.4% density, and no proliferation was measured at 0.2% (uncompressed), due to the low matrix stiffness. In the study of Ghezzi *et al.* [2011b], they also demonstrated a significant improvement in cell proliferation within dense collagen scaffolds when compared to collagen hydrogels.

1.4.3.2 Differentiation

Cells seeded in PC collagen also exhibit higher differentiation ability when compared to conventional hydrogels. Stimulation of differentiation towards mature osteoblasts and osteocytes was reported by Buxton *et al.* [2008]. By providing the pre-osteoblasts with a dense fibrillar environment, they were encouraged to com-

mit to osteogenic differentiation and further enhance the rigidity of the matrix. This has been achieved by up-regulating the expression of BSP, ALP, Collagen I, MMP-13 and Runx-2 *in vitro*.

1.4.3.3 Mineralisation

Dense collagen structure can also influence the mineralisation of osteoblasts *in vitro*. Buxton *et al.* [2008] demonstrated that osteoblasts in PC scaffolds mineralised earlier and faster than conventional collagen hydrogels. One of the explanations is that high collagen fibrillar density can provide a micro-environment more favourable to crystal formation. Marelli *et al.* [2011] further determined the correlations between the collagen fibrillar densities and the mineralisation level. They demonstrated that higher collagen fibrillar density led to higher carbonated hydroxylapatite formation within reconstituted collagen gels. Increased collagen density was in fact correlated with increased fibre entanglement, fibril-to-fibril contact points and reduced roughness. These changes in the gel microstructure had a significant effect on mineralisation level.

1.4.4 Further Engineering in Plastic Compression

Collagen gels can be hybridised at the point of self-assembly with several molecules of interest. When further introducing bio-factors into PC collagen gels, osteoblasts have been reported to have enhanced biological properties. For example, Chicatun *et al.* [2011] introduced chitosan into a PC system with MC3T3-E1 cells. Results demonstrated increased ALP production, level of mineralisation as well

as mechanical properties. However, they found no significant effects on cell proliferation when chitosan was introduced into the scaffolds. Bioactive glass particles also have been blended with collagen [Marelli *et al.*, 2010]. They demonstrated that the presence of 45S5 bioglass within dense collagen models resulted in an accelerated 3D mineralisation and differentiation. Furthermore, the incorporation of silk fibrion and anionic fibrin derived polypeptides have been demonstrated to have the ability to promote osteogenic differentiation of MSCs in collagen gels [Ghezzi *et al.*, 2011a; Marelli *et al.*, 2014].

Table 2.3 summaries some key observations in PC systems when using various types of cells, cell density and the incorporation of additional materials.

Cell Type	Cell Density/ml	Materials	Key Observations	References
HDFs	0.33×10^6	N/A	High cell viability, functional mechanical properties	Brown *et al.* [2005]
MG-63	1×10^5 - 1×10^8	N/A	Low cell density results in higher proliferation rate	Bitar *et al.* [2007]
Pre-osteoblasts	3×10^5	N/A	Enhanced expression of BSP,ALP,Col1,Runx2	Buxton *et al.* [2008]
HDFs	1×10^6 - 20×10^6	N/A	Higher cell density led to a lower proliferation rate	Hadjipanayi *et al.* [2009a]
HDFs	2.11×10^5	N/A	Increased viability, metabolic activity	Ghezzi *et al.* [2011b]
HDFs	23.2×10^6	N/A	Up-regulated expression of VEGFs	Hadjipanayi *et al.* [2011]
Chondrocytes	3×10^5	Chitosan	Increased cell viability	Imaizumi *et al.* [2007]
MC3T3-E1	2.11×10^5	nBG	Enhanced metabolic activity and ALP production	Marelli *et al.* [2011]

Table 1.1: Summary of various cell type, density and additional materials used in PC

Plastic compression of collagen hydrogels provide a mechanically strong and dense collagen structure, therefore can be better served as a 3D model for *in vitro* studies. However, there are also some limitations associated with this approach. Standard PC techniques bring scaffolds to *in vivo* levels of matrix density (11 - 18% collagen density) [Cheema *et al.*, 2011], however the mechanical properties of such scaffolds still fall far from those found in tissues. A compressed collagen sheet have a break strength of 0.6 ± 0.11 MPa and a Yong's modulus of 1.5 ± 0.36 MPa [Brown *et al.*, 2005], a double compressed collagen sheet can push the Young's modulus up to 4.7 ± 0.6 MPa [Neel *et al.*, 2006], however, these values are still far below the collagen fibres in natural tissue, which is 0.2 - 0.5 GPa [van der Rijt *et al.*, 2006]. Another problem associated with increased collagen density is that, the mass transfer of nutrients decreased, leading to potential cell death [Nazhat *et al.*, 2007]. One way to maintain suitable oxygen concentrations throughout the scaffold was incorporating micro-channelling within these matrices, such as unidirectional aligned soluble phosphate based glass fibres [Nazhat *et al.*, 2007]. Besides, although collagen hydrogels translate force to cells embedded within the scaffold very well, as the collagen matrix stiffens and remodels, less force is translated through, possibly due to the stress-shielding. Overall, PC collagen hydrogels can be served as useful 3D scaffolds/models for tissue engineering and regeneration applications, to test the properties of biomaterials and cell responses, for proliferation, differentiation, mineralisation, and other biological behaviours, over time. However, improvements are needed to further develop this approach.

1.5 Bone Regeneration

1.5.1 Bone Fracture

Bone fracture occurs when local stresses in a part of bone exceed the ultimate strength of the tissue. A fracture results in the discontinuity of the bone matrix and is normally accomplished with soft tissue damage, torn blood vessels, bruised muscles and a lacerated periosteum. The causes of bone fracture vary from trauma, infection, tumours and compromised blood supply, among which the direct trauma is the most common factor. Most fractures caused by direct trauma are either single or multiple. Fractures can also occur from pathological conditions due to the underlying bone or systemic disease, which can cause one or many of the bones of the skeleton system to be abnormal and more susceptible to fracture. Pathological fractures may occur through diseases such as bone tumours, osteoporotic bone, osteomyelitis and osteomalacia [Revell, 2012].

1.5.2 Bone Regenration

The bone healing and regeneration process normally involves three phases, the inflammatory phase, the reparative (including soft and hard callus formation) and remodelling phase.

When a fracture occurs, the bone, the associated soft tissues, including the periosteum and its surrounding muscles are torn, and the blood vessels crossing the fracture line are ruptured. The injury initiates an inflammatory response,

which is necessary for the healing to progress. The immune cells produce several factors and cytokines within that time, including Interleukin 1 (IL1), IL6, IL8, IL12, platelet derived growth factor (PDGF), tumour necrosis factor α (TNFα), vascular endothelial growth factor (VEGF), CXC Receptor 4 (CXCR4) and osteopontin/secreted phosphoprotein 1 (SPP1), which are essential for mobilisation and chemotaxis of other cells, angiogenesis and osteogenesis [Park & Barbul, 2004]. Then an accumulation of a haematoma within the medullary canal between the fracture ends occurs, and rapidly coagulates to form a clot [Gray *et al.*, 1995]. The acute inflammatory response peaks within the first 24 h and completes after 7 days. Angiogenesis happens through the secretion of several essential factors, such as fibroblast growth factor β (βFGF), VEGF and insulin-like growth factor 1 (IGF-1) [Knighton & Fiegel, 1989]. These factors induce the formation of capillaries within the clot and the loose aggregate of fibroblasts which forms the granulation tissue [Tonna & Cronkite, 1961]. Then the platelets and macrophages enter the fracture site and begin to secret inflammatory cytokines. These cytokines recruit MSCs and osteoprogenitors or chondroprogenitors from various locations, including the bone marrow, muscle and the periosteum. These MSCs then proliferate and differentiate into osteogenic cells.

The reparative phase starts after inflammation and normally lasts for a few weeks. Initially, cartilaginous tissue forms a soft callus which gives the fracture a stable structure. The progenitor cells residing in the cambial layer of periosteum and endosteum differentiate into osteoblast cells, which subsequently deposit woven bone via intramembranous ossification. The formed callus can rapidly envelope the bone ends and leads to a gradual increase in the stability of the fracture

fragments. At the same time, the granulation tissue formed after the fracture is replaced by fibrocartilagenous tissue. This process is initiated by several growth factors, including BMPs, IGF1, PDGF, transforming growth factor-beta (TGF-β) super-family and fibroblast growth factor 1 (FGF-1) [Bostrom *et al.*, 1995; Yu *et al.*, 2010]. These growth factors can stimulate fibroblast and chondrocyte proliferate and differentiate. Then the hard callus formation starts in the next stage and lasts until the fragments are united by a new bone, which normally takes 3 - 4 months.

Although the hard callus is a rigid structure providing biomechanical stability, it does not fully restore the biomechanical properties of normal bone. In order to achieve this, the fracture healing cascade initiates the next phase, to remodel the hard callus into a lamellar bone structure with a central medullary cavity. The remodelling process is carried out by a balance of hard callus resorption by osteoclasts, and lamellar bone deposition by osteoblasts. Although this process is initiated as early as 3 - 4 weeks in animal and human models, the remodelling may take years to complete and achieve a fully regenerated bone structure. In the normal adult, a cortical bone fracture takes approximately 12 weeks to heal while the remodelling phase can take several years [Browne, 1988]. Within children, the rate is normally quicker than in the adult, which consolidation taking 4 - 6 weeks [Adems & Hamblen, 1992].

To make bone remodelling successful, an adequate blood supply and a gradual increase in mechanical stability are crucial. This is demonstrated in cases where neither is achieved, resulting in the development of an atrophic fibrous non-union

(with no obvious callus formed). However, in cases where there is good vascularity but unstable fixation, the healing process progresses to form a cartilaginous callus and results in a hypertrophic non-union.

Figure 1.10a and 1.10b summarise the healing process of bone fracture.

1.5.3 Fracture Non-union

There is currently no accepted standardised definition of fracture non-union among orthopaedic surgeons. According to the definition provided by the Food and Drug Administration (FDA), a minimum time of 9 months has to elapse since the initial injury and there should be no signs of healing for the final three months for diagnosis of fracture non-union [Morshed, 2014].

The causes of non-unions can be complicated, such as problems with operative and non-operative interventions, comprising inadequate mobilisation of the fracture, distraction of fracture fragments by fixation devices or traction, repeated manipulations or excessive early motion of fractures, excessive periosteal stripping, and damage to other soft tissues during operative exposure. Besides, contamination time during operation, smoking, diabetes can also lead to non-union of fracture sites [Einhorn, 1995; Victoria *et al.*, 2009].

Fracture healing can be affected by the following factors. First of all, the type of bone involved. Cortical and cancellous bone respond to fractures differently. In

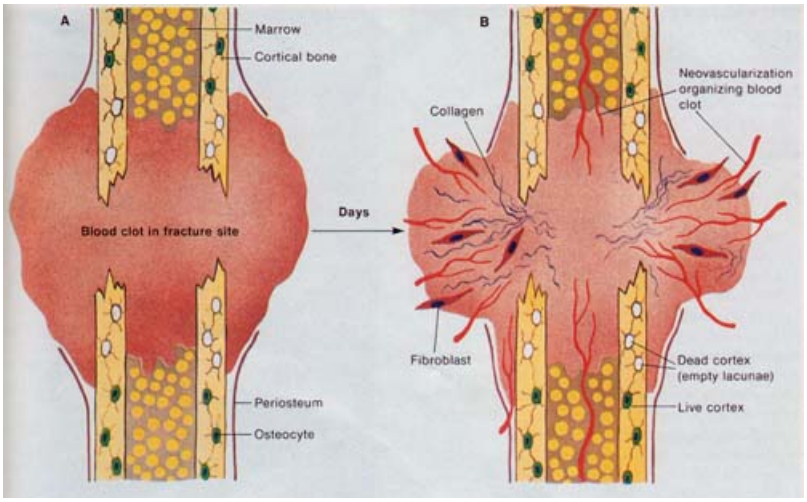

(a)

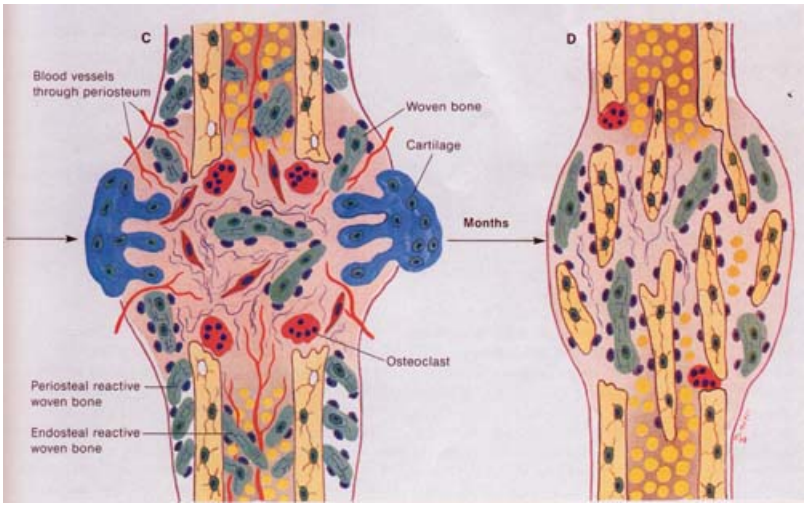

(b)

Figure 1.10: Immediately after fracture a blood clot forms and the inflammatory response is triggered. The inflammatory phase is typified by the haematoma and oedema, cells invade the fracture site. In the reparative phase, soft tissue compromising of cells embedded in glycoproteins and collagen matrix around and between the bone ends which is made up of internal callus. The cells are derived from the proliferation of osteoprogenitor cells in the endosteal layer and the external callus. Blood supply is from the periosteum, until the centrifuge supply from the endosteal is restored and regenerated. Vasularisation continue to increase as both the internal and external calluses are converted into woven bone by endochondral or intramemebraneous ossification. In the remodelling stage, the external periosteal collar is gradually resorbed whilst the medullary canal is reshaped into its original hollow form. Vascularisation is returned to normality. Figure reproduced with permission from Oryan *et al.* [2013].

cancellous bone, union occurs at points of contact, as cancellous bone has many contact points with rich blood and cells, it normally unites rapidly. Cortical bone healing is complex when compared to cancellous bone healing. The healing process can be categorised into two mechanisms depending upon the local conditions. If mobilisation is rigid, end-to-end healing of the cortical surfaces occurs with very little external callus. However, if the fragments have widespread displacement, the healing process is accompanied by the formation of callus. Secondly, the healing can also be affected by the degree of local trauma. Local trauma and trauma to the soft tissue cause a decrease in the number of MSCs and their differentiation abilities, the healing rate of the fracture site also depends on the healing of the surrounding soft tissues. Thirdly, the degree of immobilisation can have an impact on the fracture healing. Inadequate immobilisation leads to delayed union, disruption of the initial fibrin scaffolding and failure in callus formation. Besides, if infection is superimposed upon a fracture, the local defences are mobilised in order to eliminate the infection and therefore hinder the rate of healing. The healing rate is also dependent on the age of the patient. Young people heal more quickly than elderly. Studies have shown that in older rats, the expression of BMP-2 is lower when compared to other rats. Besides, serum from older donors was found to be a less potent stimulator of osteoblast differentiation when compared with that from younger patients [Kwong & Harris, 2008].

1.6 Stimulation Techniques for Bone Regeneration

1.6.1 Biological Stimulations

1.6.1.1 Osteoinductive Factors

Although the molecular basis for fracture healing is not fully understood, it has been identified that several growth factors and cytokines are involved in the process of bone repair and remodelling. Bone regeneration can be regulated by a variety of growth factors such as PDGF, fibroblast growth factor (FGF), IGF-1 and the TGF-β super-family, which includes BMPs and growth and differentiation factors (GDFs) [Sathyendra & Darowish, 2013].

FGFs have an anabolic effect on bone, as they are mitogens of osteoblasts, vascular endothelial cells and fibroblasts. It has been demonstrated that FGFs can induce MSCs to differentiate into preosteobalsts and prechondrocytes [Bostrom *et al.*, 1999]. Moreover, FGFs have been shown to enhance the callus size and the strength of the repaired fracture.

PDGFs have been demonstrated to have a stimulating effect on fracture healing. The functions of PDGFs include: stimulating the protein synthesis in osteoblasts, favouring the bone resorption, enhancing collagen synthesis, affecting the fibroblasts and smooth muscle cells [Hernandez-Gil *et al.*, 2006]. For example, when treated with PDGFs using rabbits tibial osteotomy models, more mechanically stable callus and mature osteoblast formation can be observed [Sathyendra

& Darowish, 2013].

IGF-1 can trigger osteoblasts proliferation, enhance collagen synthesis and inhibit collagen degradation, as well as mediate the osteoblast-osteoclast interaction in bone [Papachroni *et al.*, 2009]. Overexpression of IGF-I in bone under the osteocalcin or collagen type I promoter increases bone formation [Bikle, 2008]. It also has been reported that the expression of IGFs can be enhanced by mechanical loading both *in vivo* and *in vitro*. For example, by applying a mean strain of 2664 μstrain (loaded) and 350 μstrain (sham-loaded) in rats tibia, the proportion of IGF-I mRNA was found to be 29.3 $\pm$ 12.9 % for loaded tibia, 16.7 $\pm$ 4.4 % for sham-loaded tibia and 14.7 $\pm$ 4.2 % for control tibia [Reijnders *et al.*, 2007].

The TGF-β family is a group of proteins which are highly abundant in bone tissue. They have a broad range of cellular activities, including the control of proliferation and differentiated phenotype, and the synthesis of the osteoid matrix. Investigations have shown that several members of these morphogens can promote the differentiation of MSCs into the osteogenic and chondrogenic lineages. A study demonstrated that TGF-βs can increase the fracture callus size and bending strength in rabbits with mid-tibial osteotomies, however, no effects on the stiffness, bone mineral content and Harversian canal diameter have been observed [Lind *et al.*, 1993]. Moreover, Cho *et al.* [2002] conducted an *in vivo* investigation on the expression of TGF-βs on a mouse tibial over 28 days. Results demonstrated that several members of the TGF-β family are actively involved in fracture healing. For example, TGF-β1 is constitutively expressed from day 3 to day 21, TGF-β2 and TGF-β3 showed maximal expression on day 7.

Among several types of growth factor which can affect the fracture healing, BMPs are the most promising ones for clinical use [Schmitt *et al.*, 1999]. BMPs can aid the transformation from connective tissue into bone tissue, mediate the recruitment of cells to the repair site, with the potential to stimulate maturation of mesenchymal osteoprogenitor cells to osteoblasts, in addition to influencing the proliferation of these cells at various stages of the healing process [Bodamyali *et al.*, 1998; Yamaguchi *et al.*, 2000]. Cho *et al.* [2002] studied the temporal expression of members of the BMPs during fracture healing using a mouse tibia model over a 28-day period. Within 24 hours of the fracture occurred, there was an increase in the activity of BMP-2, suggesting its role as an early response in the cascade of healing events. Through the period of day 14 to 21, when the resorption of calcified cartilage and osteoblastic recruitment were the most active, there were increased expressions of BMP-3, BMP-4, BMP-7, and BMP-8. Moreover, BMP-5 and BMP-6 were constitutively expressed from day 3 to day 21. BMP-2s have been shown to induce osteoblastic differentiation by acting on the MSCs, increasing the expression of the osteogenitic transcription factors osteix and Runx2 [Phimphilai *et al.*, 2006]. Urist [1965] reported that BMP-4 is considered as a factor related to the healing of bone fractures, and this growth factor has been widely studied since then. Sato *et al.* [1999] further suggested that BMP-2 and BMP-4 accelerate differentiation of the cells into osteogenic/chondrogenic cells, as well as lead to bone-like structure formation with associated increase in osteoblast differentiation and improved mineralisation of constructs; BMP-6 was detected in differentiated chondrocytes, and the expression can last for a few weeks until cartilage callus was resorbed and replaced by bone.

1.6.1.2 Osteoconductive Materials

Osteoconduction is a process that supports the ingrowth of the sprouting capillaries, perivascular tissue and osteoprogenitor cells from the recipient host bed into the 3D structure of an implant or graft [Einhorn, 1995]. Osteoconductive materials include calcium phosphate ceramics, such as hydroxyapatite (HA), tricalcium phosphate (TCP) and bioactive glasses, or natural materials, such as coral. The rational of these materials is that, normal osteoblasts or osteoblastic cell lines have the ability to form bone on the appropriate surface. That surface must have the necessary physical and chemical composition to support the attachment, migration and differentiation of the cells. Therefore the investigations of these materials on the stimulation of bone formation and repair have been conducted for many years.

HA has been widely studied as an osteoconductive material for bone healing applications as it shares the similar composition with bone. Immature bone has deficient amounts of calcium and hydroxyl ions. With age, the bone crystal progresses to the stoichiometric hydroxyapatite formula of $Ca_{10}(PO_4)_6(OH)_2$ [Posner, 1978]. Naturally formed apatite has carbonate substitutions ($CO_3{}^{2-}$), with additional substitution of sodium (Na^+), magnesium (Mg^{2+}), potassium (K^+). fluoride (F^-), chloride (Cl^-), and trace elements such as strontium (Sr^{2+}), lead (Pb^{2+}) and barium (Ba^{2+}). $CO_3{}^{2-}$ are the most abundant ions found in bone minerals, and can substitute for the phosphate and hydroxyl group in apatite [Driessens *et al.*, 1983]. There has been increasing interest in using precipitated

nano scale HA particles (nHA) for bone regeneration therapies, own to the fact that it mimics the size of HA crystals in natural bone more closely. nHA has been demonstrated to promote the adhesion, proliferation and differentiation of osteoblasts *in vitro* [Huang *et al.*, 2004; Murugan & Ramakrishna, 2005; Wei & Ma, 2004].

The first calcium-phosphate based bone graft substitute approved by FDA was the Interpore (Interpore International Irvine California) [Bucholz *et al.*, 1989]. Interpore is a predominantly HA biomatrix formed by the conversion of a marine coral calcium phosphate to crystalline HA. The structure formed can serve as a template for host bone and new bone formation, presumably on the basis of its chemical and architectural composition. Clinical trails have been conducted to demonstrate the effects of this material in the treatment of osseous defects and fractures with loss of the bone [Bucholz *et al.*, 1989]. Other examples of the clinically approved material include Collagraft (Collagen Corporation, Palo Alto, California), which is a mixture HA, TCP and fibrillar collagen.

On the other hands, infection is one of the reasons that causes fracture non-union. Nano zinc oxide (nZnO), with its well demonstrated antimicrobial properties [Brayner *et al.*, 2006], can be introduced into the system to enhance fracture non-union by reducing bacterial growth. The antimicrobial property of nZnO can be contribute to the generation of reaction oxygen species and damage cell membrane with subsequent interaction of the nanoparticles with intracellular contents. In addition to the antimicrobial property, recent studies from Memarzadeh *et al.* [2015] also demonstrated a stimulating effects of nZnO on the proliferation and

ALP activity of osteoblastic cell lines. These results support the use of nZnO incorporated scaffolds as an outstanding candidate for promoting bone growth and inhibiting infection.

1.6.2 Physical Stimulations

1.6.2.1 Mechanical Stimulations

Tracing back to the 19th century, Cowin [1986] firstly hypothesised that bone remodels in response to stress and strain, due to the fact that the structure of bone adapts to changes in its stress environment. This process is also known as mechanotransduction, which involves the conversion of a biophysical force into a biochemical response leading to changes in gene expression and cellular adaptation.

Mechanotransduction can be categorised into four distinct phases, including mechanocoupling, biochemical coupling, transmission of signal and the effector cell response. Mechanical loads first cause deformations in bone that stretch bone cells, and also create fluid movement within the canaliculae of bone [Duncan & Turner, 1995]. In biochemical coupling, mechanical forces can be transferred to osteoblasts through several mechanosensors, includes integrins, calcium channels, cell-cell adhesion elements (cadherins, gap junctions), surface processes (primary cilia, stereocilia), other membrane elements (caveolae, surface receptors), cytoskeleton constituents (microfilaments, microtubules, intermediate filaments), ECM elements (collagen, fibronectin, proteoglycans, basement membrane) and

other cell-ECM adhesions (focal adhesions) [Frost, 2003]. Osteoblasts, osteocytes, and bone lining cells may act as sensors of mechanical signals and may communicate the signal through cell processes. These cells also produce paracrine factors that may signal osteoprogenitors to differentiate into osteoblasts [Duncan & Turner, 1995]. At the molecular level, mechanotranduction also induces secretion of growth factors, including IGF, VEGF, PDGF, FGF, TGF-β and the BMPs, which are considered to be principal local regulators of osteogenesis [Papachroni *et al.*, 2009].

In bone, external mechanical loads cause local deformations in the tissue, which is known as the strain. The amount of strain influences the cellular response, the formation of capillaries, and the resultant tissue formed at a fracture site [Sathyendra & Darowish, 2013], hence can potentially lead to increased bone volume, bone strength [Robling *et al.*, 2000] and bone formation rate [Kotani *et al.*, 2002; Schriefer *et al.*, 2005] *in vitro* and *in vivo*. A number of reports have suggested that ion channels in the membrane are strain-sensitive. *In vivo* loading can also increase the gene expression of vital matrix proteins such as osteocalcin (OC), collagen type I and alkaline phosphate (ALP) [Moalli *et al.*, 2000; Pavlin *et al.*, 2001]. These studies indicated that mechanical strain transduction may be related to direct mechanical deformation of ultrastructural organelles or proteins, which would convert mechanical signals into biochemical information.

It is worth noting that the effects of mechanical loading are dependant upon the magnitude, duration, and rate of the applied load. Some amount of strain at the fracture site is beneficial to healing, whereas excessive strain will result in for-

mation of granulation tissue or fibrous tissue and eventually disrupt the healing process [Wallace *et al.*, 1994]. Lanyon [1984] and Rubin & Lanyon [1985] studied the response of bone during normal loading *in vivo*. Strains smaller than 500 μstrains were not found to have a stimulation effect, and those between 500 and 1500 appeared to maintain bone mass and strains over 1500 μstrains increased bone mass, while peaked at 3000 μstrains. Application of over 10 000 μstrain results in a de-differentiation of the osteoblasts [Jones *et al.*, 1991]. When the strain increases to above 30 000 μstrains, microcracks and even failure of the bone can be observed. However, most of the cell culture mechanostimulus systems have been designed to deliver peak strains in the range of 10,000 - 100,000 μstrains [Brown, 2000], which were 5 - 100 times greater than the normal strain level found in living cells [Duncan & Turner, 1995].

1.6.2.2 Magnetic Stimulations

Pulsed electromagnetic fields (PEMFs) have also been identified to play a role in bone fracture healing treatments through the similar principles as mechanical stimulation applications. Application of PEMFs to the fracture site is meant to induce currents in the high conductive extracellular fluids as well as mechanotransduction. Much evidence has suggested that PEMFs can enhance a number of activities of osteoblasts, i.e., proliferation [De Mattei *et al.*, 1999], differentiation [Landry *et al.*, 1997], extracellular matrices [Heermeier *et al.*, 1998], expression of bone morphogenic protein 2 and 4 [Bodamyali *et al.*, 1998], net flux and the uptake of calcium [Fitzsimmons *et al.*, 1994]. There are a number of USA FDA approved devices aimed to enhance bone fracture related diseases by using

PEMFs, including the Physio-Stim by Orthofix, the EBI Bone Healing system by Biomet Inc and the Orthologic (OL) 1000 by OrthoLogic.

There are several mechanisms proposed for the effects of PEMFs on bone healing. Firstly, PEMFs have been shown to stimulate the calcification of the fibrocartilage of the gap between the bony segments. Secondly, the PEMFs have been demonstrated to have an inhibitory effect on the resorptive phase, leading to the early formation of osteoids and calluses. Thirdly, PEMFs can have an effect on increasing rate of bone formation by osteoblasts [Shupak *et al.*, 2003]. However, some studies failed to show the effects of PEMFs on fracture healing applications. For example, PEMFs with 0.3 T/s, 15 Hz were ineffective in the treatment of un-united tibia fractures [Shupak *et al.*, 2003]. Although PEMFs treatment have been succeeded in lots of clinical applications, the fundamental understanding of the ways in which magnetic forces are transduced into cellular and molecular events is still under investigation.

Static magnetic fields (SMFs) have also been demonstrated to have the ability to promote bone healing. SMFs have been identified to affect a number of biological functions in osteoblasts, such as proliferation, differentiation, extracellular matrix synthesis and mineralisation [Cai *et al.*, 2015; Chiu *et al.*, 2007; Meng *et al.*, 2013; Rosen, 2003]. At the molecular level, it has been proposed that the magnetic force can affect the molecular structure of excitable membranes, hence modify the function of embedded ion specific channels. This process can be achieved by the activation of mechanosensitive Ca^{2+} ion channels or the reorientation of the cytoskeleton [Dobson *et al.*, 2006]. However, despite the success

of SMFs stimulations with several *in vitro* studies, there remains a concern that bone responds to dynamic loading rather than static, it is believed that the stimulation is related to the peak strain magnitude and the loading frequency [Rubin & Lanyon, 1985]. Therefore in some cases, the SMFs failed to demonstrate a stimulating effect on cell proliferation, etc.

An overview of the details of magnetic stimulation will be provided in the following sections, including the use of static magnetic fields as well as magnetic nanoparticles.

1.7 Magnetic Stimulation

1.7.1 Static Magnetic Fields

SMFs can be categorised into three classifications, by their magnetic field strength, including weak ($<$ 1 mT), moderate (1 mT - 1T) and strong (1T - 5T) [Rosen, 2003]. Each type of SMFs influence biological systems differently.

Biogenic magnetite, which presents in various bacteria (such as *E.Coli*), cells (such as fibroblasts), and organs (such as brain), can respond to weak magnetic field of the Earth (about 5 μT) [Hong, 1995]. For example. weak SMFs have been demonstrated to enhance the efflux of Ca^2+ ions in chick brain and therefore the brain functions [Dini & Abbro, 2005]. Several studies tried to explain the biological effects of weak SMFs [Gartzke & Lange, 2002; Kavaliers & Ossenkopp, 1994;

Markov *et al.*, 1993; Reiter, 1993]. Belyaev *et al.* [1997] proposed that the effects of low magnetic field is related to high frequency oscillations in the cell nuclei. Lednev [1996] further explained that the bioeffect induced by low magnetic field is proportional to the polarization degree of the ion's vibration.

Moderate intensity SMFs are capable of influencing a number of biological systems, due to the fact that many inorganic and organic compound in the cells/ cell membranes have some degree of diamagnetic properties. Moderate intensity SMFs have an effect on the molecular structure of excitable membranes, potentially by rotating the membrane's phospholipid molecules, hence modify the function of embedded ion-specific channels. This could lead to, for example, changes in cellular shape [Chionna *et al.*, 2003], cytoskeleton arrangement [Paradisi *et al.*, 1993], ion flux [Rosen, 1996], ion channels [Ottaviani *et al.*, 2002] and formation of cell protrusions [Ross *et al.*, 1989]. For osteoblasts, these changes can up-regulate the osteogenesis process.

Differences in exposure systems, conditions and cell types complicate the evaluation of the effects of SMFs on biological behaviours. The effects as regards to the proliferation of osteoblasts are not significant, with decreased and unchanged cell proliferation having been documented with different intensities of SMFs, and different cell types and exposure time. For instance, Chiu *et al.* [2007] found that the proliferation of MG-63 cells was inhibited by SMFs (400 mT) after 3 days, and Cunha *et al.* [2012] indicated a reduced cell number of MG-63 by SMFs (320 mT) after 7 days. Imaizumi *et al.* [2007] demonstrated that the proliferation of MC3T3-E1 was unchanged after 1 day but decreased by the exposure to SMFs

(250 mT) after 4 and 7 days. Reduced cell viability has also been observed in the studies of Paradisi *et al.* [1993] and Chionna *et al.* [2003]. On the other hand, SMFs can have no effects on the cell proliferation at all. After treatment with SMFs with 160 mT, the proliferation of primary calvaria cells, ROS 17/2.8, and UMR-106 was not altered [Yamamoto *et al.*, 2003] after 4, 6, 8 and 10 days, similar conclusions can be drawn from the studies of Yoshizawa *et al.* [2002] and Aldinucci *et al.* [2003]. Other cell types have also been investigated. Hsu & Chang [2010] demonstrated that, under a exposure of 290 mT SMFs alone, the proliferation of dental pulp cells (DPCs) was not affected up to 7 days, and decreased afterwards. Jouni *et al.* [2013] found that the viability and proliferation of rat bone MSCs were decreased under SMFs of 4, 7 and 15 mT after 3 days, and the decrease rate was related to the magnetic field intensity. However, one exception was reported by Cai *et al.* [2015]. They observed increased cell proliferation of MC3T3-E1 cells when exposed under 100 mT SMFs between 4 hours and 7 days of culture. Generally, it can be concluded that the biological effects of moderate intensity SMFs on cells are non-toxic, however, the effects of SMFs on cell proliferation are dependent on the magnetic field strength and exposure time. Enhanced proliferation can be observed with short culture period (within 7 days) and low magnetic field intensity (100 mT).

SMFs are generally believed to have a positive influence on cell differentiation. Yamamoto *et al.* [2003] studied the effects of SMFs on calvaria cells, ROS 17/2.8, and UMR-106, and results indicated that SMFs can promote the ALP productions after 10 days. Besides, it was shown that moderate SMFs promoted the differentiation of MG-63 cells with increased expression of ALP and ECMs pro-

duction [Chiu *et al.*, 2007; Feng *et al.*, 2010]. In the study of Huang *et al.* [2006], they examined the effect of 400 mT SMFs on the expression of several genes in MG-63 cells, the data suggested that the local regulatory factors produced by SMFs treated cells, including collagen Type I, ALP and OP were greater than those of the untreated ones after only 3 days. However, Imaizumi *et al.* [2007] found that the SMFs have no significant effects on cell differentiation by using MC3T3-E1 cells. After SMFs treatment of 250 mT, the ALP activity was not altered after 4 days. Ba *et al.* [2011] had gained similar results that the ALP production of MC3T3-E1 cells was not promoted by SMFs. However, Cai *et al.* [2015] found that by exposing under 100 mT, the ALP production of MC3T3-E1 cells can be promoted after 14 days. Meng *et al.* [2010] also indicated a stimulating effect of SMFs on the differentiation of MC3T3-E1 cells after 14 days. It can be concluded that the SMFs can have a significant influence on the differentiation of certain types of osteoblasts, especially MG-63 cells, and this is possibility due to the up-regulation of several key genes including collagen Type I, ALP and osteopontin (OP). SMFs can also affect the differentiation of MC3T3-E1 cells, however, this happens slower than that of the MG-63 cells.

Many studies have indicated that SMFs exposure can enhance the level of mineralisation [Huang *et al.*, 2006; Imaizumi *et al.*, 2007]. Imaizumi *et al.* [2007] demonstrated that by exposing under 250 mT SMFs for 1 month, the mineralisation level increased significantly in MC3T3-E1 cells. Furthermore, significant increase in the mineralisation level of ROS 17/2.8, and UMR-106 were observed after 8 days of culture Yamamoto *et al.* [2003]. Huang *et al.* [2006] further expalined that the promotion in the mineralisation level was caused by promoting

the expression of osteonectin (ON) and osteocalcin (OC).

Table 1.2 summaries the major effects of SMFs on cultured cells. The bioeffects of moderate intensity SMFs are exposure system and cell type dependent. The SMFs alone can only enhance cell proliferation at a relatively low intensity (100 mT) and within a short period of time (7 days). The SMFs has a significant influence on cell differentiation, but this effect is cell type and exposure time dependent. The ALP production of MC3T3-E1 cells cannot be enhanced significantly within a short period of culturing time. The effects of SMFs on cell mineralisation are consistence, regardless the cell type, magnetic field strength and exposure time.

Strong SMFs have been demonstrated to have an impact on the alteration of the preferred orientation of a variety of diamagnetic anisotropic organic molecules [Rosen, 2003]. Hirose *et al.* [2003] reported that A172 cells embedded in collagen gel were oriented perpendicular to the direction of strong SMFs of 10 T. In addition, Kotani *et al.* [2002] showed that after exposure to 8 T high SMFs, both MC3T3-E1 cells *in vitro* and the newly formed bones *in vivo* were oriented to the SMFs direction. In the same study, they also demonstrated that the differentiation and matrix synthesis of MC3T3-E1 cells were accelerated.

Cell Type	SMFs Intensity	Exposure time	Effects	References
MSCs	4, 7, 15 mT	1-3 days	Reduced cell proliferation	Jouni *et al.* [2013]
DPCs	290 mT	1-7 days	Unchanged proliferation	Hsu & Chang [2010]
Rat Calvaria Cells	160 mT	2-20 days	Increased ALP	Yamamoto *et al.* [2003]
UMR-106	160 mT	2-20 days	Unchanged proliferation, increased level of mineralisation	Yamamoto *et al.* [2003]
ROS 17/2.8	160 mT	2-20 days	Increased level of mineralisation, ALP production	Yamamoto *et al.* [2003]
MC3T3-E1	100 mT	1 - 21 days	Increased proliferation, ALP production	Cai *et al.* [2015]
MC3T3-E1	250 mT	1 - 7 days	Decreased cell number, unchanged ALP, increased mineralisation	Imaizumi *et al.* [2007]
MG-63	320 mT	1-7 days	Reduced cell number	Cunha *et al.* [2012]
MG-63	400 mT	1-3 days	Inhibited proliferation, enhanced ALP production	Chiu *et al.* [2007]
MG-63	400 mT	1-5 days	Inhibited proliferation, enhanced ALP and ECM synthesis	Feng *et al.* [2010]
MG-63	400 mT	1-3 day	Increased the expression of Collagen type I, ALP, OP	Huang *et al.* [2006]

Table 1.2: Summary of major effects of moderate intensity SMFs on cells.

1.7.2 Magnetic Nanoparticles

The fundamental source of material magnetism is the magnetic moments of electrons, which constitute electron shells of atoms and form electron structure of molecules and crystals [Skomski, 2008]. If the electron shell of an isolated atom is not closed, the atoms will experience non-zero magnetic moment. The iron atom, for example, has a strong magnetic moment due to unpaired electrons in its 3D orbits. There are several categories of magnetisms, including diamagnetic, paramagnetic, ferromagnetic, ferrimagnetic and antiferromagnetic. Ferromagnetic materials are strongly attracted by magnetic fields and can be magnetised to become permanent magnets, producing magnetic fields themselves. Like ferromagnetism, ferrimagnets retain their magnetisation in the absence of a field. However, unlike ferromagnets, neighbouring pairs of electron spins in ferrimagnetic materials tend to point in opposite directions, resulting in smaller magnetisation. Paramagnetic substances are weakly attracted to an applied magnetic field, whereas diamagnetic substances are weakly repelled. Antiferromagnets have a zero net magnetic moment due to opposite electrons.

Magnetic nanoparticles (MNPs) have been widely applied into biomedical applications. They have controllable sizes ranging from a few nanometres up to tens of nanometres, which can be compared to those of a cell (10 - 100 μm), a virus (20 - 450 nm), a protein (5 - 50 nm) or even a gene (2 nm wide and 10 - 100 nm long). Due to the small sizes, MNPs can achive the activation of individual ion channels or surface receptors on specific cells precisely. MNPs can be manipulated by an external magnetic field without direct contact. Miltenyi

et al. [1990] demonstrated that when MNPs are attracted to a high magnetic flux density, these particles can attract biomolecules or living cells *in vitro*. This "action at a distance", combined with the intrinsic penetrability of magnetic fields into human tissue, can be applied to reach the internal organisms of the human body [Pankhurst *et al.*, 2003]. They can be manipulated to penetrate into tissues deeply under SMFs, reaching a single cell and acting directly on its organelles without being shielded by the membrane potential [Sapir *et al.*, 2014]. Stress parameters of the MNPs can also be varied dynamically simply by varying the strength of the applied field.

MNPs can be categorised into metallic nanoparticles, magnetic alloys and magnetic oxides nanoparticles. Metallic nanoparticles exhibit interesting properties in many applications own to the larger magnetisation compared to metal oxides or alloys. Among many metallic materials, iron, cobalt and nickel are the most widely studied. Metals like cobalt and nickel are seldom used in clinical applications, as they can be toxic if used *in vivo* without a biocompatible coating. Iron, on the other hand, is relatively safe to be applied *in vivo*, as well as exhibiting high magnetic moment density of 220 emu/g. However, there still remains a complicated task to prepare nanoparticles consisting of pure iron as they often contain oxides, carbides and other impurities; besides, metallic nanoparticles are not air stable and are easily oxidised, resulting in the change or loss of their magnetisation. Although iron metal itself is a good candidate for magnetic applications, it is seldom used as a core material for the synthesis of magnetic nanoparticles unless they are coated with an inert, protective coating. Iron is exceptionally vulnerable to corrosion in the presence of water, resulting in rusting,

for instance.

Magnetic alloys, such as iron platinum (FePt), are more popular as core materials for magnetic nanoparticles compared to pure iron metal. FePt possess high uniaxial magnetocrystalline anisotropy, making them exhibit large coercively at room temperature. The surface chemistry of FePt nanoparticles allows for binding of carboxylate and amine based surfactants which may be utilised to improve the water solubility. Sun *et al.* [2000] demonstrated that polyethylene glycol (PEG) coated FePt nanoparticles are stable in biological media such as phosphate-buffered saline (PBS), however, there remains an unclear understanding about the toxicity of the FePt nanoparticles, as well as limited reports of cytotoxicity assays.

Magnetic oxides exist in many forms like iron oxide, cobalt oxide and nickel oxide. It has been well documented in the literature that nanoparticles such as $CoFe_2O_4$, $NiFe_2O_4$ have been used in many biomedical applications. However, the use of these mixed oxide nanoparticles can be hampered by the high toxicity of these transition metals. Iron oxide nanoparticles (IONPs), on the other hand, presents low toxicity and are well tolerated in the human body. Iron oxide fluids have also demonstrated good cardiovascular tolerance, their infusion has been shown not to change blood pressure, heart rate or respiratory rate [Lübbe *et al.*, 2001].

The use of iron oxide based nanoparticles in biomedicine has received considerable attention in a wide range of applications, such as magnetic resonance imaging (MRI) [De *et al.*, 2011], magnetic drug delivery and magnetic hyperther-

mia [Huang *et al.*, 2012], as they are non-toxic and relatively safe for clinical use. Iron oxides exist in many forms in nature, such as magnetite (Fe_3O_4), maghemite (γ-Fe_3O_4) and hematite(α-Fe_2O_3). Magnetite nanoparticles have ferromagnetic properties, maghemite have ferrimagnetic properties and hematite are weakly ferromagnetic or antiferromagnetic in nature, therefore magnetite nanoparticles have the strongest magnetisation when compared to the other two [Teja & Koh, 2009]. Magnetite possesses a magnetic moment density of 90 emu/g (bulk) and 30 - 50 emu/g (nanoparticles). Magnetite is also one of the iron oxides approved by the FDA for *in vivo* use. Iron oxide nanoparticles (IONPs) with a diameter between 2 - 20 nm display superparamagnetic behaviour at room temperature [Cornell & Schwertmann, 2003].

Although IONPs are considered as biocompatible and appear to be promising for various biological applications, it is important to know the safe dosage of IONPs for such uses, i.e, their toxic potential is still a major concern. The total body iron store is $\sim$ 4000 mg in a normal male adult. Small quantities of iron may not pose iron-linked toxicity issues, but higher amounts may lead to increased plasma iron concentration, hence the formation of oxidative stress and various toxicities [Glickstein *et al.*, 2006].

The toxicity of IONPs induced is dependent on the concentration. Studies from Karlsson *et al.* [2008] showed that IONPs (20-30 nm) are safe and non-cytotoxic to cells with concentrations up to 80 μg/ml *in vitro*. Naqvi *et al.* [2010] also studied the toxicity of IONPs (30 nm) *in vitro*. Their results indicated that these IONPs do not show toxicity effect at concentrations up to 100 μg/mL. By

further increasing the concentration to 25-200 μg/mL, the cell viability reduced to 95 %. When the IONPs concentrations have been increased to 300-500 μg/mL, the cell viability further reduced to 55-65 %.

Surface modifications of IONPs, such as alginate [Ma *et al.*, 2007], silica [Chekina *et al.*, 2011] and chitosan [Kievit *et al.*, 2009], can be employed to enhance the biocompatibility of IONPs. Gupta & Wells [2004] examined the cytotoxicity of uncoated and poly(ethylene glycol) (PEG) coated IONPs with concentrations of 0 - 1000 ug/ml. Uncoated IONPs (10 - 15 nm) showed significant loss in viability of about 25 % at concentration of 250 μg/ml, whereas PEG-coated IONPs (40 - 50 nm) revealed no cytotoxic effects to cells up to 1000 μg/ml. One possible explanation for the enhancement in cell viability can contribute to the hydrophilic property of PEG, and it protects uncoated IONPs from interacting with cells or proteins. Some *in vivo* studies also evaluated the toxicity of IONPs. Kim *et al.* [2006] found that intraperitoneally injected SiO_2 coated IONPs (50 nm) were found to be safe at 25-100 μg/ml dose for 4 weeks.

Table 1.3 summarises some of the main findings from previous studies about the toxicity of uncoated and coated IONPs *in vitro*.

Coating Material	Size (nm)	Concentration (μg/ml)	Results	References
Uncoated	20 - 30	80	non-toxic	Karlsson *et al.* [2008]
Uncoated	30	0 - 250	no cytotoxicity up to 100 μg/ml, 55-65 % cell viability with 250 μg/ml	Hussain *et al.* [2005]
Uncoated	10 - 15	0 - 1000	75 % cell viability with 250 μg/ml	Gupta & Wells [2004]
PEG	40 - 50	0 - 1000	non-toxic up to 1000 μg/ml	Gupta & Wells [2004]
Tween 80	30	25 - 5000	non-toxic up to 100 μg/ml, 90 % viability up to 200 μg/ml, 55 - 65 % up to 500 ug/ml	Naqvi *et al.* [2010]
Dextran	15	50	reduce proliferation	Berry *et al.* [2003]
Albumin	9.6	50	induce proliferation	Berry *et al.* [2003]
Silica	50	25 - 100	non-toxic	Kim *et al.* [2006]
Chitosan	13.8	123.52	Cell viability reduced to 10 %	Ge *et al.* [2009]

Table 1.3: Summary of toxicity of IONPs with and without biocompatible coatings.

1.8 Thesis Objective and Structure

1.8.1 Objectives

The aim of this thesis is to devise a reliable 3D bone model for the *in vitro* evaluation of the effects of SMFs on the osteogenesis process. The objectives of this thesis are listed as below:

1. To develop a biocompatible magnetic bio-reactor with moderate intensity to support cell growth *in vitro*.

2. To develop a 3D model, with suitable scaffold, cell lines and biofactors incorporated, for the *in vitro* stimulations of osteoblasts under static magnetic fields. The biological behaviours, including cell proliferation, differentiation and mineralisation will be investigated.

3. To evaluate the mechanism of static magnetic field stimulation on the molecular levels. This includes the study of gene expression, and the microstructural analysis of the 3D model, especially the cell/matrix interactions.

1.8.2 Structure

The structure of the thesis is outlined below:

1. In Chapter 2, details of experimental materials and methods will be provided, including the design and fabrication of the magnetic bio-reactor,

magnetic nanoparticles, 3D collagen models, and the *in vitro* evaluation for the biological behaviours of osteoblastic cell lines, such as proliferation, differentiation, mineralisation, gene expression and microstructural analysis.

2. In Chapter 3, a magnetic bio-reactor with moderate intensity (100 - 160 mT) will be designed. ANSYS Maxwell will be applied to simulate the magnetic field strength, and 3D printing technique will be employed to fabricate the reactor.

3. In Chapter 4, the development of the 3D model will be demonstrated, this includes the investigations of the scaffolds, cell lines and biofactors. The effects of SMFs will also be studied.

4. In Chapter 5, the effects of the SMFs and the incorporation of IONPs on osteogenesis will be examined. The proliferation, differentiation and mineralisation of osteoblasts when seeded within collagen scaffolds. The mechanisms of SMFs on osteoblasts at molecular levels will then be investigated. This includes the examination of cell/matrix interactions and the expression of Runx-2, ON, BMP-2 and BMP-4.

5. In Chapter 6, a general discussion and conclusion of the thesis will be given, as well as suggestions for future studies.

Chapter 2

Development of the Experimental Techniques

2.1 Overview

This chapter details the development of the materials and methods used to evaluate the magnetic stimulation on osteogenesis, including the set-up of the magnetic bio-reactor, the preparation of iron oxide nanoparticles (IONPs), the fabrication of 3D PC collagen scaffolds and the *in vitro* biological evaluations of bone cells. This includes, the alamarBlue (AB) assays for proliferation, alkaline phosphatase (ALP) for differentiation, alizarin red s staining (ARS) for mineralisation, polymerase chain reaction (PCR) for gene expression, Histology for cellular responses and transmission electron microscopy (TEM) for micro-structural analysis.

2.2 Materials

For IONPs fabrication, iron (II) chloride tetrahydrate ($FeCl_2 \cdot 4H_2O$) (<99.0 %), iron (III) chloride hexahydrateand ($FeCl_3 \cdot 6H_2O$) (97%), and ammonium hydroxide solution (28.0 - 30.0%) were purchased from Sigma-Aldrich and used as received without any further treatment.

For collagen gel preparation, 10X Eagles MEM solution was purchased from Gibco, Paisley, UK, and Dulbeccos Modified Eagles Medium (DMEM) was purchased from Sigma-Aldrich. Rat tail type I collagen in acetic acid (protein concentration of 2.10 mg/ml) was ordered from First Link, Birmingham, UK. sodium hydroxide (NaOH), which was used to neutralise the mixture, was also purchased from Sigma-Aldrich.

For cell culture, MG-63 (Homo sapiens, osteosarcoma, ATCC), UMR-106 (Rattus norvegicus, osteosarcoma, ATCC) and MC3T3-E1 (Mus musculus, preosteoblast, ATCC) were used in this study. DMEM, fetal bovine serum (FBS), penicillin-streptomycin (P/S) L- glutamine (L-G) and trypsin/EDTA were purchased from Sigma-Aldrich.

For *in vitro* assays, alamar blue (alamarBlue, Bio-Rad) was used to measure the cell proliferation activity, 4- nitrophenyl phosphate disodium, trizma hydrochloride and $MgCl_2$ were used for the quantification of the ALP production, alizarin red s (ARS) reagent, cetylpyridinium chloride, haemotoxylin and eosin (H & E) reagent were used for cell staining. RNeasy Mini Kit (Qiagen

74104 and 74106) was used for PCR studies. All chemicals were ordered from sigma without further treatment.

2.3 Methods

2.3.1 Computational Simulation of Magnetic Field Strength

In this study, ANSYS Maxwell has been employed to simulate the magnetic field strength of several designs, and helped to select the one with desired range. ANSYS Maxwell is an industry leading electromagnetic field simulation software for the design and analysis of a wide range of electromagnetic or magneto-static devices. In the case of static magnetic field, the magneto-static solver can be applied. ANSYS Maxwell magnetic field formulation is founded on Maxwell's equation:

$$\nabla \times \vec{E} = -\frac{d\vec{B}}{dt}(Faraday'sLaw) \quad (2.1)$$

$$\nabla \times \vec{H} = \vec{J}(Ampere'sLaw) \quad (2.2)$$

$$\nabla \times \vec{B} = 0(Gauss'sLaw) \quad (2.3)$$

in which $\vec{E}$ is the electric field strength, $\vec{B}$ is the magnetic flux density, $\vec{H}$ is the magnetic field strength, and $\vec{J}$ is the electric current density.

In the case of SMFs, the current flowing through can be considered as steady or zero, therefore the Faraday's law will not be employed. On the other side,

the relations between the magnetic field strength and magnetisation, $\vec{M}$ can be described as below:

$$\vec{B} = \mu_0(\vec{H} + \vec{M}) \tag{2.4}$$

So the equations applied for the magneto-static solver are:

$$\nabla \times \vec{H} = \vec{J} \tag{2.5}$$

$$\nabla \times \vec{B} = 0 \tag{2.6}$$

$$\vec{B} = \mu_0(\vec{H} + \vec{M}) \tag{2.7}$$

The details of the simulation are described briefly as below. Firstly, the type of solver has to be determined. In the case of 3D static magnetic field, the 3D magnetostatic solver was selected. Secondly, the bio-reactor has to be computational designed and modelled. Then the following parameters may be defined for a material, includes, relative permeability, bulk conductivity, magnetic coercivity and composition. Thirdly, the boundary conditions in 3D has to be assigned. The boundary conditions define behaviour of the magnetic field at the interfaces or the edges of the problem region. For the boundaries on the interface between objects, H field is continuous across the boundary; for exterior boundaries of solution domain, H field is tangential to the boundary and flux cannot cross it. Then the mesh can be applied on the object. Maxwell uses the finite element method (FEM) to solve Maxwell equations. In order to obtain the set of algebraic equa-

tions to be solved, the geometry of the problem is discretised automatically into basic building blocks, such as tetrahedra in 3D. The assembly of all tetrahedra is referred to as the finite element mesh of the model or simply the mesh. Mesh plays important role in accuracy of the computed results. In the current study, the mesh is automatically refined to achieve the required level of accuracy in field computation. Finally, the analysis set-up has to be added. In this case, the B field (in Tesla) has been selected.

2.3.2 Magnetic Field Strength Validation by Tesla Meter

The actual magnetic field strength was measured by a Digital AC/DC Magnetic Field Gauss Meter (BST600, Hangzhou BST Magnet Co. Ltd) (shown in Figure 2.1). The magnetic field of the bio-reactor was measured at nine points of the field to create a distribution map, as illustrated in Figure 2.2. Points A, D and G are 1 cm from the left magnet, whereas points C, F and K are 1 cm apart from the right magnet. Point B, E and H locate at the central vertical axis of the field. Points A, B, C and G, H, K are 1 cm from the top-edge and the bottom edge, respectively. Points D, E and F are at the central horizontal axis of the field. E is the centre point of the whole field. The pink area in the middle has a diameter of 2 cm, which represent the location of the scaffold. Five repeating readings were taken at each point.

Figure 2.1: Illustration of the tesla metre. The tesla meter has a working range of 0 - 2000 mT with a resolution of 0.1 mT.

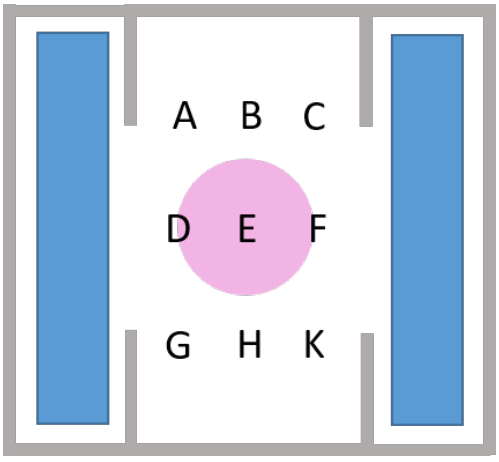

Figure 2.2: Illustration of tested points in the magnetic fields. Points A, D and G are 1 cm from the left magnet, points C, F and K are 1 cm away from the right magnet. Point B, E and H locate at the central vertical axis of the field. Points A, B, C and G, H, K are 1 cm from the top-edge and the bottom edge, respectively. Points D, E and F are at the central horizontal axis of the field. E is the centre point of the whole field. The pink area in the middle has a diameter of 2 cm, which represents the location of the scaffold.

2.3.3 Permanent Magnets Selection

The use of a permanent magnet provides an important advantage for bone cell stimulation in that it does not require a power device and thereby reduces the unexpected continuations or thermal effects on treated cells. SMF has been identified as capable of affecting a number of biological behaviours of osteoblast cells, and it is particularly interesting to researchers because it can be easily achieved with permanent magnets. Neodymium magnets (NdFeB) and samarium-cobalt magnets (SmCo) have been applied in clinic studies [Cai *et al.*, 2015; Kim *et al.*, 2005; Riley *et al.*, 2001], due to their biocompatibility and strong intensity. Table 2.1 summarises the magnetic properties of two commonly used neodymium magnets, NdFeB30 and NdFeB35, and two types of commonly used samarium-cobalt magnets, SmCo24 and SmCo28. These magnets will be analysed and compared in the following study to develop a suitable magnetic bio-reactor.

Property	NdFeB30	NdFeB35	SmCo24	SmCo28
Remanence (Br) /mT	1080	1170	950	1030
Coercive force (Hcb) / kA/m	796	867	700	756
Intrinsic coercive force (Hcj) /kA/m	≥ 955	≥ 955	≥ 1433	≥ 1435
Max. energy product (BH) kJ/m^3	223	263	175	207

Table 2.1: Magnetic properties of NdFeB30, NdFeB35, SmCo24 and SmCo28.

2.3.4 3D Printing

Once the magnets had been set up with the desired strength, the design was 3D printed by Selective Laser Sintering (SLS) technique. SLS is a powder based 3D

model fabrication method for rapid prototyping and rapid tooling, can achieve large-scale production [Kumar, 2003]. Generally, laser beams are used to heat the materials (in powders) in predetermined sizes and shapes. The laser beam is selectively scanned over the powder following the cross-sections of the computer-aided design (CAD) models. After the first layer is scanned, a second layer of loose powder is deposited over it, and the process is repeated from the bottom to top until the product is completed. The conventional materials used in SLS technique are polymers and nylon. In this study, SLS (EOSINT P100, layer height of 0.1 mm) has been employed.

2.3.5 Synthesis and Preparations of Iron Oxide Nanoparticles

The size and shape of magnetite particles are generally controlled by the synthesis method. A variety of methods have been reported in the literature on the synthesis of magnetite nanoparticles, including co-precipitation [Mascolo *et al.*, 2013], thermal decomposition [Lu *et al.*, 2008], sol-gel [Teja & Koh, 2009], microeulsion and hydrothermal synthesis [Lu *et al.*, 2007], in which the thermal decomposition and co-precipitation are the most widely used methods.

Table 2.2 compares the synthetic conditions of four different methods.

Synthetic method	Co-precipitation	Thermal decomposition	Microemulsion	Sol-gel
Size	10-50 nm	5-50 nm	4-15 nm	20-200 nm
Distribution	broad	narrow	very narrow	broad
Temperature	20-90 °C	100-320 °C	20-50 °C	40-120 °C
Period	minute	hours-days	hours	hours
Morphology	Spherical	Spherical	Spherical with high porosity	Cubic or spherical
Magnetisation	20-50 emu/g	>20 emu/g	>30 emu/g	10-40 emu/g
Advantages	Simple condition Large quantities	Useful for protective coatings and thin film deposition	Uniform properties	Desired shape and length
Disadvantages	Uncontrolled oxidation	Require high temperatures	Surfactants are difficult to remove	Contains sol-gel matrix components

Table 2.2: Summary of synthetic methods for iron oxides

The thermal decomposition method relies on the pyrolysis of organic precursors of iron, such as Fe $(CO)_5$, which is toxic and hence may limit the biomedical applications. As for the co-precipitation method, which mainly relies on the hydrolysis of ferric and ferrous ions under a proper molar ration, Fe^{2+} and Fe^{3+} ions are generally precipitated in alkaline solutions such as ammonium hydroxide, sodium hydroxide and potassium hydroxide. The reactions occurs during the magnetite formation are as follows:

For Fe^{3+},

$$Fe^{3+} + 3OH^{-} = Fe(OH)_3(s), \quad (2.8)$$

$$Fe(OH)_3(s) = FeOOH(s) + H_2O, \quad (2.9)$$

For Fe^{2+}

$$Fe^{2+} + 2OH^{-} = Fe(OH)_2(s), \quad (2.10)$$

$$2FeOOH(s) + Fe(OH)_2(s) = Fe_3O_4(s) + 2H_2O. \quad (2.11)$$

Hence the overall reaction can be re-written as

$$2Fe^{3+} + Fe^{2+} + 8OH- = 2Fe(OH)_3Fe(OH)_2(s) \longrightarrow Fe_3O_4(s) + 4H_2O \quad (2.12)$$

IONPs were prepared by the co-precipitation method [Chekina *et al.*, 2011]. The method involves addition of a base (NaOH or NH_4OH) to ferric (Fe^{3+}) and ferrous (Fe^{2+}) chloride solutions under ambient pressure at an elevated temper-

ature. Briefly, 5.41 g of $FeCl_3 \cdot 6H_2O$ were mixed with 1.99 g of $FeCl_2 \cdot 4H_2O$, followed by an addition of NH_4OH of 400 ml. The resulting solution was left to grow for 30 mins and then washed 7 times by using centrifugation and DI water. However, the particles obtained by this method are not uniform in size distribution and tend to agglomerate. In order to reduce the agglomeration, sonication was introduced. The suspension was mixed under sonication (Digital Sonifier 250, Branson Ultrasonics, Danbury, CT, USA) at 40 W in between each wash. Besides, permanent magnets was also employed under the suspension to enhance the precipitation process.

The results regard to the characterisation of IONPs are attached in Appendix.

2.3.6 Synthesis and Preparations of Nano-hydroxylapatite and Nano-zinc oxide

Nano-hydroxylapatite (nHA) with calcium/phosphate ratios of 1.67 was prepared and synthesised based on a precipitation reaction between calcium hydroxide ($Ca(OH)_2$) and orthophosphoric acid (H_3PO_4) (both AnalaR grade, BDH, UK) [Huang *et al.*, 2007]. 0.3 M H_3PO_4 solution was added drop wise to 0.5 M $Ca(OH)_2$ solution under continuous stirring at room temperature, the pH was kept above 10.5 by the addition of ammonia solution. Stirring was maintained for a further 16 h after the reactants had been added. The precipitate obtained was further aged for one week.

Nano-zinc oxide (nZnO) were synthesised using the flame pyrolysis method as used by Johnson Matthey plc (JMTC).

2.3.7 Formation of Collagen Gel

By neutralising native acid soluble collagen, a hydrogel scaffold can be generated due to collagen fibrillogenesis. In the fibrillogenesis process, collagen molecules spontaneously assemble with neighbouring molecules in a quarter staggered arrangements to form fibres, and those fibres form as collagen monomers in solution continue to aggregate, until the fibrillogenesis is complete.

There are some key factors which can influence the fibrillogenesis process, including the type of collagen used, the collagen density, the pH of the solution, the synthesis temperature and the incorporation of other biofactors (such as cells, growth factors or biocompatible materials). The preferred temperature for collagen fibrillogenesis is defined at 37 °C. Temperature higher than this can potentially denature the collagen protein, whereas temperature lower than this can delay the process. Besides, the desirable pH for fibrillogenesis to happen is 6.5 - 8. At low pH, collagen fibres are formed with poor structure; at high pH, banding patterns of fibrils can be observed [Harris & Reiber, 2007].

Acellular collagen gels were made by titrating the pH of rat tail type I collagen (2.10 mg/ml in acetic acid). To make a total volume of 10 ml solution, 8 ml of acid soluble collagen was needed, with the addition of 1 ml 10 X DMEM. The

obtained solution was neutralised with 1M or 5M NaOH, until a colour change from yellow to pink was observed [Brown *et al.*, 2005]. The neutralised gel requires the same pH value to ensure a consistency. The remaining 1ml was made up with DMEM (with and without cells). This collagen gel was then set in a 24 well plate with an amount of 1 ml per well, followed by incubation at 37°C with 95 % relative humidity and 5 % CO_2 for 30 minutes.

2.3.8 Plastic Compression

There are two methods developed for the fabrication of plastic compressed collagen gels, downward flow compression [Brown *et al.*, 2005] and upward flow compression [Alekseeva *et al.*, 2011]. Downward flow means the direction of the fluid flow out of the collagen gels is towards the bottom of the set-up (as can be observed from Figure 2.3, the liquid flows out from the bottom.). While upward flow refers to that where the water will be sucked up from the top (As shown in Figure 2.4). During the down flow process, customised shape and size of the PC model can be fabricated, while upward flow can produce multiple models simultaneously and hence reduce the production time. Therefore, the upward flow process has been employed.

The plastic compression protocol is modified from Brown *et al.* [2005]. Briefly, collagen gels were set in 24-well plate and covered by several layers of filter paper (Whatman grade I) on the top. A cylinder plunger roll (height=3.7 cm, diameter=1.5 cm) made by filter paper (process shown in Figure 2.5) was laid on the

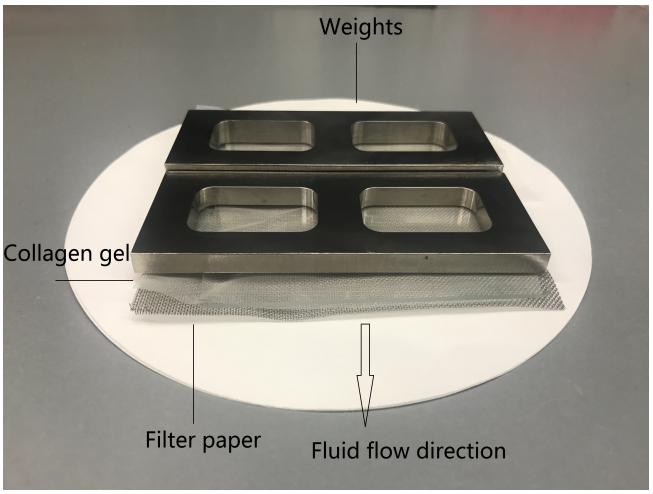

Figure 2.3: Illustration of downward flow plastic compression (PC) process. Diagram shows the conventional assembly of PC of pre-formed collagen gels. The liquid in the collagen hydrogel was expelled from the bottom by the application of compressive mechanical loads on the top.

top of each gel for 5 minutes. Extra weights can be added on top of the filter paper roll to accelerate the process, with approximately 15 g per well. The extra liquid component was absorbed by the plunger and left a thin layer of collagen gel with a thickness of 75-100 μm. IONPs can be embedded inside the collagen matrix at the point of self-assembly. After the completion of plastic compression, the plunger roll was removed. Cell medium (1 ml) was then added to each well immediately to keep the samples hydrated. The filter paper discs separating the plunger and the hydrogel can then be removed at this point. Samples were then used or cultured as required.

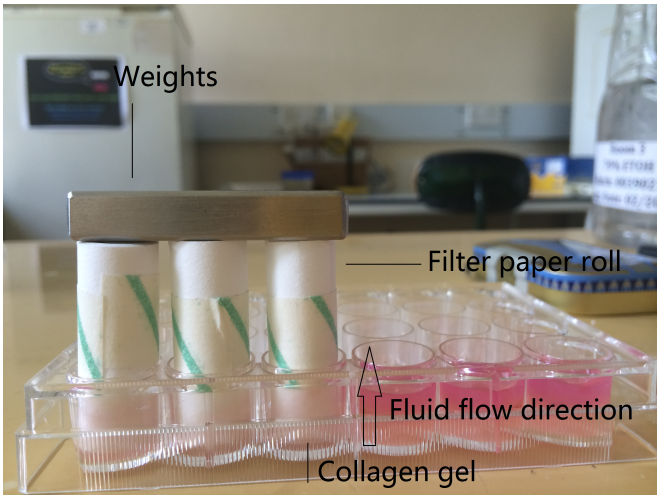

Figure 2.4: Illustration of upward flow collagen plastic compression (PC) process. Collagen gels are neutralised in a 24-well plate, with several layers of filter paper placed on top, then a paper roll made of filter paper serve as a weight to expel the water component out of the collagen gel. Additional weights can be added on top of the gel to accelerate the process. The weights used are 15g per well.

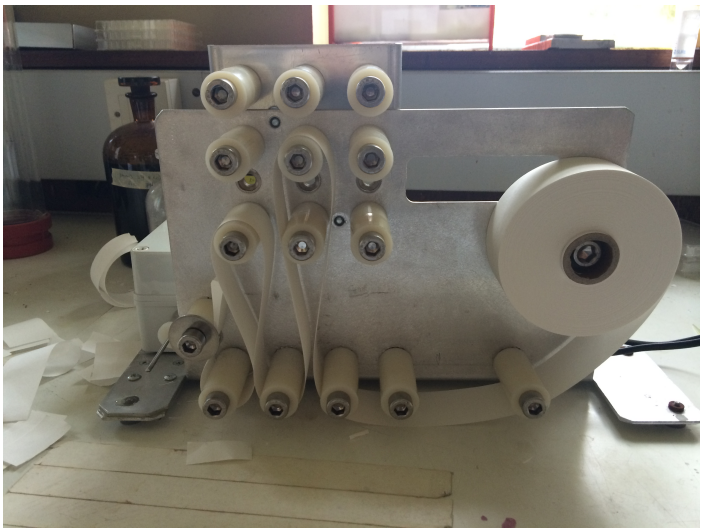

Figure 2.5: Illustration of the rolling process. The cylinder plunge rolls are made by filter paper, with dimensions of height=3.7 cm, diameter=1.5 cm for each. The size was chosen to fit in a single well of a 24-well plate. Customised plunge size can be designed and fabricated by the same technique.

2.4 Characterisations

2.4.1 Transmission Electron Microscopy (TEM)

The investigation of the morphology of the IONPs was conducted by transmission electron microscopy (TEM) (JEOL JEM-1011). TEM is a microscopy technique where a beam of electrons is transmitted through an ultra-thin specimen, interacting with the specimen as it passes through it. Depending on the density of the specimen, electrons are either passing through or scattering away. An image will be formed when the transmitted electrons hit onto an image device, such as a fluorescent screen. In this study, IONPs in ethanol were collected using copper grids coated with carbon film. The accelerating voltage applied was 200 keV.

A Philips CM120 transmission electron microscope was used to examine the cellular structure of cell-seeded collagen tissues. Biological tissue is delicate and must be protected in the harsh internal environment of the electron microscope (high vacuum and a stream of electrons). Cell seeded collagen scaffolds were stabilised in karnovsky's fixative (2.5% glutaraldehyde/ 2% paraformaldehyde/ 0.1 M PBS) to preserve structure details, follow by dehydration and then infiltrated with a liquid resin, which is hardened by gentle heat. Resin blocks containing the tissue can therefore be sectioned and stained for observation in the TEM. Firstly, pieces of the fixed tissue were placed in screw cap microtubes with PBS and washed 3 times of 10 mins each. Secondly, the PBS was discarded and the samples were postfixed in 1% osmium tetroxide solution for 1 hour at 4 °C. Then osmium solution was removed with a pipette. Samples was washed 3 x 15 mins with distilled water, followed by dehydration through graded ethanol solutions of

30%, 50%, 70% and 90% with 2x 15 mins each, and finally in 100% ethanol 3x 15 min. The infiltration with liquid resin was achieved by infiltrating the tissue in 40% resin for 3 hours, overnight in 60% resin and then 100% resin for 6 hours at room temperature. After final infiltration, tissues were placed in labelled embedding moulds with fresh resin and polymerised in the oven at 70 °C overnight to be examined. The specimens were sectioned into 1 μm and used to find the area of interest; then ultra thin sections (70nm) were taken to be placed on grid for further examinations. The grids have then been stained in uranyl acetate for 2 hrs, followed by lead citrate for 5 min. The voltage applied was 80.0 kV.

2.4.2 Scanning Electron Microscopy (SEM)

Scanning electron microscopy (SEM) is a technique for surface structure characterisation. Thin layers of neutralised collagen gels were prepared by adding 10 μl collagen solution onto the surface of each cover slip, followed by air drying. The collagen gels were treated with two conditions, one with SMFs and one without SMFs. The morphological characterisation of the thin collagen gel were investigated by using a Jeol JSM-6300 F with a field emission electron gun operated at 5 kV. In order to enhance the electrical conductivity, the samples were first coated with ultra-thin layers of gold atoms (120 seconds) by using a rotary-pumped sputter coater (Quorum) before being mounted into the vacuum chamber.

2.5 *In vitro* Study

2.5.1 Cell Lines

Frozen cells were gently thawed and cultured in high glucose DMEM with 10 % FCS, 1 % penicillin, and 1 % L- glutamine and were then maintained at 37°C, with 5 % CO_2. MG-63, UMR-106 and MC3T3-E1 cells were used to assess the effects of SMFs on biological behaviours. MG-63 cell lines were used to further study various aspects of cellular responses to IONPs, nHA and nZnO incorporated into collagen scaffolds. Ethical considerations and guidelines were followed regarding obtaining and usage of biological cell lines.

2.5.2 Subculture of Adherent Cell Lines

MG-63, UMR-106, MC3T3-E1 cell lines were stored in DMEM and incubated at 37°C, with 95 % relative humidity and 5 % CO_2 until 80 % confluence was achieved. For sub-culturing the adherent cell lines, cell culture medium was removed and the monolayer of cells was washed with PBS (10 ml). Typsin was added to the flask at 0.03 ml/cm^2, 2 mins was then required for most cells to detach, until culture medium was added to neutralise the trypsin. The cell suspension was centrifuged at 800 rpm for 5 mins to pellet the cells. The supernatant was removed and medium was added by gently mixing to disrupt the cell pellet. Cells were then dispersed, suspended and counted using a haemocytometer.

2.5.3 AlamarBlue Assay

The alamarBlue (AB) assay is a proven cell viability indicator that uses the natural reducing power of living cells to convert resazrin to the fluorescent molecule, resorufin. Upon entering cells, resazurin is reduced to resorufin which shows a red fluorescence. The non-fluorescent blue dye responds to the reductive environment by forming a fluorescent red dye, and the fluorescence intensity of the dye can be detected. The amount of fluorescence is proportional to the number of living cells, and corresponds to the metabolic activity of the cells. In general, damaged or non-viable cells have lower innate metabolic activity and thus generate a proportional lower signal than healthy cells.

The proliferation of MG-63 cell lines was assessed by using Alamar Blue. The reagent was diluted with normal growth medium (1:10 Dilution) and stored at 4°C prior to use. Approximately 10^4 osteoblasts were seeded into the compressed collagen scaffolds incorporated with nanoparticles. Seeded scaffolds were left for periods of 1, 3, 7 and 14 days in the incubator (37°C, with 5 % CO_2). 1 mL of DMEM was added to each well and replaced every two days. At each time point, 100 μl of the reagent was added into each well. The plate was then incubated at 37°C, with 5 % CO_2 for a period of 2 h (optimal time for this study only) to allow the reaction. Afterwards, 100 μl of the supernatant was then removed from relevant wells (n=3) and added to a 96-well plate (Falcon). Fluorescence was measured using a fluorescent plate reader (FLUOstar OPTIMA) at wavelengths of 544 nm (excitation) and 590 nm (emission).

2.5.4 Alkaline Phosphatase Quantification

Alkaline phosphatase (ALP) activity is an early indicator of osteogenesis. It is one of the key substances that indicate whether osteoblasts have entered the period of extracellular matrix development and maturation. The differentiation ability of MG-63 cell lines can be identified by employing the Alkaline phosphate (ALP) biochemical marker. The method of determination of ALP produced by differentiating osteoblasts is based on the conversion of an artificial substrate of ALP, paranitrophoenol phosphate. When dephosphorylated by ALP, it results in a coloured (yellow) product.

In this project, approximately 10^4 cells were incorporated in 1 ml of collagen gel with various nanoparticles, followed by compression and incubation at 37°C, with 5 % CO_2. DMEM changes were carried out every two days. After incubation for 7, 14 and 21 days, the scaffolds were removed into a 24-well plate and washed by PBS. Equal amounts (500 μl) of substrate reagent was added to each well. One tablet of 4-nitrophenyl phosphate disodium (Sigma, Dorset, UK) was mixed with 8 mL 0.1 M trizma hydrochloride (3.94 g Tris in 500 ml DI water, pH=9.5) and 15 μl of 2M $MgCl_2$ (9.521 g $MgCl_2$ in 50 ml DI water). The 24-well plate was left at room temperature for 15 mins for the reaction to take place. 100 μl of 0.5 M NaOH (10 g NaOH in 500 ml DI water) was then used to stop the reaction. Subsequently, 100 μl was removed from each well (n=3) and transferred into a 96-well plate and the absorbance read at 405 nm (reference at 670 nm) using a plate reader (FLUOstar OPTIMA).

2.5.5 Alizarin Red S Staining

Alizarin red s (ARS) staining has been used for decades to evaluate calcium-rich deposits by cells in culture. Unlike von kossa's staining, which visualises the phosphate and carbonate anions, ARS can pick up the calcium content in tissue through chelation. It is particularly versatile in that the dye can be extracted (by cetylpyridinium chloride) from the stained monolayer and assayed. Therefore ARS has been employed in this study to highlight regions of mineralised collagen matrix. ARS reacts with the calcium cation to form a chelate, therefore the calcium content in the tissue show an orange-red colour after staining, while non-mineralised tissue present colour-less.

The samples were examined after 1, 21 and 42 days of culture. Scaffolds were washed three times with PBS and fixed with 4% paraformaldehyde for routine wax embedding and sectioning. The sectioning process was done by a microtome with a thickness of 5 μm each. Sectioned samples were then been collected in hot water and dried for 30 mins. After drying, specimens have to be de-waxed by de-waxing and cleaning in xyline for 2 mins, followed by several washes of 100% ethanol, 90% ethanol and 70% ethanol. A protocol for staining has been developed for this study. Basically, 1g ARS dye was dissolved in 50 ml deionized water and the pH was adjusted to 4.1 - 4.3 with 10% ammonium hydroxide. 1 ml of ARS solution was added on each slide for 30 seconds and DI water was used to wash off the excess dye adsorbed on the scaffold surface. If stained less than 30s, the staining can be easily washed off by DI water; if overstained, the mineralised modules are difficult to observe. Presence of mineral deposition (red-

orange colour) was evaluated using a Nikon eclipse TE2000-5 optical microscope.

A method for quantifying the level of mineralisation has also been developed. Briefly, the stained samples were desorbed with the use of 10% (w/v) cetylpyridinium chloride in 10 mM sodium phosphate (pH 7.0). The dye was then collected and absorbance read at 540 nm using a plate reader (FLUOstar OPTIMA).

2.5.6 Histology

Histology specimens were fixed with 4% paraformaldehyde for routine wax embedding and sectioning. The sectioning process was done using a microtome with a thickness of 5 um each. Sectioned samples were then collected in hot water and dried for 30 mins. After drying, specimens have to be de-waxed and cleaned in xylene for 2 mins, followed by several washes of 100% ethanol, 90% ethanol and 70% ethanol. After air drying, haemotoxylin and eosin (H&E) was applied for sample staining. A staining protocol was developed for this study. Briefly, haemotoxylin was firstly added onto the sample surface for 30 seconds, followed by rinsing under running water. Then eosin was then applied for another 30s, followed by water rinsing. The optimal staining time (30s) was determined after a series of trail experiments. If stained too short, the staining will be easily rinsed off; whereas longer staining time resulting over-dyeing of the cells and tissue. After staining, specimens have to be dehydrated by 70% ethanol, 90% ethanol and 100% ethanol and xyline for future storage, with cover slips mounted on top.

Histology samples were examined under a Nikon eclipse TE2000-5 optical microscope to investigate the cellular responses between cells and nanoparticles. Images were analysed by image analysis software (Image J) to further quantify the cell number. Generally, three different sections were cut from each sample with two magnifications (10X and 40X). The cell number in each image were counted and plotted with average and standard deviation (n=3). The results were also validated by a blind test.

2.5.7 Gene Expression

2.5.7.1 RNA Extraction

Isolation of RNA from cell-seeded collagen scaffolds was the first step in gene expression quantification. RNeasy Mini Kit (Qiagen 74104 and 74106) was used to extract the RNA from the samples. Firstly, 350 μl Buffer RLT (lysis buffer) was added to the sample in a micro-centrifuge tube and mixed well to release cells. Samples were stored at -80 °C if not used immediately. Secondly, 250 μl ethanol (96 - 100 %) was added to the diluted RNA and mixed well by pipetting, followed by transferring the samples (700 μl) to an RNeasy Mini spin column placed in a 2 ml collection tube. 350 μl of Buffer RW1 (wash buffer) was then added to the RNeasy column. 10 μl DNase I stock solution was added to 70 μl Buffer RDD (provides efficient on-column digestion of DNA and also ensures that the RNA remains bound to the column). This was mixed well by gently inverting the tube. Then the DNase I incubation mix (80 μl) was directly added to the RNeasy column membrane and left for 15 mins at 20-30 °C. Then 350

μl Buffer RW1 was added to the column, followed by 2× of 500 μl Buffer RPE (concentrated wash buffer), with the addition of 4 volumes of 96 - 100 % ethanol for a working solution, to wash the membrane. Centrifugation at $\geq$ 8000 × g for 15 s was needed in between each step. Finally, the RNeasy spin column was placed in a new 1.5 ml collection tube with an addition of 40 μl RNase-free water directly to the spin column membrane, centrifuged for 1 mins at $\geq$ 8000 × g to elute the RNA.

The isolated RNA was quantified by a Nanodrop spectrometer. The spectrometer is equipped with a lower pedestal, an upper pedestal and an arm. A source fibre is embedded within the lower pedestal and a receiving fibre is embedded in the upper pedestal. Light emitted from the LEDs transverses the sample, and absorbance is measured using a silicon photodiode. Briefly, place 0.5 - 2 μl of sample directly on top of the detection surface, when closing the arm, a column between the ends of optical fibres are created due to surface tension. Thus the measurement optical path is formed. The pedestal then moves to automatically adjust for an optimal path length (0.05 - 1 mm). Then the concentration of nucleic acid can be quantified.

2.5.7.2 Reverse Transcription with Elimination of Genomic DNA for Quantitative, Real-Time PCR

To eliminate the genomic DNA, 2 μl of buffer GE, 50 ng of template RNA with variable RNase-free water were used to make a total volume of 10 μl reaction. The samples were incubated for 5 mins at 42 °C and then placed on ice imme-

diately. Then the reverse transcriptase master mix was prepared by adding 4 μl 5× buffer BC3, 2 μl of RE3 Reverse Transcriptase Mix and 4 μl of RNase-free water to make a total volume of 10 μl solution. This master mix was incubated at 42 °C for 5 mins. Then the template RNA and reverse transcriptase master were mixed together, followed by incubation at 42 °C for 15 mins and 95 °C for 5 mins. The rise in temperature was to denature RNA secondary structures that will inhibit cDNA production. Then 30 μl RNase-free water was added to each reaction and mixed by pipetting up and down several times.

The RT SYBR Green Mastermix was prepared as below. 0.5 μl of 10 μ mol of forward primer and 0.5 μl of 10 μ mol of reverse primer was added together with 4 μl of SYBR Green and 3 μl of RNase-free water to make a 8 μl solution. Finally, 2 μl of the cDNA and 8 μl of the SYBR Green Master Mix was added into one well to make one reaction. For PCR amplification, the following sets of specific primers were designed via Primer-Blast (shown in Table 2.3). The procedures of primer designing are listed as below. First of all, copy the sequence which has to be amplified in PCR. Then set the range of acceptable lengths and melting temperature of the PCR products, followed by the selection of Exon junction span. Finally, a primer pair specific check has to be completed to exclude primers that could amplify outside the target sequence.

The reaction conditions were modified as follows: incubation at 95 °C for 2 mins, denaturation at 95 °C for 10s, annealing at 60 °C for 5s and polymerisation at 72 °C for 25s, followed by a final extension at 76 °C for 1s, for 45 cycles.

Quantitative analysis was performed based on relative quantification and modified for this study. Briefly, the threshold cycle (Ct) value was calculated from amplification plots, the Δ Ct value for each sample was obtained by subtracting the Ct values of housekeeping genes (GAPDH), respectively. The Δ Ct values calculated can then been plotted into graph and presented by box and whiskers graph. The data are represented for triplicate readings.

2.5.8 Statistical Analysis

The experiments of biological property evaluation were performed in triplicate. The results are represented as mean ± standard deviation for n=3 samples. Statistical analysis was carried out by analysis of variance (ANOVA) to determine the presence of any significant differences between groups, and significant level was set at $p < 0.05$.

2.6 Summary

The project described in this chapter was to develop a 3D model for the *in vitro* evaluation of magnetic stimulation on osteogenesis. In this chapter, the setting-up of the magnetic bio-reactor has been reviewed, which includes the employment of computational simulations, the selection and comparison between different types of permanent magnets, and the use of tesla meter to validate the simulation results. Besides, the methods and materials used to develop the 3D collagen model have been introduced, from the formation of collagen gel, to the plastic

Oligo Name	μl for 100 μM	Sequence (5'-3')
GAPDH-F	803	5' TGCACCACCAACTGCTTAGC 3'
GAPDH-R	744	5' GGCATGGACTGTGGTCATGAG 3'
ACTB-F	619	5'CTGGAACGGTGAAGGTGACA 3'
ACTB-R	513	5'AAGGGACTTCCTGTAACAATGCA 3'
Runx2-F	511	5' CCAACCCACGAATGCACTATC 3'
Runx2-R	470	5' TAGTGAGTGGTGGCGACATAC 3'
ALP-F(1)	579	5' GACCCTTGACCCCCACAAT 3'
ALP-R(1)	656	5' GCTCGTACTGCATGTCCCCT 5'
ALP-F(2)	1046	5' CGGATCCTGACCAAAAACC 3'
ALP-R(2)	1130	5' TCATGATGTCCGTGGTCAAT 5'
Osteonectin-F(1)	482	5' ATTGACGGGTACCTCTCCCA 3'
Osteonectin-R(1)	541	5' GAAAAAGCGGGTGGTGCAAT 5'
Osteonectin-F(2)	462	5' GCGAGTTTGAGAAGGTGTGC 3'
Osteonectin-R(2)	456	5' TTTGCAAGGCCCGATGTAGT 5'
Osteonectin-F(3)	498	5' CGTCCTGGTCACCCTGTATG 3'
Osteonectin-R(3)	525	5' CTTCTTCACCCGCAGCTTCT 5'
BMP2-F(1)	425	5',TTTCAATGGACGTGTCCCCG 3'
BMP2-R(1)	410	5' AGCAGCAACGCTAGAAGACA 3'
BMP2-F(2)	536	5' GGACGCTCTTTCAATGGACG 3'
BMP2-R(2)	695	5' GCAGCAACGCTAGAAGACAG 5'
BMP2-F(3)	582	5' TGTCTTCTAGCGTTGCTGCTT 5'
BMP2-R(3)	538	5' GCAACTCGAACTCGCTCAGG 3'
BMP4-F(1)	525	5' CGTCCAAGCTATCTCGAGCC 3'
BMP4-R(1)	566	5' CGGAATGGCTCCATAGGTCC 3'
BMP4-F(2)	586	5' TTGTCTCCCCGATGGGATTC 3'
BMP4-R(2)	591	5' GAATGGCTCCATAGGTCCCTG 3'
BMP4-F(3)	492	5' TCCAAGCTATCTCGAGCCTG 3'
BMP4-R(3)	543	5' ATGGCTCCATAGGTCCCTGC 3'

Table 2.3: Primers designed and used for PCR studies.

compression process. The protocol used for the *in vitro* studies have also been described. Based on standard protocols, novel methods have been developed for the current study. These developed methods can also be applied to future studies.

Chapter 3

Development of a Magnetic Bio-reactor for Magnetic Stimulation

3.1 Overview

The objective of this chapter is to describe the design of a magnetic bio-reactor with the desirable intensity. It has been proposed that SMFs with 1 mT to 1 T are capable of influencing a number of biological systems, including proliferation, differentiation and mineralisation of osteoblasts. From previous investigations (as reviewed in Chapter 1), SMFs with field strength below 15 mT or 250 mT were not able to enhance osteoblasts proliferation, whereas SMFs with field strength between 100 mT and 160 mT had most effective effect. Therefore, the aim of this chapter was to design and fabricate a magnetic bio-reactor with field strength within this range. SMFs can be set up by employing permanent magnets. The

magnetic field between two magnets depends on the dimensions and physical properties of the magnets, as well as the relative position of the magnetic poles. Therefore the effect of various parameters on the magnetic field strength will be first studied. Then the designed magnetic bio-reactor will be constructed by SLS technique, followed by validation using a Tesla meter. A map of strength distribution will also be plotted.

3.2 Development of a Magnetic Bio-reactor

3.2.1 Computational Simulation of Magnetic Fields

In order to investigate the effects of different types of magnets, the relative position of the poles and the separation distances on the strength of the magnetic field, several designs were tested. Four different types of magnets were involved, NdFeB30, NdFeB35, SmCo24 and SmCo28. All other variables used are illustrated in Figure 3.1.

The first target was to investigate the effect of different types of magnets on the magnetic field strength. NdFeB30 and NdFeB35 are the most commonly used neodymium magnets in biomedical studies, Figure 3.2a and 3.2b represent the difference in magnetic filed strength from these two types of magnets, given that all other parameters were fixed. The magnetic field strength of interest is at the centre of the design with a diameter of 2 cm. The magnetic field strength is in the range of 62 - 184 mT and 72 - 215 mT, respectively.

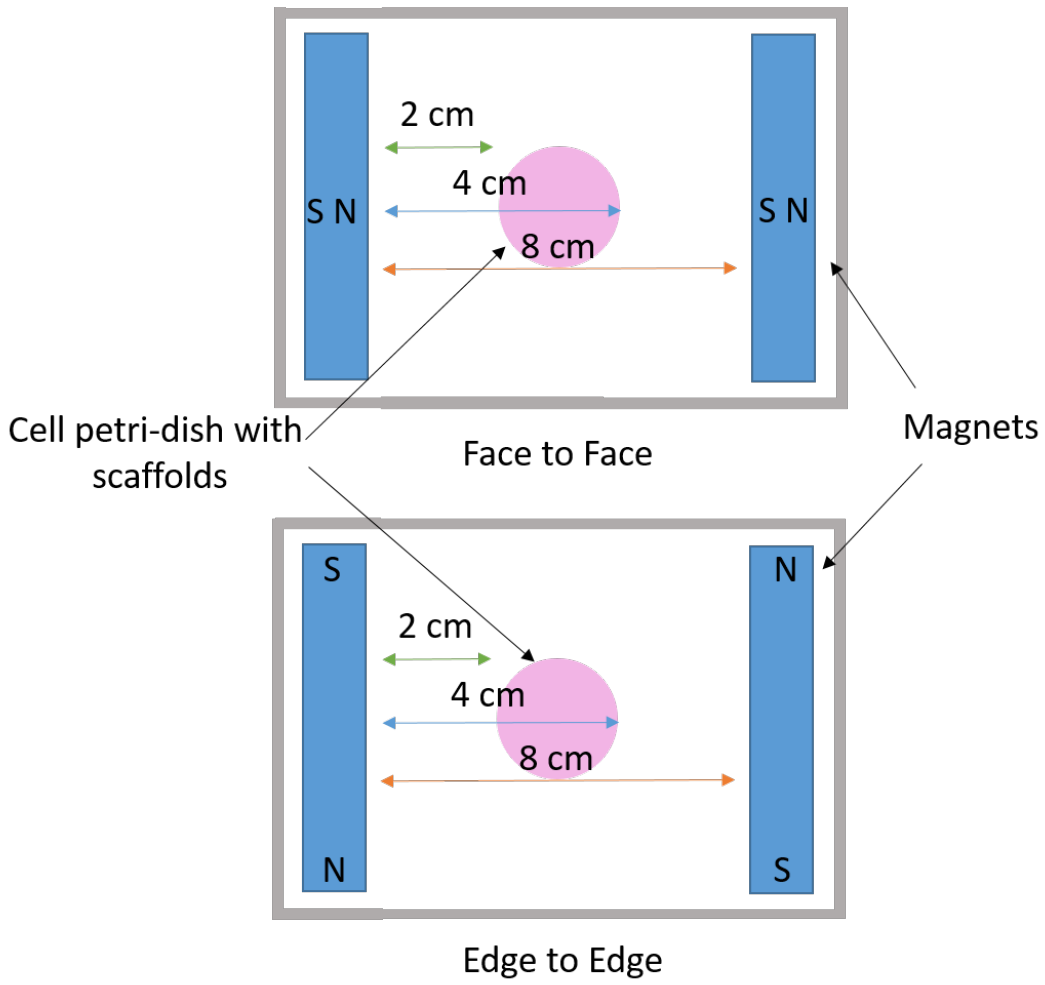

Figure 3.1: The separation distances used are 2, 4, and 8 cm, and the relative position of magnetic poles varied are face to face and edge to edge. The pink circle represents the location of the scaffolds with a diameter of 2 cm in cell petri-dish.

Apart from neodymium magnets, samarium-cobalt magnets have also been applied in clinic. SmCo24 and SmCo28 were modelled and simulated, with the results presenting in Figure 3.3a and 3.3b. The magnetic filed strength generated at the centre (with a diameter of 2 cm) is in the range of 57 - 169 mT and 61 - 181 mT, respectively.

Then the magnet to magnet distance and relative position of the magnetic poles were investigated. NdFeB35 magnets were chosen for the following studies, due to its highest strength when compared to others.

Firstly, the magnets were placed with a gap of 2 cm. In this case, two positions were studied, with N-S face to face and N-S edge to edge (shown in Figure 3.4a and 3.4b). As can be observed, the B field at the centre of the face to face case are in the range of 140 mT to 279 mT, which is larger than that in the edge to edge case, which is 76 mT to 151 mT. The edge to edge position generated a smaller field when compared to the face to face one.

As the distance increased to 4 cm, the B field decreased to 105 - 209 mT (face to face) (figure 3.5a) , and 37 - 72 mT (edge to edge) (Figure 3.5b). A reduction of the magnetic field strength can be observed when compared to the case where the separation distance is 2 cm.

The third design is to further increase the separation distance to 8 cm. As is shown in Figure 3.6a and 3.6b, the magnetic field with 8 cm gap generated a field

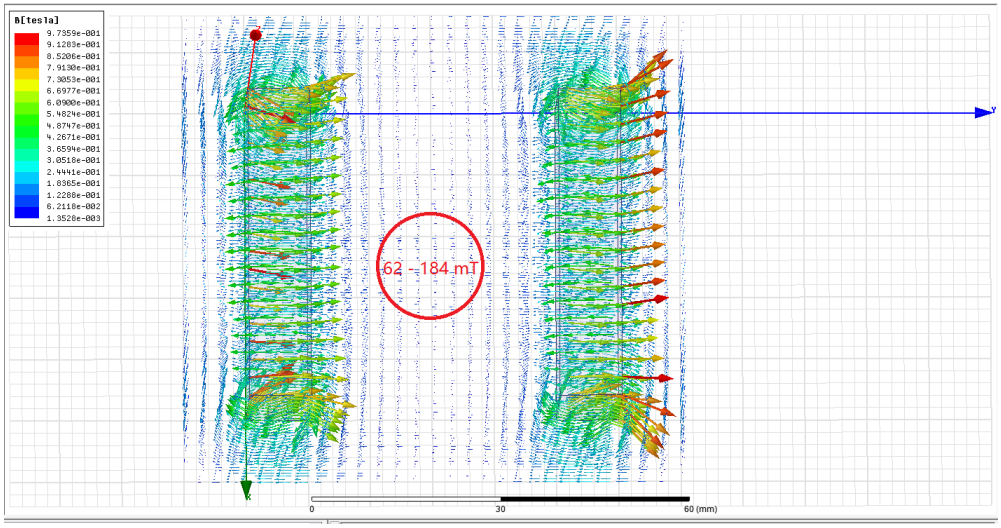

(a)

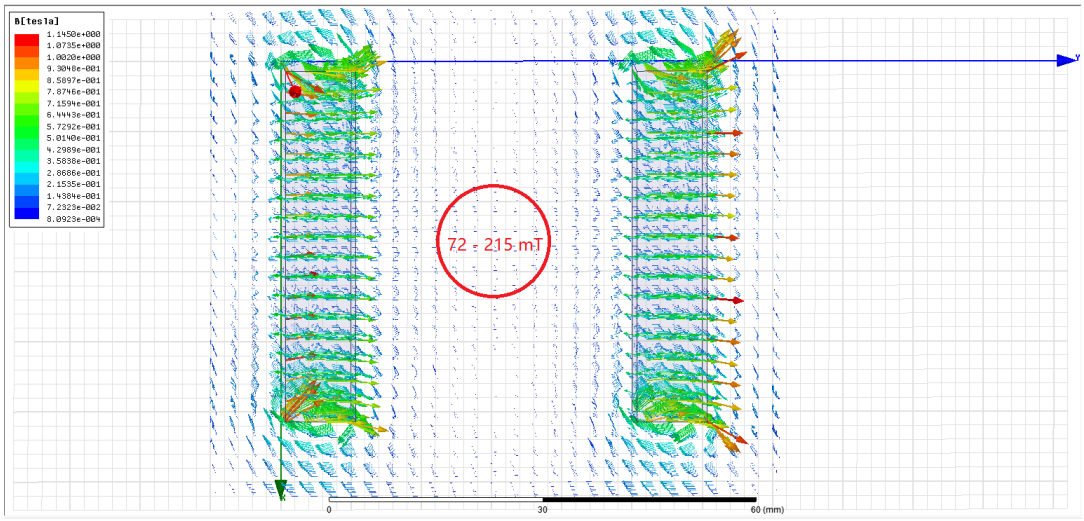

(b)

Figure 3.2: The simulation of (a) NdFeB30 and (b) NdFeB35 magnets with internal gap of 4 cm. The magnetic field strength at the centre of the field is 62 - 184 mT and 72 - 215 mT, respectively.

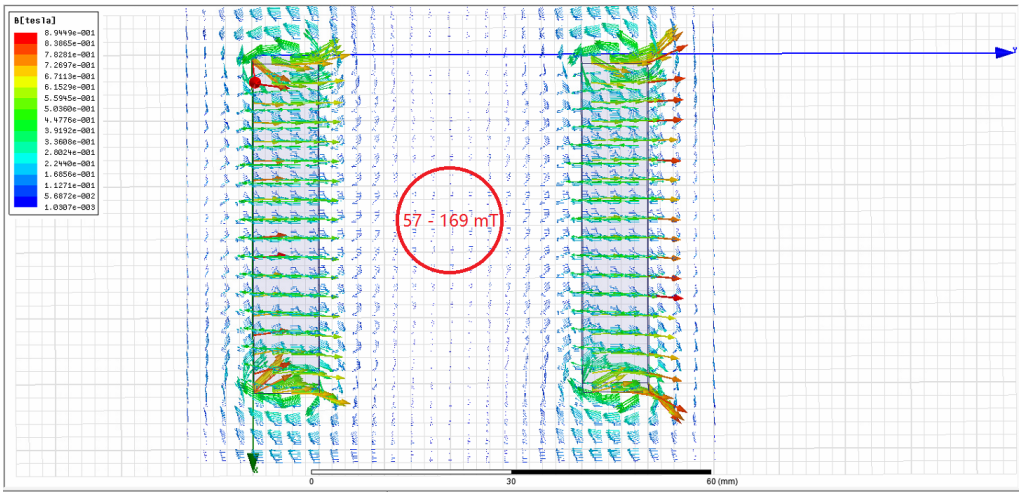

(a)

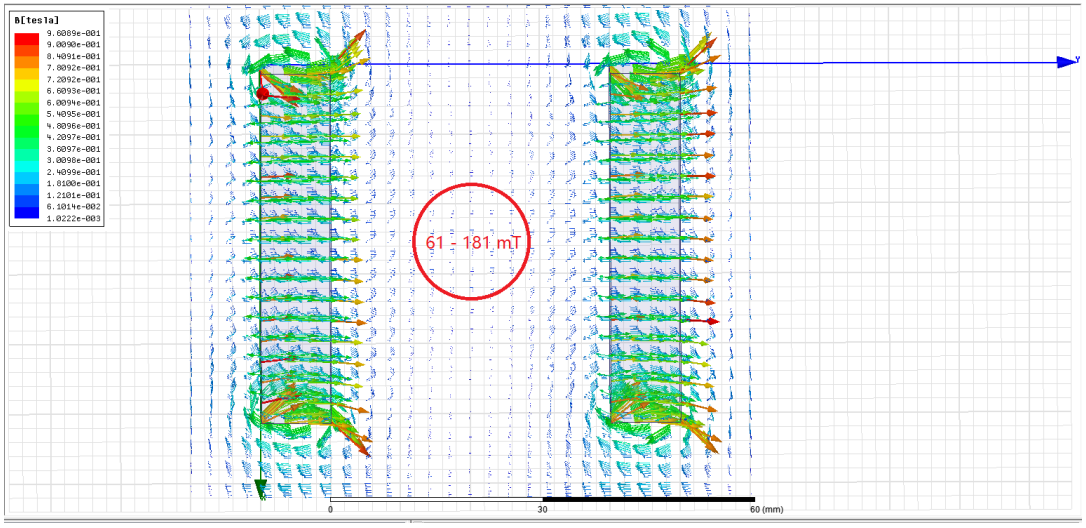

(b)

Figure 3.3: The simulation of (a) SmCo24 and (b) SmCo28 magnets with internal gap of 4 cm. The magnetic field strength at the centre of the field is 57 - 169 mT and 61 - 181 mT, respectively.

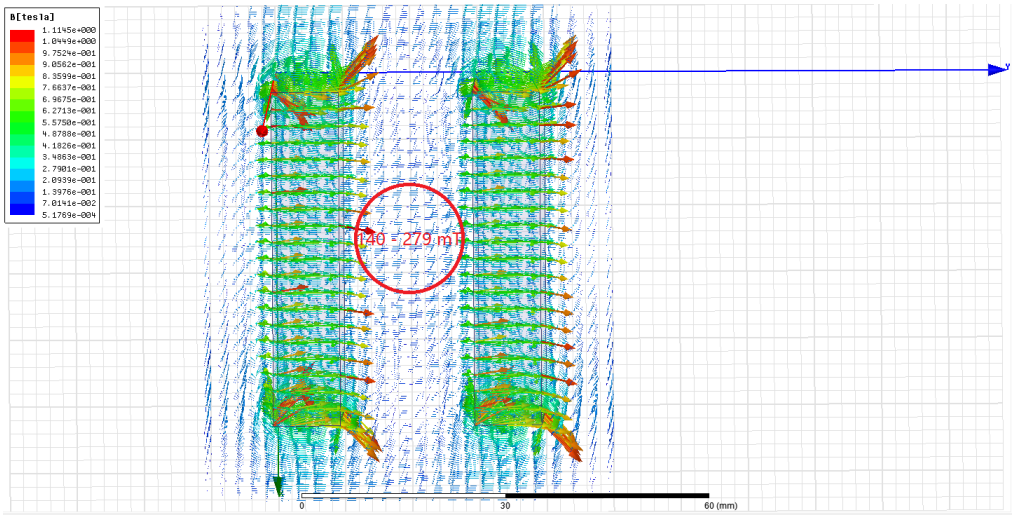

(a)

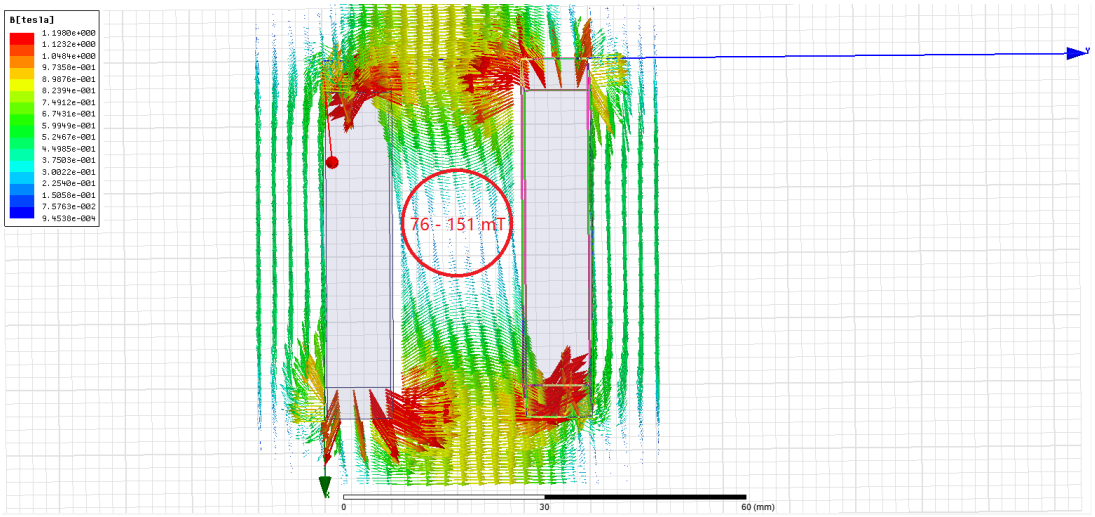

(b)

Figure 3.4: The simulation of (a) face to face and (b) edge to edge position with internal gap of 2 cm. The magnetic field strength at the centre of the field is 140 - 279 mT and 76 - 151 mT, respectively.

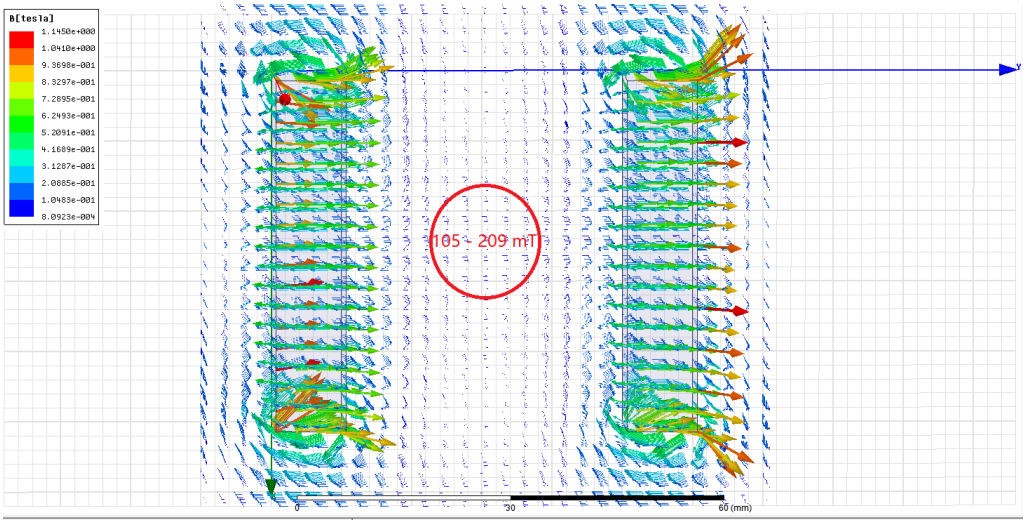

(a)

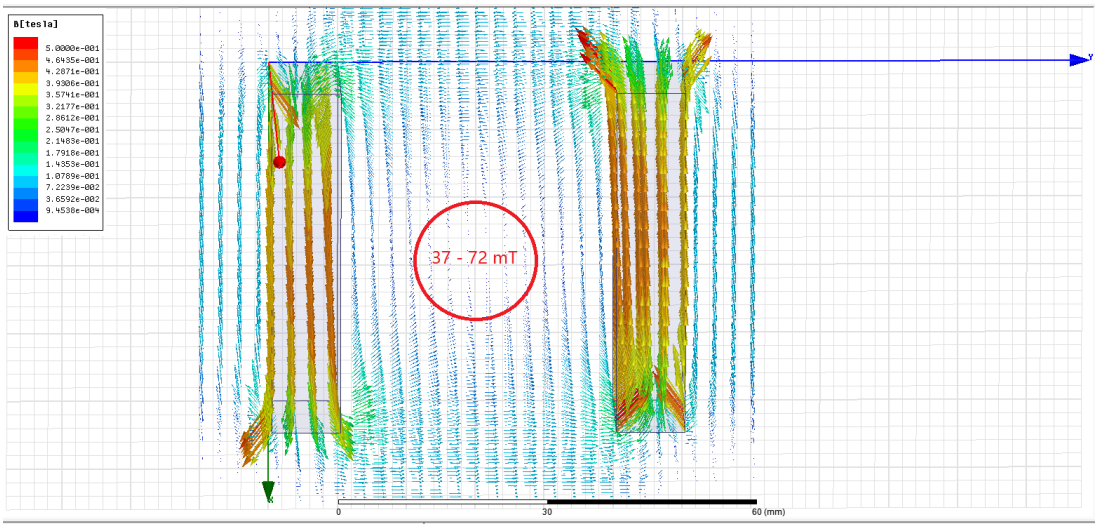

(b)

Figure 3.5: The simulation of (a) face to face and (b) edge to edge position with a distance of 4 cm. The B field at the centre of the field is 105 - 209 mT and 37-72 mT, respectively.

strength of 0.45 - 71 mT when the magnets are placed face to face, and 0.125 - 36 mT when the magnets were placed edge to edge.

Table 3.1 summaries the magnetic field strength from different designs.

Position	Distance / cm	Magnetic Field Strength / mT
Face to Face	2	140 - 210
	4	105 - 209
	8	0.45 - 71
Edge to Edge	2	76 - 151
	4	37 - 72
	8	0.125 - 36

Table 3.1: Summary of the simulation results from different designs.

As can be compared from the above results, the design with face to face position, 4 cm internal gap give the closest value as the hypothesised magnetic filed (100 - 160 mT). Therefore this design will be used for the following studies.

3.2.2 Designing of the Magnetic Bio-reactor

A magnet holder has to be designed to accommodate the magnets. There are two pockets designed on the side of the holder to not only accommodate the magnets but also prevent the magnets colliding with each other (as shown in Figure 3.7). The magnets were fitted in two pockets with magnetic poles facing each other. A 3 cm diameter Petri-dish was able to successfully fit in the centre of the holder.

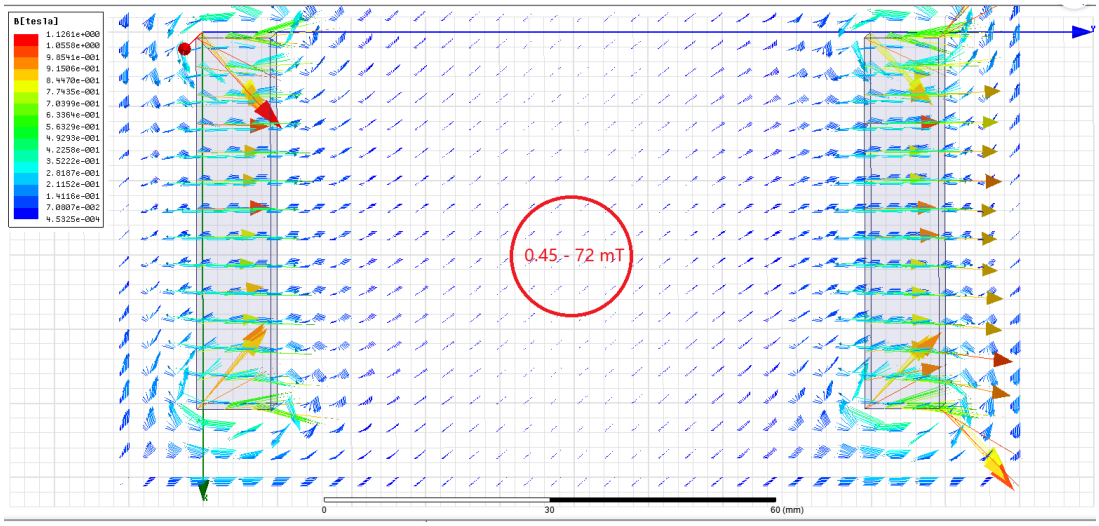

(a)

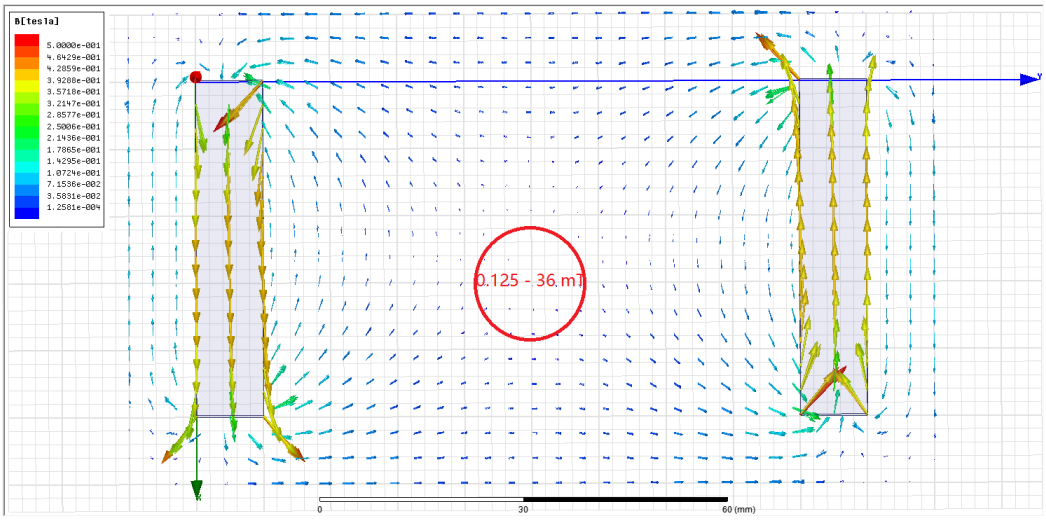

(b)

Figure 3.6: The simulation of (a) face to face and (b) edge to edge SMFs with a gap of 8 cm. The field strength at the centre of the field is 0.45 - 72 mT and 0.125 - 36 mT, respectively.

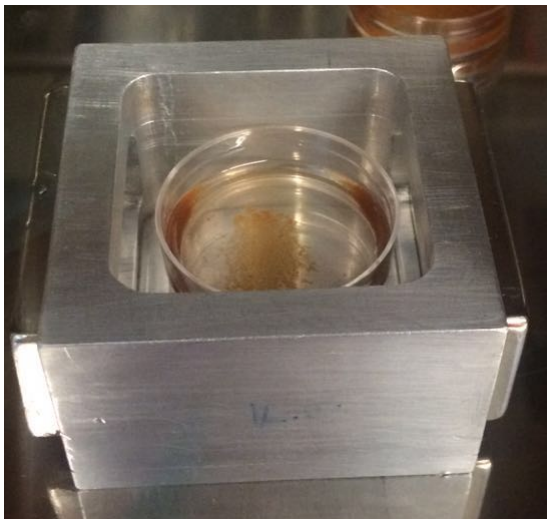

Figure 3.7: Initial design of the magnets holder. The holder is made of aluminium, with an internal diameter of 4 cm, and the magnets can be inserted from two sides of the holder.

However, there are some potential problems encountered with this design. First, the pocket deign would lead to higher possibility of infections for the cells, due the gap between the pockets and the magnet. Exposing the magnets outside the reactor is also not safe. Second, it is difficult to ensure that the cell Petri-dish is located in the centre of the magnetic field, as the size of the Petri-dish is slightly smaller than the inner space of the holder.

Based on the feedback from the initial design, a modified version was fabricated. The CAD model is shown in Figure 3.8a. The problem introduced by the side pockets from the initial design can be eliminated by placing the magnets inside the holder, with two thin barriers preventing the magnets from moving. Besides, a Petri-dish platform was designed to hold the Petri-dish in the centre of

the magnetic field. The actual dimensions are shown in Figure **??**. In addition, the holder has to be strong enough to hold the magnets in place, as well as to be biocompatible for biological studies. Therefore, Nylon (PA 2200) was selected as the candidate material. Figure 3.8b represents final the 3D printed bio-reactor.

3.2.3 Final Validation of the Magnetic Bio-reactor

The magnetic holder was tailor-made and fabricated, there remained an issue of the effects of the Nylon holder barriers on the magnetic field strength. It was therefore necessary to simulate the magnetic field strength of the final reactor. The simulated results were shown in Figure 3.9. As can be seen, the field strength of the new design was reduced to 72 - 144 mT. Although the strength was decreased, it still remained in the desired range, therefore the new design were accepted.

The magnetic field strength of the designed bio-reactor has then been validated by a tesla meter, with results presented in Figure 3.10. The average magnetic field strength at each point ranged from 90 to 129 mT, and they lie within the range of the simulated results (72 - 144 mT at the centre and 144 - 215 mT at the corner), which validated the simulation results. The differences between the simulated and experimental results might be due to the the accuracy of instrumentation and the effect of the magnet field of the earth.

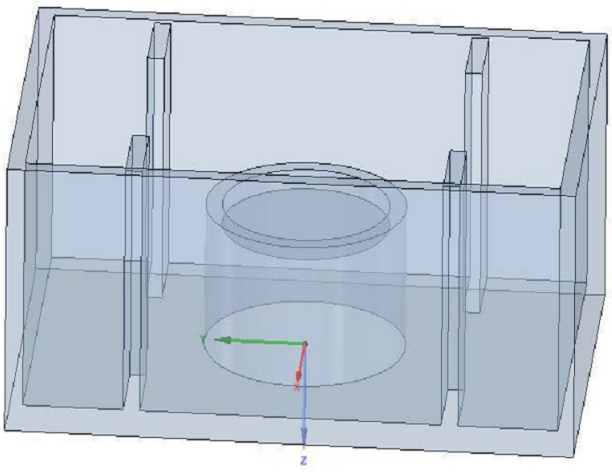

(a)

(b)

Figure 3.8: Illustrations of (a) the CAD drawing of the magnetic bio-reactor, with a magnet to magnet distance of 4 cm and a Petri dish platform in the centre of the magnetic field and (b) final product, which was fabricated by SLS technique with biocompatible Nylon PA 2200. The magnetic bio-reactor has an overall dimension of 56mm, 68mm and 28mm in x, y and z dimension, respectively.

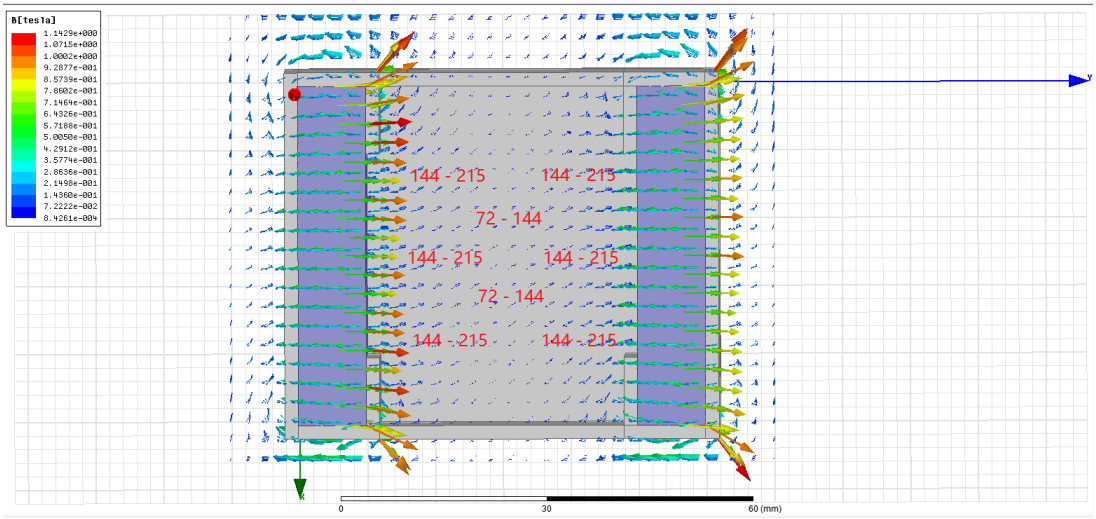

Figure 3.9: Computational simulation of the magnetic bio-reactor, with magnetic field strength of 72 -144 mT.

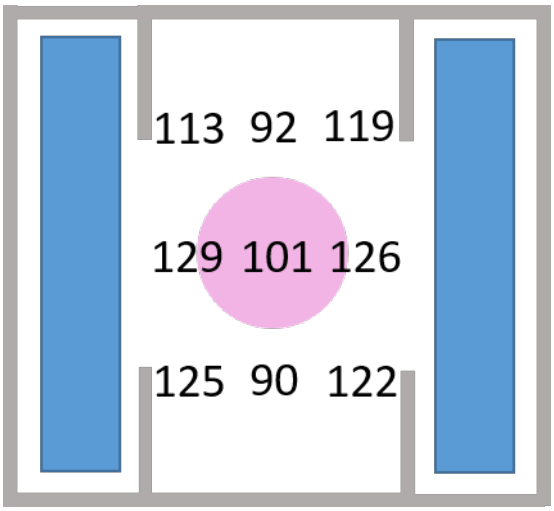

Figure 3.10: The magnetic fields measured by the Tesla meter is in the range of 90 - 129 mT.

3.3 Discussion

The magnetic field strength is the most crucial factor that influences the cell behaviours (who were exposed under SMFs). Degen & Stetsula [1971] firstly reported the promoting effect of SMFs on fracture repair. Among all types of SMFs, SMFs with 1 mT - 1T have been identified as capable of affecting a number of biological behaviours of osteoblast cells, including cell proliferation, differentiation and mineralisation. However, the results with regards to various strength within that range are highly controversial. For example, Chiu *et al.* [2007] found that the proliferation of MG-63 cells was inhibited by SMFs of 400 mT. Imaizumi *et al.* [2007] demonstrated that the proliferation of MC3T3-E1 was decreased by the exposure of 250 mT SMFs. On the other hand, in the study of Yamamoto *et al.* [2003], they showed that SMFs of 160 mT stimulated bone formation by promoting differentiation of osteoblasts (rat calvaria cell, ROS 17/2.8 and UMR-106). Cai *et al.* [2015] further demonstrated that 100 mT SMFs was capable of enhancing MC3T3-E1 cell differentiation. However, when low SMFs have been employed (3, 4, 7 and 15 mT), either the cell attachment nor proliferation of osteoblasts can be observed [Kim *et al.*, 2005]. As can be concluded from these studies, SMFs with field strength above 250 mT or below 15 mT were not been able to promote osteoblasts to proliferate, whereas SMFs with field strength in between 100 mT to 160 mT had a stimulating effect. Therefore the hypothesis was to build a magnetic bio-reactor with magnetic field strength of 100 mT - 160 mT.

In order to build a magnetic field with desired strength (100 mT - 160 mT),

several designs were simulated computationally firstly, with the results ranging from 0.125 mT to 279 mT. The magnetic field strength is dependent on several factors, for example, types of magnets, distance in between the magnets as well as the relative position of the magnetic poles.

Among a wide range of permanent magnets, neodymium and samarium-cobalt magnets are the most commonly used. Both types have been applied in clinical applications [Bondemark *et al.*, 1994; Darendeliler *et al.*, 1995], whereas NdFeB magnets showed negligible cytotoxicity and stronger magnetic strength during *in vitro* tests. The computational simulation gave similar range of magnetic field strength by using both types of magnets, due to bio-compatibility considerations, neodymium magnets were chosen as the source of permanent magnets in this study. Once the type of the magnets were decided, the magnetic field strength is then dependant on the relative position of the magnets, i.e, the distance between two magnets, the position of the magnetic poles (the poles are at the edges or the faces of the magnets).

Placing the magnetic poles face to face, or edge to edge lead to different strength. Taking all three distances simulated (2 cm, 4 cm and 8 cm), face to face position induced larger magnetic field strength when compared to edge to edge one. The magnetic field at any given point is specified by both direction and magnitude (or strength) as such it is a vector field. When multiple magnets are placed near to each other, they exert forces and torques on each other. The forces are modelled as tiny loops of current, called magnetic dipoles, which produce their own magnetic field. Calculating the net force in between two magnets

is complicated, as it is determined by summing up all these interactions between the dipoles of the first magnet and that of the second. When magnetic poles are placed face to face, the magnetic field in the middle is the same as that at the edge. However, when two magnets are placed edge to edge, the magnetic dipoles come from N to S of one magnet is in the opposite direction with that come from the other magnets, resulting in a smaller magnetic field strength in the centre of the field.

As for the distance between magnets, it can be concluded that the closer the magnets, the stronger the magnetic field. Classically, the force between two magnetic poles is given by a formula,

$$F = \frac{\mu q_{m1} q_{m2}}{4\pi r^2} \tag{3.1}$$

where F is force, q_{m1} and q_{m2} are the magnitudes of magnetic poles, μ is the permeability of the intervening medium and r is the separation distance. As can be observed from the equation, given the same permeability, smaller separation distance induces larger magnetic force in between.

In this study, a magnetic bio-reactor constructed with neodymium N35 magnets with a separation distance of 4 cm was selected, which resultant in a magnetic field strength of 72 - 144 mT (computational) and 90 - 129 mT (experimental).

3.4 Summary

In this chapter, a magnetic bio-reactor was designed and validated. A static magnetic field can be constructed by using the permanent magnets, and the field strength of the bio-reactor is highly dependent upon the properties of the magnets, the relative position of the magnetic poles and the separation distances. As can be concluded from the results, when the magnetic poles are placed face to face, the magnetic field in the centre is stronger than that when the magnetic poles are placed edge to edge. Besides, the smaller the separation distance, the larger the magnetic field strength. This can be explained by using the force between two poles formula, where smaller separation distance lead to stronger magnetic force. The final design of the magnetic bio-reactor was fabricated by SLS technique and simulated to have a 72 - 144 mT magnetic field strength. The actual magnetic field strength was measured by a tesla meter with result lying in the range of 90-129 mT. These data validated the simulation results from ANSYS.

Chapter 4

Development of a 3D Collagen Model for the *In Vitro* Evaluation of Magnetic Stimulation on Osteogenesis

4.1 Overview

A tissue model consists of three key components, the scaffold, the cells and the biofactors. Collagen hydrogels have been widely used as tissue models/scaffolds. However, conventional collagen hydrogels lack of mechanical strength and low in collagen density (only containing 0.2 - 0.6 w/w % collagen protein). They can be quickly resorbed *in vivo* [Tabata *et al.*, 2000]. Plastic compression of collagen gels can improve the collagen density and the mechanical properties, by expelling the extra aqueous components, while maintaining the structure and cell viability.

Compared to hydrated collagen gels, cells seeded within compressed scaffolds also show increased proliferation, differentiation and mineralisation over time. Plastic compressed hydrogels have been used as tissue models/scaffolds with the ability to incorporate various types of cells, such as fibroblasts, osteoblasts, etc. The aim of this project was to investigate the effects of SMFs on osteogenesis, therefore osteoblasts will be the focus of the study.

One of the advantages of PC collagen models is that they offer the possibility of incorporating various bio-factors together with cells. It has been reported by several studies that incorporating biofactors into the plastic compressed collagen scaffolds, such as chitosan and bioactive glass particles, can promote the differentiation and mineralisation of the cells. IONPs can be manipulated by an external magnetic field without direct contact, therefore can be used to evaluate and potentially enhance the effect of SMFs on osteogenesis. Besides, HA is one of the most popular ceramic materials for bone repair, own to the fact that it is the primary constitution of bone mineral [Cheema *et al.*, 2011]. On the other hand, infection is one of the reasons that causes fracture non-union. nZnO have been demonstrated to have antimicrobial properties [Brayner *et al.*, 2006] and can be introduced into the system to enhance fracture non-union by reducing bacterial growth.

The aim of this chapter was to design and evaluate a suitable *in vitro* model for the investigation of SMFs on osteogenesis. The effects of SMFs on various cell lines (MG-63, UMR-106 and MC3T3-E1), 2D/3D collagen models, as well as the incorporation of IONPs, nHA and nZnO (concentrations of 1, 10, 100 and

1000 μg/ml) will be studied. Alamar blue (AB) assays have been employed to investigate the proliferation of cells.

4.2 Effects of SMFs on Cell Cultures

The effects of SMFs on the proliferation of three different cell lines, MG-63, UMR-106 and MC3T3-E1 were tested by using AB assay. Cells were seeded in collagen scaffolds for 1, 3, 7 and 14 days with a population of 1×10^4 cells, respectively, and grow with/without the exposure of SMFs (shown in Figure 4.1a). Figure 4.1a compares the proliferation of three cells under conditions and with SMFs. Without the exposing of SMFs, all cells were able to proliferate over time. MG-63 cells proliferated faster than the other two cell lines, whereas the lowest was found with UMR-106 cells. MC3T3-E1 cells show a steady growth rate when compared to the others. When subjected to SMFs, all cells were able to proliferate over 14 days. The proliferation of MG-63 cells peaked at day 14, whereas UMR-106 remained with the lowest. A comparison of the effects of SMFs on different cell lines are illustrated in Figure 4.1b. As can be observed, all cells were stimulated significantly by SMFs after 7 days.

4.3 Effects of SMFs on 2D/3D Models

2D model (cell monolayers) and 3D plastic compressed collagen scaffolds were prepared and tested in the magnetic bio-reactor. A population of 1×10^4 MG-63

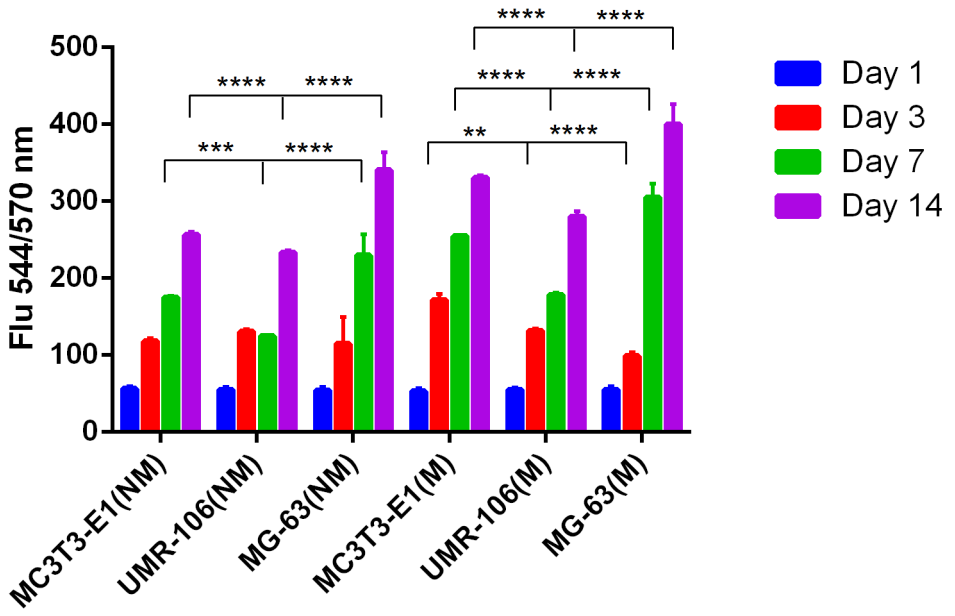

(a)

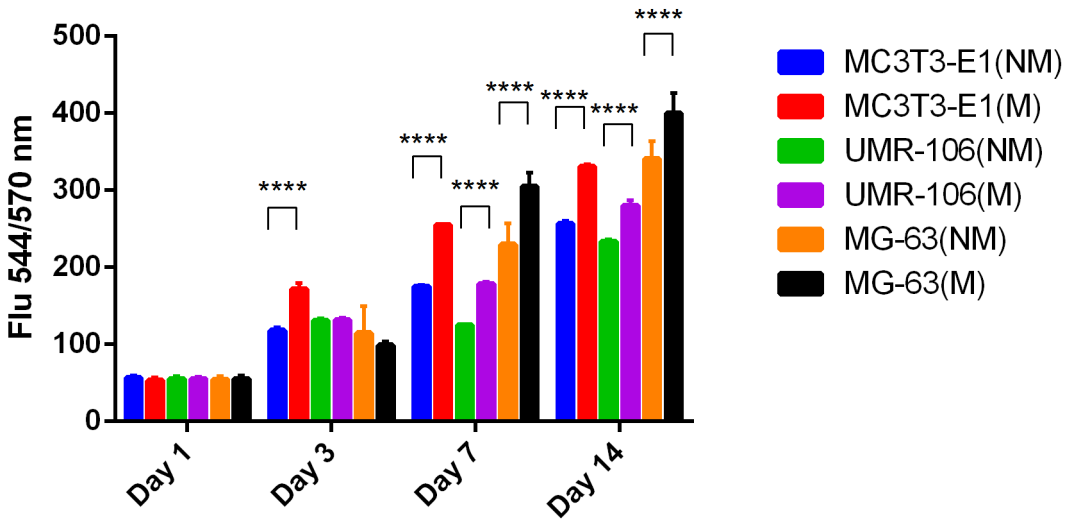

(b)

Figure 4.1: Comparisons of cell proliferation of MG-63, UMR-106 and MC3T3-E1 cell lines using an alamar blue assay with (M) and without (NM) SMFs (n=3, $*p<0.05$, $**p<0.01$, $***p<0.001$, $****p<0.0001$). (a) Cell proliferation with and without SMFs. All three cell lines are able to proliferate under SMFs. (b) Effects of SMFs on each cell lines compared at the same time point. As being exposed under SMFs, MG-63 and MC3T3-E1 cell lines respond more significantly as compared to UMR-106.

cells was seeded onto/into the each sample. AB assays were performed at day 1, 3, 7 and 14 after culture with results presented in Figure 4.2a. As can be observed, when being seeded in a 3D collagen model, MG-63 cells proliferated faster when compared to 2D monolayers from day 3. When further subjected to SMFs, the proliferation rate was enhanced. A peak growth reached after 7 days. However, a decrease in proliferation was found at day 14. This could due to the fact that cells are entering the stage of differentiation, therefore the proliferation subsides. Figure 4.2b further compares the effects of SMFs on cell proliferation with time. The stimulation effects of SMFs can be observed after 1 day in collagen scaffolds. Significant cell growth continued until day 14 for both 2D and 3D samples. This demonstrates that the SMFs have a stimulating effect on the cell proliferation of MG-63 cells, with higher proliferation in 3D collagen scaffolds.

4.4 Effects of SMFs on 3D Collagen Model with Various Bio-factors

4.4.1 IONPs Incorporated Collagen Models

AB assay was conducted to evaluate the cell proliferation when in contact with IONPs at different concentrations, 1, 10, 100 and 1000 μg/ml, as shown in Figure 4.3a and 4.3b.

Results indicate that MG-63 cell lines were able to proliferate within the IONPs embedded collagen scaffolds at low concentrations (1, 10 and 100 μg/ml),

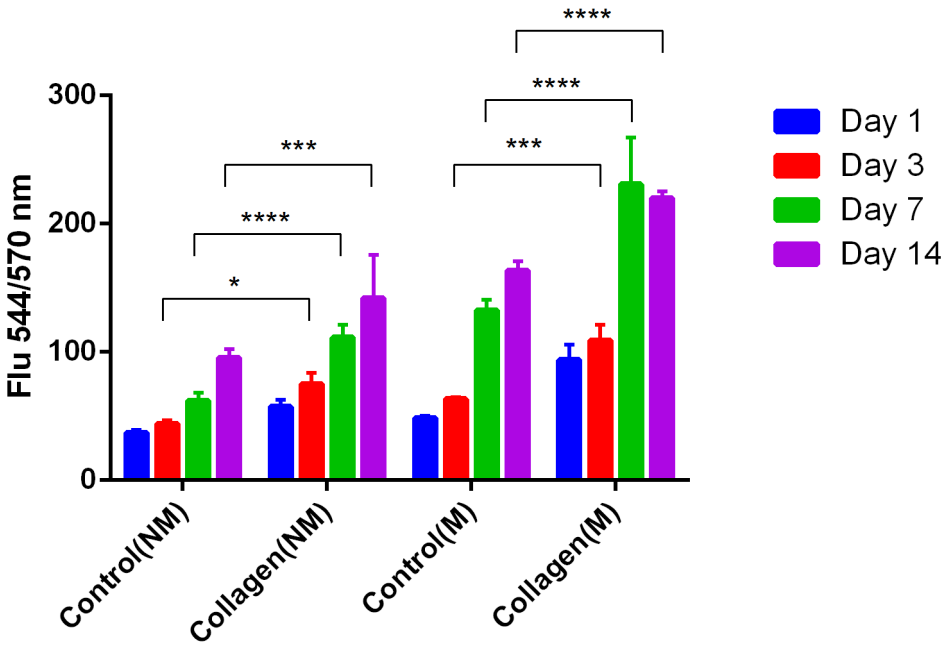

(a)

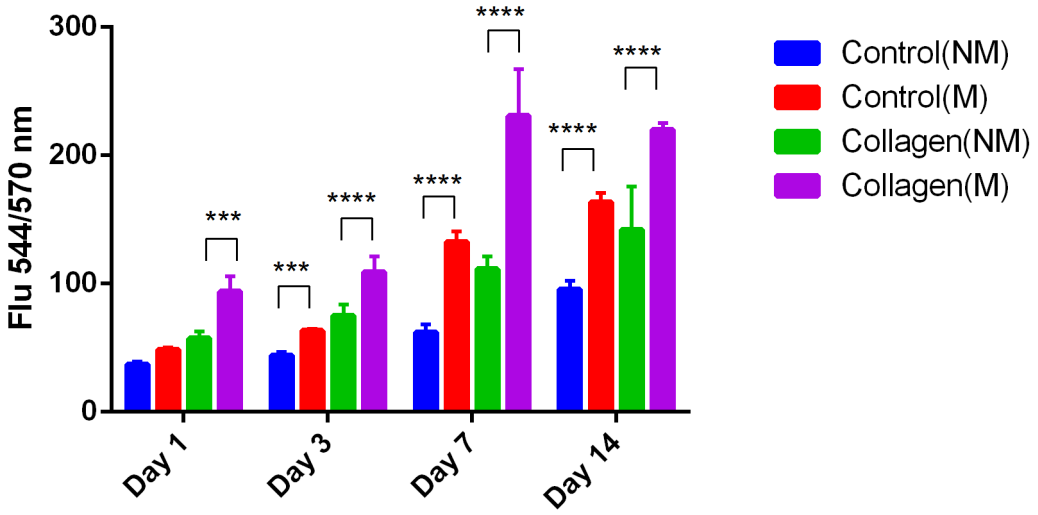

(b)

Figure 4.2: Comparisons of cell proliferation of MG-63 on cell culture monolayers (control) and collagen models using an alamar blue assay with (M) and without (NM) SMFs. (a) Cell proliferation with and without SMFs. As can be observed, cell proliferation can be affected by SMFs on all scaffolds. (b) Effects of SMFs on cells seeded on each scaffolds. Collagen scaffolds stimulated higher cell growth when compared to 2D monolayers (n=3, $*p<0.05$, $**p<0.01$, $***p<0.001$, $****p<0.0001$).

with an increasing growth rate over time. When high concentration of IONPs, which is 1000 μg/ml in this case, a decrease in proliferation was observed. It demonstrates that high IONPs concentration has an inhibition effect on MG-63 cell growth. Statistical results from day 1 and day 3 indicate that there is a significant increase when 100 μg/ml IONPs are used (when compared to controls). After 7 days, the cell growth in scaffolds incorporated with 10 μg/ml IONPs increased significantly as well. Finally, after 14 days of culture, the increase in cell proliferation was proven to be significant for all three concentrations, with the peak value located at concentration of 100 μg/ml. Furthermore, the cell proliferation at each time point increased with the IONPs content up to 1000 μg/ml, suggesting a positive correlation between the magnetite content and the cell proliferation up to a certain concentration. The IONPs incorporated scaffolds were then placed under external SMFs to evaluate the effect of a magnetic field on cell proliferation. When being exposed under SMFs, the growth of MG-63 cell lines increased for all nanoparticle concentrations except 1000 μg/ml (shown in Figure 4.3b), which further confirmed the toxicity of IONPs at high concentration. Again, 100 μg/ml resulted in the most significant effect when compared to other concentrations.

4.4.2 nHA Incorporated Collagen Models

The cell proliferation on nHA incorporated collage scaffolds were also examined at day 1, 3, 7, and 14, with concentrations of 1, 10, 100 and 1000 μg/ml, respectively.

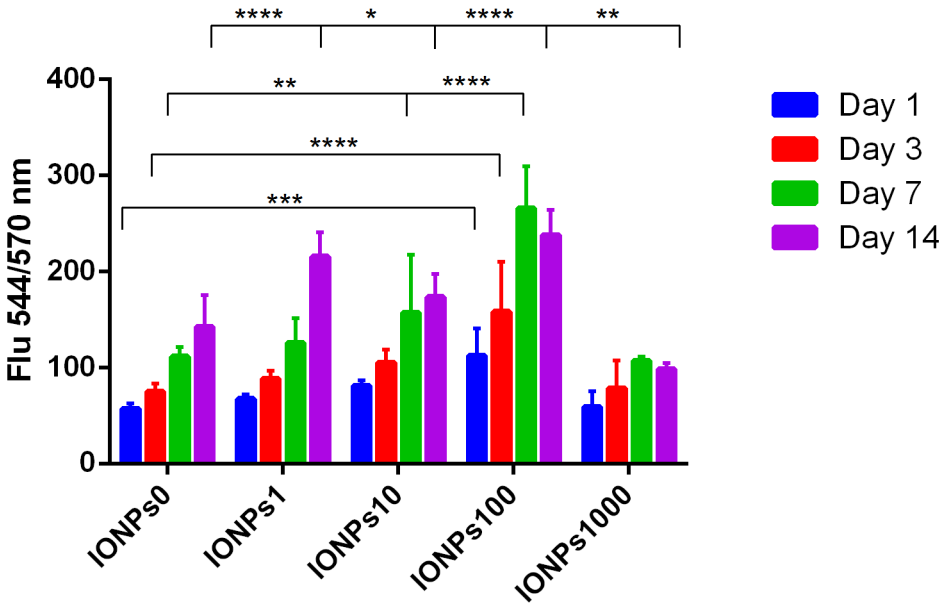

(a)

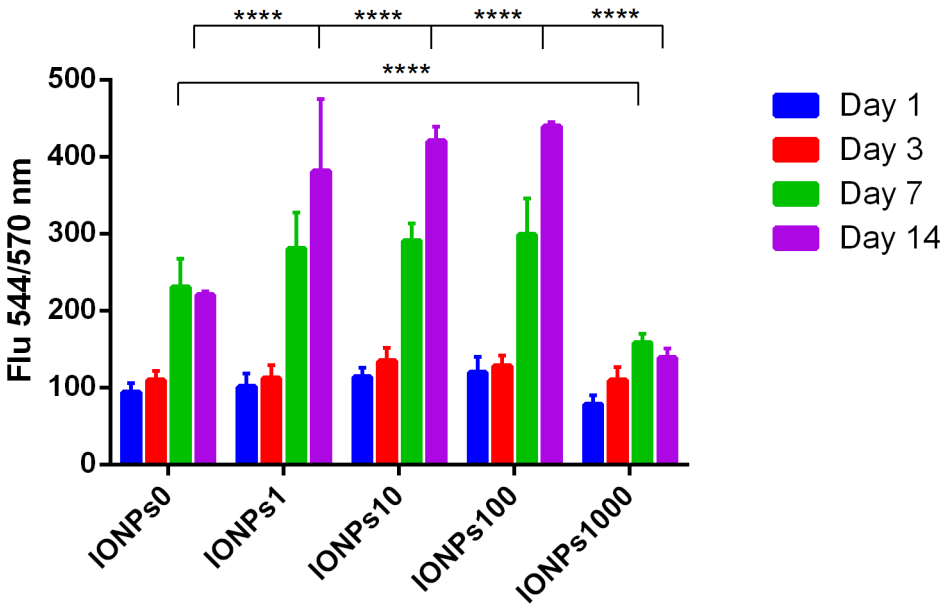

(b)

Figure 4.3: A comparison of cell proliferation of MG-63 cell lines using an alamar blue assay when in contact with IONPs (a) under non-SMFs and (b) under SMFs. 0, 1, 10, 100 and 1000 μg/ml IONPs were incorporated for 1, 3, 7 and 14 days. 1000 μg/ml were proved to be toxic to the cells under both conditions, and 100 μg/ml demonstrates the highest enhancement of the proliferation of the cells (n=3, $*p<0.05$, $**p<0.01$, $***p<0.001$, $****p<0.0001$).

For cell cultured without the exposure to SMFs, significant increase in cell proliferation was observed at day 3 for nHA concentrations of 10, 100 and 1000 μg/ml. For longer culturing times, all concentrations were identified to have a stimulating effect, even for concentration as low as 1 μg/ml, with the results shown in Figure 4.4a. This finding suggests that nHA has an stimulating effect on MG-63 cell proliferation. It also demonstrates that the nHA used in this study is bio-compatible up to a concentration of 1000 μg/ml. When external SMFs were applied, the increase in proliferative activity with the presence of nHA was not significant when compared to the control (as illustrated in Figure 4.4b). This suggests that nHA do not response to SMFs significantly.

4.4.3 nZnO Incorporated Collagen Models

In order to examine the cell growth of MG-63 cells in nZnO incorporated scaffolds, AB assays were conducted at different time points, i.e, 1, 3, 7 and 14 days, with concentrations of 1, 10, 100 and 1000 μg/ml. Figure 4.5a and Figure 4.5b represents the data.

For non-SMFs treated samples, when adding in 1 and 10 μg/ml nZnO, positive effects on cell growth were observed after 3 days. However, by further increasing nZnO concentration, a significant reduction in cell metabolic activity was noticed after 7 days. The cell proliferation with nZnO of 1000 μg/ml was halved when compared to the controls. It can be concluded that the nZnO can only stimulate MG-63 cell growth at low concentration for a shorter culture period, while being

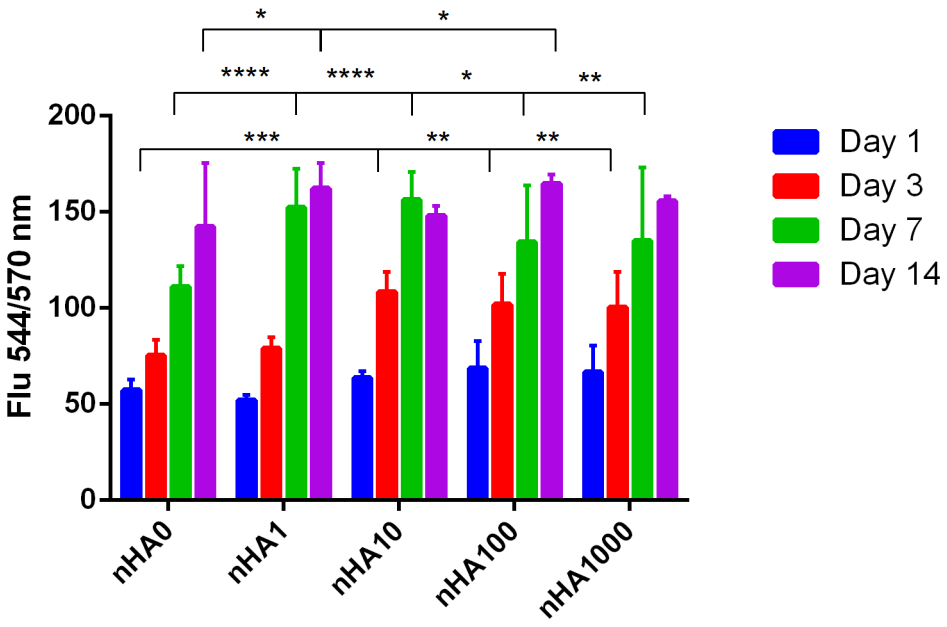

(a)

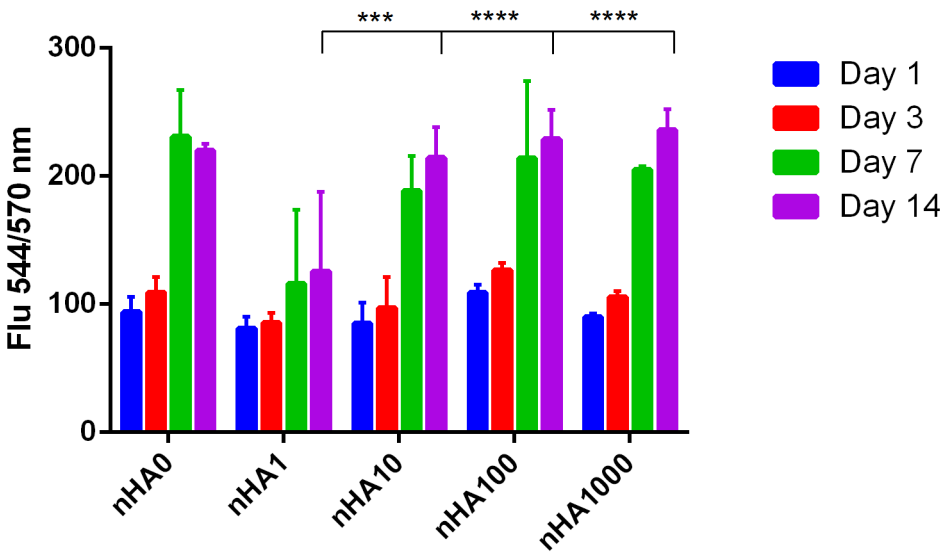

(b)

Figure 4.4: A comparison of cell proliferation of MG-63 cell lines using an alamar blue assay when in contact with nHA (a) under non-SMFs, (b) under SMFs. Without the exposure of SMFs, the nHA have a stimulating effect on the proliferation of cells when compared to the control samples, however, when further exposing them under SMFs, the effects of nHA on cell proliferation cannot be observed (n=3, $*p<0.05$, $**p<0.01$, $***p<0.001$, $****p<0.0001$)

toxic to the cells at higher concentrations for longer culture time.

Similarly, under the exposure of SMFs, nZnO demonstrated an unfavourable effect on cell proliferation. This further proved the toxicity of nZnO on MG-63 cell lines when embedded within collagen substrates.

4.5 Discussion

4.5.1 Effects of SMFs on Various Cell Lines

While a number of osteoblastic cell lines have been well characterised, few studies have directly compared their behaviour in order to determine their suitability for use in a tissue model. In this chapter, the proliferation behaviour of MG-63, UMR-106 and MC3T3-E1 cell lines were studied, with and without the exposure to SMFs. Enhanced proliferation of all MG-63, UMR-106 and MC3T3-E1 cells were demonstrated under SMFs. Indeed, the MG-63 cells respond to the SMFs most significantly when compared to the others, the proliferation of MC3T3-E1 cells were promoted steadily, whereas UMR-106 cells were not influenced much.

It was proposed that on the cell culture surfaces, the saturation density is influenced by the cell size. Smaller sizes of cells lead to high value of saturation density, therefore it was expected to have higher proliferation in smaller cells when compared to larger cells. A morphometric analysis of several osteoblastic cell lines from Pautke *et al.* [2004] indicated that the sizes of MG-63 cells were

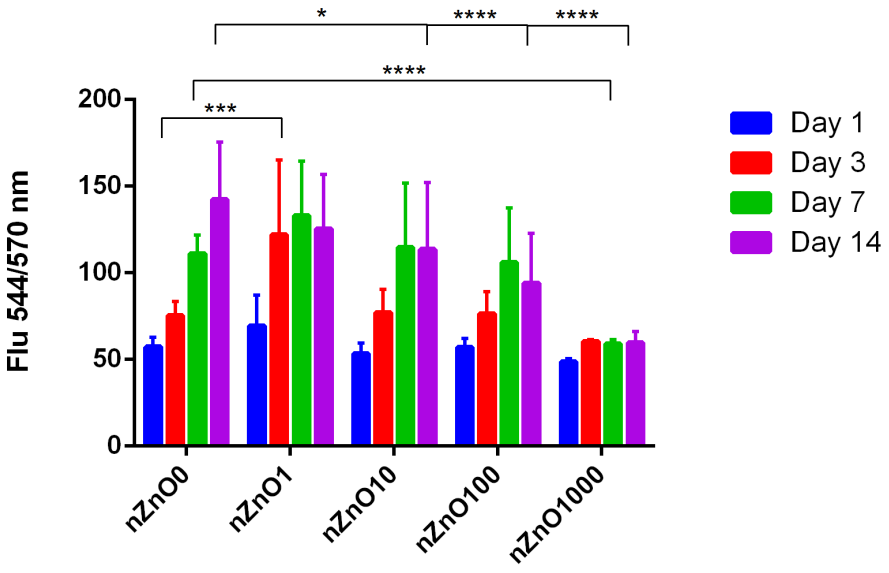

(a)

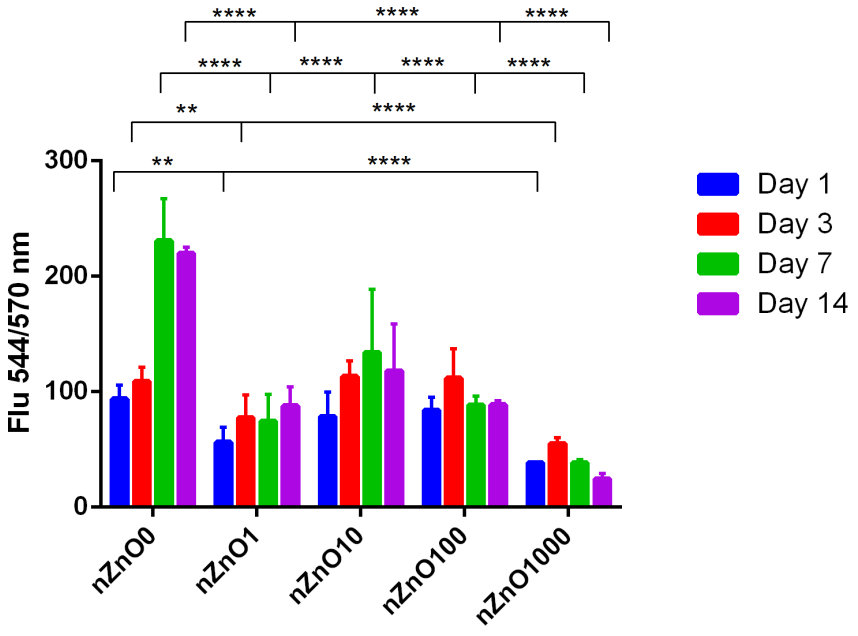

(b)

Figure 4.5: A comparison of cell proliferation of MG-63 cell lines from alamar blue assay when in contact with nZnO (a) under non-SMFs and (b) under SMFs. The incorporation of nZnO have an inhibition effect on MG-63 cells, especially at higher concentrations (n=3, $*p<0.05$, $**p<0.01$, $***p<0.001$, $****p<0.0001$).

smaller than that of MC3T3-E1 cells, therefore they tend to proliferate faster than other cell lines with bigger sizes. Furthermore, Czekanska *et al.* [2014] demonstrated that the MC3T3E1 cells have a similar proliferation behaviour as primary cells, whereas MG-63 cells proliferate much faster. Similar observations have also bee reported by Pautke *et al.* [2004]. This explains the higher proliferation of MG-63 when compared to the other two cell lines. When further exposing under SMFs, enhanced proliferation of all three cell lines were observed. Although contradictory results have been reported (as summarised in Chapter 1), the successful demonstration of the effects of SMFs on cell proliferation in this study are contributed to the magnetic field strength and the collagen/cell interactions. Previous studies were focused on 2D or synthetic polymeric scaffolds, whereas 3D collagen scaffolds were employed here.

Primary cells and different types of cell lines possess their own advantages and disadvantages when used as *in vitro* cell models. Primary cells undergo the same osteoblastic differentiation *in vivo*, therefore are the most representable cells for *in vitro* use, as well as clinical studies. However, they exhibit several disadvantages which limit their use. First of all, they have limited accessibility and have to be prepared under long and complex isolation procedures. Second, the primary cells normally contain heterogeneous phenotype which may complicate the model. In addition, primary cells are sensitive to donor related factors, such as age and gender, which may rise inconsistent results. Therefore cell lines have been widely applied on *in vitro* investigations. Cell lines are mostly used due to the availability of unlimited number of cells, ease of culturing and higher phenotypical stability comparing to primary cells [Kartsogiannis & Ng, 2004]. Moreover,

in the case of human derived cell lines, both normal and malignant, the concern about the effect of species differences can be avoided [Czekanska *et al.*, 2012]. One example can be found as MG-63 cell lines. They have been reported to exhibit no interspecies differences to human primary cells and express similar level of ALP and collagen deposition. However, they may proliferate much faster when compared to primary cells *in vitro*.

4.5.2 Effects of SMFs on 2D/3D Models

The effects of culturing cells in 3D collagen scaffolds have also been examined. Compared to the 2D monolayers, collagen scaffolds provide a 3D, ECM-like environment, which promote the cell growth significantly both with and without SMFs. Comparing to 2D monolayers, 3D plastic compressed collagen gels offered more advantages. First of all, collagen scaffolds are self-assembled from natural material. One of the advantages of using natural materials is that these molecules are naturally recognised by cells and are more likely to stimulate physiological responses in cells. Collagen, for example, has the structure same to the ECM of bone, hence can better simulate the migration, proliferation, remodelling of matrix of osteoblasts, which will be further discussed in Chapter 5. The other main advantage of collagen as a scaffold material is its properties as a 3D cell substrate. 3D *in vitro* collagen hydrogels models have the advantage of suspending collagen/cells in a tissue-like matrix, and also enables real-time assessment of the accessible construct. Plastic compressed collagen scaffolds provide the desired properties, including water retention capacity, nano/micro-porosity to allow cells

to grow and arrange in 3D, biodegradability, and pore inter-connectivity that would allow free flow of oxygen and nutrients [Dutta & Dutta, 2009]. Collagen can also provide cells with native tissue like environment, mechanical properties, topographical features and orientation cues.

4.5.3 Effects of SMFs on 3D Collagen Model with Various Bio-factors

The effects of adding in IONPs, nHA and nZnO particles into cell seeded collagen models have also been studied. Starting from the lowest nanoparticles concentration employed in this study, which was 1 μg/ml, IONPs demonstrate a stimulating effects on the proliferation of MG-63 cell lines, while this behaviour was not observed with nHA and nZnO incorporated samples. Similar conclusions can be drawn for the concentrations at 10 μg/ml. For concentrations beyond 100 μg/ml, the presence of nHA induced significantly enhanced cell proliferation, whereas nZnO still showed a toxic effect to cells. IONPs has a significant stimulating effect on cell proliferation under SMFs. As the concentration increased to 1000 μg/ml, IONPs and nZnO demonstrated toxic effects to cells while nHA significantly encouraged the cell growth. However, nHA do not respond to SMFs significantly.

When incorporating IONPs into the collagen scaffolds without SMFs, growth of MG-63 cell lines were enhanced up to a concentration of 100 μg/ml, which peaked at 100 μg/ml at 7 days culture. However, toxicity effects were observed

when a concentration of 1000 μg/ml was employed. By further employing exterior SMFs, a promoting effect on cell proliferation can be observed when in contact with IONPs, with the optimal concentration at 100 μg/ml. This suggests that the applied SMFs played a positive role on the cell proliferation.

IONPs smaller than 20 nm in size behave with superparamagnetic properties [Cornell & Schwertmann, 2003]. They are non-magnetic in the absence of an exterior magnetic field. Once exposed under an exterior magnetic field, they will be rapidly magnetised to saturation and respond to the exterior magnetic field to provide magnetic properties. When introduced into the scaffolds and exposed under SMFs, those particles can be attracted by the magnetic fields, leading to movements inside the scaffolds. Although been embedded inside the collagen gel, the particles tend to travel towards the magnetic poles, overcome the friction provided by the gels, resultant in a motion within the matrix. This motion caused by the particles can potentially affect the cell behaviours during cell/particles interactions. Therefore, due to the incorporation of IONPs, the SMFs is not only providing a static field, it will also create a dynamic environment to the cells. Besides, uncoated iron oxides are often negatively charged in water due to the adsorption of OH^- ions onto their surface. The resulting electric field may attract counter ions and hence promote protein adsorption [Mahmoudi *et al.*, 2010].

IONPs can be toxic to cells, and this is dependent on the concentration. For example, Naqvi *et al.* [2010] studied the toxicity of IONPs (30 nm). Their results indicated that IONPs do not show a toxicity effect at concentrations up to 100 μg/ml. By further increasing the concentration to 25-200 μg/ml, the cell viabil-

ity reduced to 95 %. When the IONPs concentrations were increased to 300-500 μg/ml, the cell viability further reduced to 55-65 %. In this study, the average size of the IONPs used was characterised to be 13 $\pm$ 5 nm (detailed characterisations are attached in Appendix), and the safe concentration was identified as 100 μg/ml. More importantly, this concentration can also promote cell growth. This is partially due the culturing system. The toxicity of IONPs at high concentrations can be explained as, the Cl^- ions that present in the cell culture medium can bind to the Fe ions, thus altering the pH of the medium together with the surface characteristics of the nanoparticle. Such interactions with the cell culture medium, resulting in alterations in the ionic concentration and protein function, may cause cell detachment and subsequently may lead to cell death [Mahmoudi *et al.*, 2010].

By adding in nHA into the collagen scaffolds without SMFs, cell proliferation can be enhanced at various concentrations up to 1000 μg/ml. This confirmed the stimulating effect of nHA on osteoblasts. Studies by San Thian *et al.* [2008] demonstrated that, by seeding human osteoblasts on nHA coated surfaces, the number of cells growing increased with culturing time and tended to multiply significantly. When samples were further exposed under SMFs, a slightly higher proliferation can be observed when compared to non-SMFs treated samples. This suggests that the exterior SMFs have a beneficial effect on stimulating the cell proliferation in collagen scaffolds, but the effect was limited. This results can be validated by Zeng *et al.* [2012]. Their study investigated the effects of exterior magnetic field on MC3T3-E1 cells when in contact with IONPs and HA. Results indicated that HA particles have no observable influence on the cell proliferation

under magnetic fields, whereas this stimulating effect was magnified in the presence of IONPs.

Moreover, results demonstrated that nZnO with a concentration higher than 10 μg/ml are toxic to the MG-63 cell lines. It can be concluded that the nZnO can only stimulate MG-63 cell growth at a low concentration, whereas being toxic to the cells at a high concentration. Similarly, under the exposure of SMFs, nZnO shows an unfavourable effect on cell proliferation. This further proved the toxicity of nZnO on MG-63 cell lines when embedded within collagen substrates. In the study of Bai *et al.* [2010], they demonstrated the toxicity of nZnO at concentrations of 50 - 100 μg/ml. In addition, Heng *et al.* [2010] found that nZnO is toxic to human bronchial epithelial cells (BEAS-2B) above a concentration of 10 μg/ml, and this result also agreed with the study from Xia *et al.* [2008]. The enhancement of cell proliferation when in contact with nZnO (on 2D substrates) have been observed by Memarzadeh *et al.* [2015]. Therefore, due to the biocompatibility of nZnO (at low concentrations) and the well-established antimicrobial properties, a controllable concentration of nZnO can be suggested as an antimicrobial agent in the scaffold.

4.6 Summary

Different cell types possess different properties, and they all have advantages and disadvantages when used as *in vitro* cell models. Their use should be limited to appropriate and specific research questions with careful extrapolation of results,

rather than as widespread use for recapitulating general bone biology and disease as is currently the case [Czekanska *et al.*, 2012]. MG-63, UMR-106 and MC3T3-E1 cells all respond to SMFs by increasing proliferation. Among which, MG-63 cells have the highest proliferation when compared to the others. When further incorporating IONPs, nHA and nZnO, a stimulating effect of IONPs incorporated scaffolds can be observed under SMFs, up to a concentration of 100 μg/ml. nHA can encourage the cell proliferation without the exposure of SMFs, with no significant improvements under SMFs. nZnO demonstrates the lowest stimulating effects on cell proliferation, while being toxic to the cells at concentrations above 10 μg/ml. Therefore, 100 μg/ml of IONPs were considered as the optimal bio-factor to be added into the PC scaffolds for the evaluation of SMFs *in vitro*. Apart from being a tissue model, this system developed here can also serve as a novel scaffold for cell stimulation applications.

Chapter 5

Cellular and Molecular Evaluation of the 3D Collagen Model under Static Magnetic Fields

5.1 Overview

In 1986, Cowin [1986] firstly hypothesised that bone remodels in response to stress and strain through mechanotransduction (further details can be found in Chapter 1). This process involves the conversion of a biophysical force into a biochemical response leading to changes in gene expression and cellular adaptation. Based on the principle of mechanotransduction, magnetic stimulation has been proposed for the applications of bone regeneration and fracture non-union.

SMFs have been demonstrate to have the ability to influence a number of biological functions in osteoblasts, such as proliferation, differentiation, extra-

cellular matrix synthesis and mineralisation [Cai *et al.*, 2015; Chiu *et al.*, 2007; Meng *et al.*, 2013; Rosen, 2003]. However, despite the success of SMFs stimulations with several *in vitro* studies, there remains a concern that bone responds to dynamic rather than static loading, it is believed that the stimulation is related to the peak strain magnitude and the loading frequency [Rubin & Lanyon, 1985]. Therefore in many studies related to the SMFs stimulation, the promotion effect on cell proliferation were not observed [Chionna *et al.*, 2003; Chiu *et al.*, 2007; Cunha *et al.*, 2012; Imaizumi *et al.*, 2007]. However, the cell behaviours are not only dependent on external physical stimulations, it is also dependent on the effect of other biochemical cues, as well as cell/ECM interactions. One hypothesis is that the proliferation (as well as other cell behaviours, such as differentiation and mineralisation) of osteoblasts can be stimulated when embedded inside the 3D bio-mimic collagen matrix, with the incorporation of additional IONPs, under the exposure of SMFs. The mechanisms at molecular levels are also of interest to be investigated. The hypothesis of the mechanisms is that, SMFs can affect the reorientation of cell membrane phosphilipids, as well as the cell/matrix interactions, hence activate the calcium ion channels in the cell membrane, encouraging more calcium ion flux. During the interaction, the expression of Runx2, ON, BMP-2 and BMP-4 can be stimulated by the combination of SMFs, IONPs and dense collagen matrix, leading to an enhancement of the osteoblastic differentiation process.

The objectives of this chapter are described as below. The effects of SMFs, the collagen matrix and the incorporation of IONPs on the osteogenesis process of MG-63 cell lines were studied firstly, this includes the examination of cell prolif-

eration by alamar blue (AB) assay, the measurement of alkaline phosphatase production by ALP assay, and then the assessment of cell mineralisation by alizarin red s (ARS) staining. The next focus was to understand the mechanisms of SMFs and IONPs on osteogenesis at molecular levels. Firstly, the expression of several key genes, Runx2, ON, BMP-2 and BMP-4 will be investigated by PCR study. Secondly, the histology of the cells/matrix exposed under SMFs will be evaluated. Furthermore, a detailed microstructural analysis of the cell/ECM interaction will be examined under TEM.

5.2 Cell Proliferation

The proliferation of MG-63 cells was tested by alamarBlue assay. The cells were cultured for 1, 3, 7 and 14 days, under four conditions, with/without the exposure of SMFs, and with/without the incorporation of IONPs. The results are shown in Figure 5.1. From day 1, the incorporation of IONPs, the exposure of SMFs and both jointly all had stimulating effect on cell proliferation, and this effect continued until day 7. After 7 days, the cell proliferation with treatments almost doubled to that found at day 1. This indicates the that the SMFs and IONPs had a significant influence on the cell proliferation during day 1 and day 7. However, when further cultured up to 14 days, the SMFs or IONPs alone did not have significant impact on cell proliferation when compared to that at day 7. However, it was observed that the proliferation of the cells incorporated with IONPs and exposed to SMFs was up-regulated after 14 days.

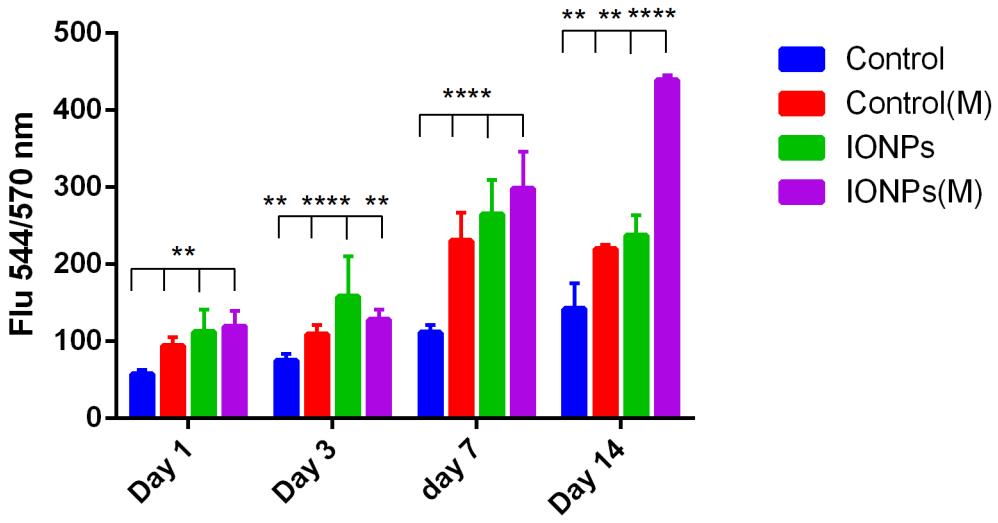

Figure 5.1: A comparison of cell proliferation of MG-63 cells when cultured within collagen scaffolds with/without the incorporation of IONPs, with (M) and without the exposure of SMFs. Cell proliferation can be enhanced under SMFs with the incorporation of IONPs, indicating a stimulating effect (n=3, $*p<0.05$, $**p<0.01$, $***p<0.001$, $****p<0.0001$).

5.3 Cell Differentiation

Alkaline phosphatase (ALP) activities of collagen scaffolds with/without SMFs, and with/without the incorporation of IONPs were determined. As shown in Fig 5.2, no significant effect of SMFs, IONPs or a combination on ALP production can be observed up to 14 days. By exposure to SMFs for 21 days, the ALP production of the cells was up-regulated compared to the control, whereas little difference was found with the incorporation of IONPs alone. When further combining the effect of IONPs and SMFs, the ALP production was significantly stimulated.

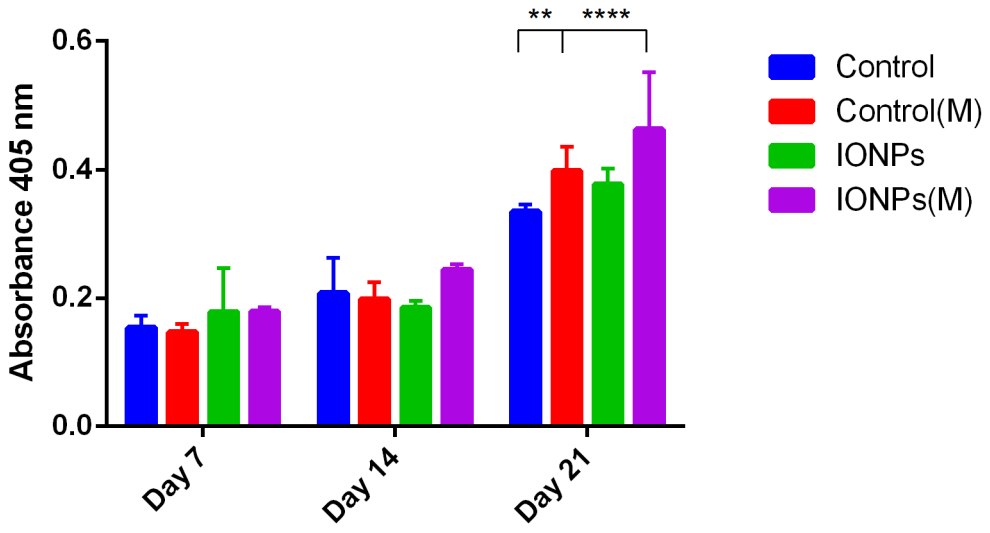

Figure 5.2: A comparison of cell differentiation using the ALP assay with (M) and without SMFs exposure. Cell-loaded collagen scaffolds were incorporated with IONPs with a concentration of 100 μg/ml, results were collected at 7, 14 and 21 days of culture time. The combination of SMFs and IONPs stimulates the ALP production of the cells (n=3, $*p<0.05$, $**p<0.01$, $***p<0.001$, $****p<0.0001$).

5.4 Cell Mineralisation

Figure 5.3a, 5.3b, 5.3c, 5.3d, 5.3e and 5.3f represent the ARS staining results of cell-seeded collagen scaffolds with and without SMFs. As can be observed in Fig 5.3a and 5.3b, the scaffolds were not stained at day 1, indicating the absence of mineralisation. At day 21, early mineralisation can be observed in both samples, more significantly in those samples which received the SMFs treatment (shown in Fig 5.3c, 5.3d). After 6 weeks, the mineralisation was observed with all samples, as shown in Fig 5.3e, 5.3f. At this time point, significant differences were not observed. ARS staining was also applied to the collagen scaffolds which incorporated IONPs, as shown in 5.4a, 5.4b, 5.4c, 5.4d, 5.4e and 5.4f. At day 1, mineralisation was not observed for both conditions. After 21 days, significant differences in the degree of mineralisation was identified, with a higher level for scaffolds treated with SMFs. After 42 days, all samples were fully stained by ARS, indicating complete mineralisation. Quantification of mineralisation was accomplished by using ARS extraction as shown in Fig 5.5. Results indicated that SMFs can induce early mineralisation *in vitro*, with more significant simulation when IONPs were incorporated. After 42 days, extraction levels remained, indicating that the SMFs and IONPs were not able to promote mineralisation at this period.

The quantification of mineralisation was accomplished by using ARS extraction, with the difference in absorbance shown in Fig 5.5. Results indicated that SMFs can induce early mineralisation *in vitro*, with more significant simulation when incorporating the IONPs. After 42 days, the extraction remains at similar levels, indicating that all samples achieved complete mineralisation.

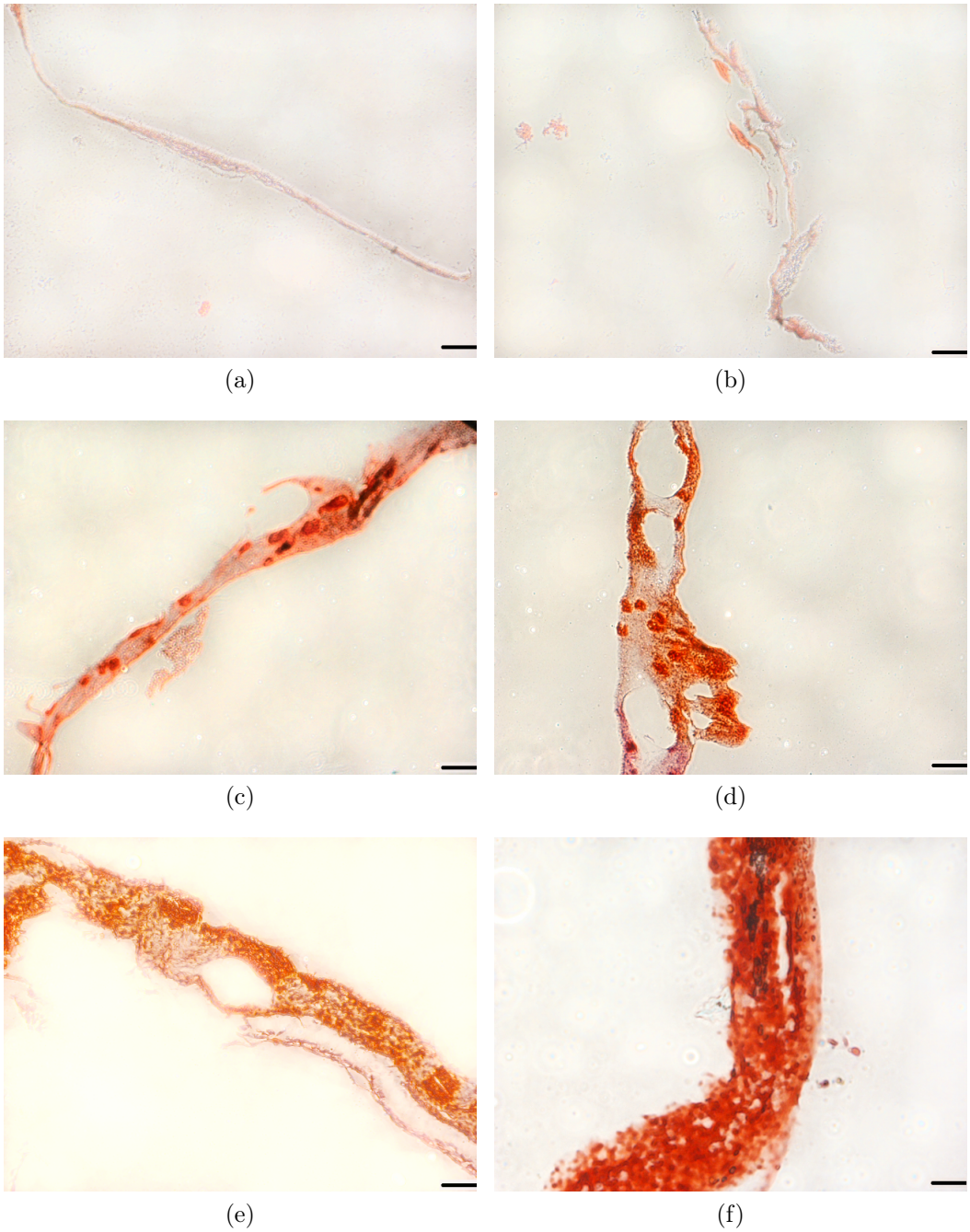

(a) (b) (c) (d) (e) (f)

Figure 5.3: A comparison of cell mineralisation by ARS staining of collagen scaffolds at day 1 (a) without SMFs, (b) with SMFs, collagen scaffolds at day 21 (c) without SMFs, (d) with SMFs, and collagen scaffolds at day 42 (e) without SMFs, (f) with SMFs (n=3). Scale bar = 100 μm.

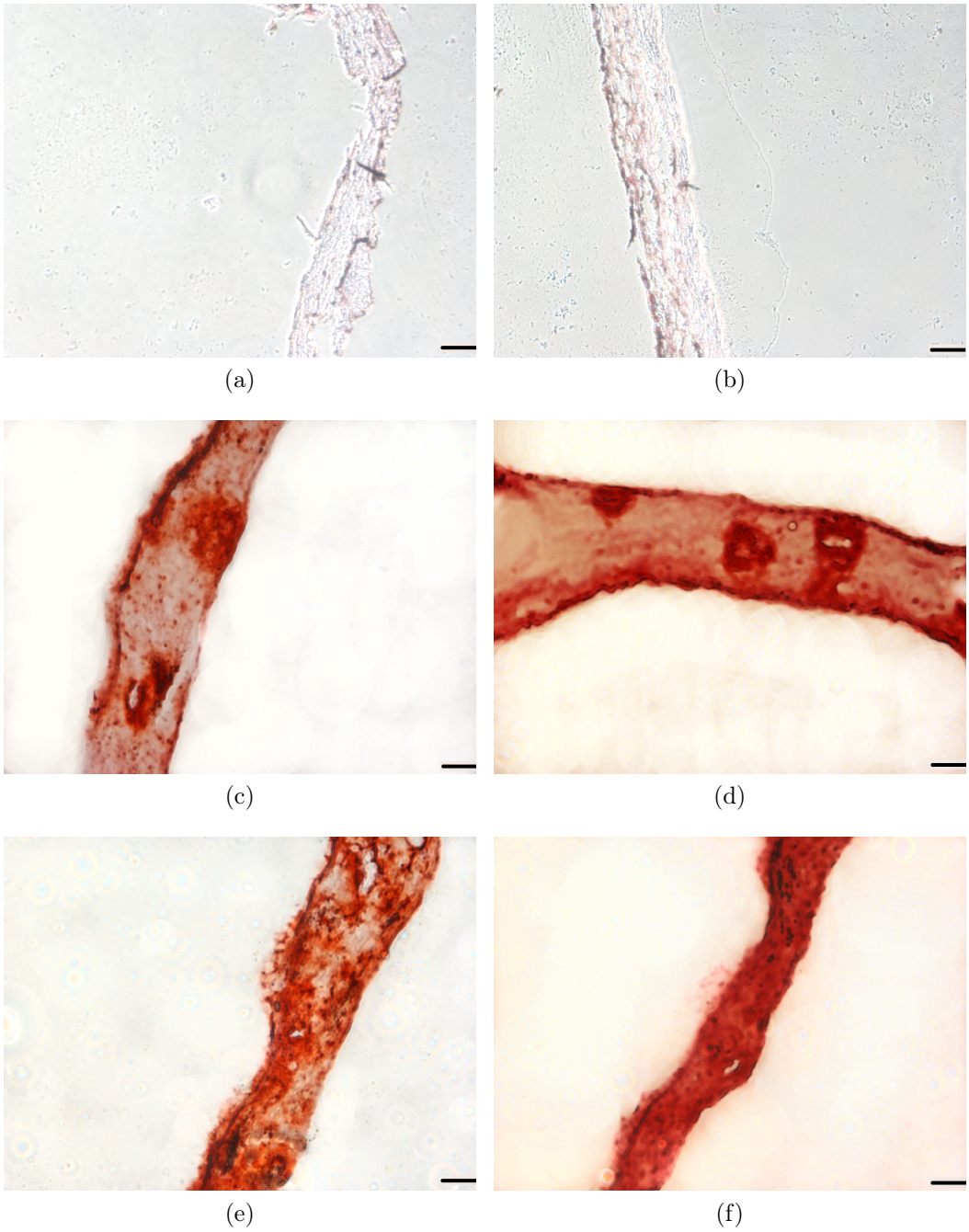

Figure 5.4: A comparison of cell mineralisation by ARS staining of IONPs incorporated collagen scaffolds at day 1 (a) without SMFs, (b) with SMFs, collagen scaffolds at day 21 (c) without SMFs, (d) with SMFs, and collagen scaffolds at day 42 (e) without SMFs, (f) with SMFs (n=3). Scale bar = 100 μm.

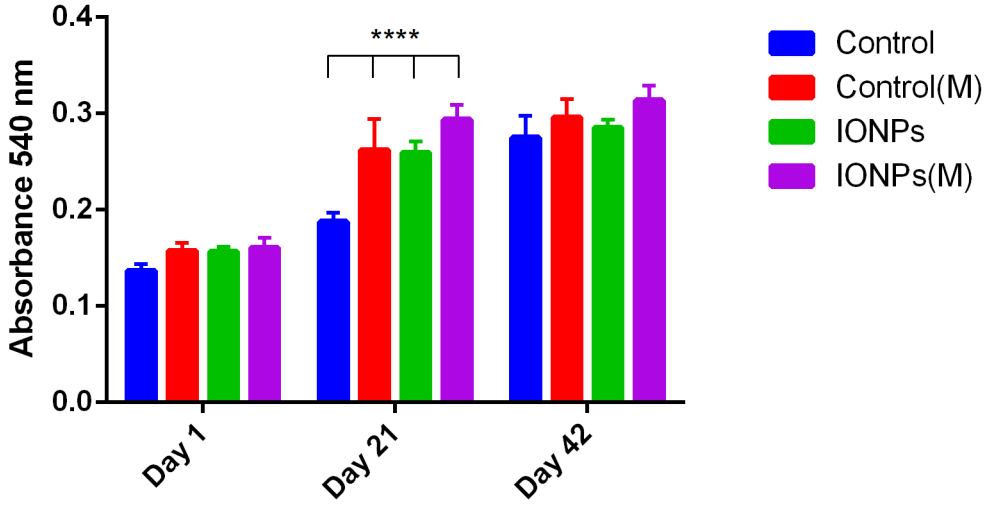

Figure 5.5: A comparison of cell mineralisation by extracting and quantifying ARS staining from scaffolds treated with (M) and without SMFs exposure (n=3, $*p<0.05$, $**p<0.01$, $***p<0.001$, $****p<0.0001$). Cell-loaded collagen scaffolds were incorporated with IONPs with a concentration of 100 μg/ml, results were collected at 1, 21 and 42 days of culture time.

5.5 RNA Extraction

The total mRNA of samples cultured for 1, 7 and 14 days were isolated following a standard protocol. Due to the low amount of RNA produced by samples cultured for 1 day, this was not sufficient for quantifying. The mRNA yields (ng/μl) were plotted against sample types and presented in Figure 5.6. After 7 days, the effects of SMFs, IONPs alone, and the combination on the mRNA production can be seen. The combination of SMFs and IONPs appear to have the strongest influence, however, due to large deviations, the results are not sufficient to prove the effects of IONPs and SMFs on RNA production. With a time increased to 14

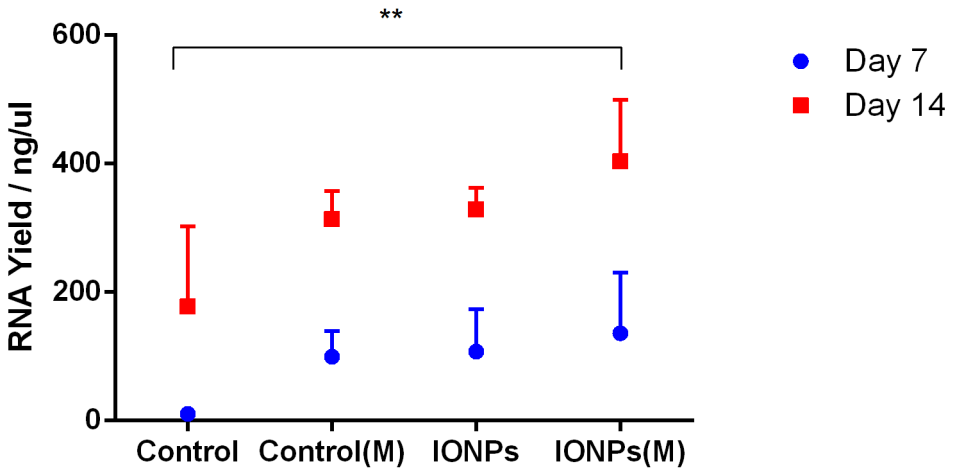

Figure 5.6: Total RNA isolated against samples with(M)/without SMFs, and with/without the incorporation of IONPs (n=3, ∗p<0.05, ∗∗p<0.01, ∗∗∗p<0.001, ∗ ∗ ∗∗p<0.0001). The combination of SMFs and IONPs has a stimulating effect of the total mRNA production of osteoblasts-seeded collagen scaffolds.

days, significant influences of SMFs and the combination of both can be observed, with a smaller standard deviation.

5.6 Gene Expression : Real-time Polymerase Chain Reaction

To understand the responses of cell-seeded collagen scaffolds to IONPs and SMFs at the molecular level, the expression of Runx-2, ON, BMP-2 and BMP-4 were investigated by PCR. The expression of Runx2 normalised to GAPDH are illustrated in Figure 5.7. A 7 day treatment of SMFs alone had no significant effect on the expression of Runx2, whereas increased expression can be found in the SMFs and IONPs treated samples. After 14 days, the expression of Runx-2 in

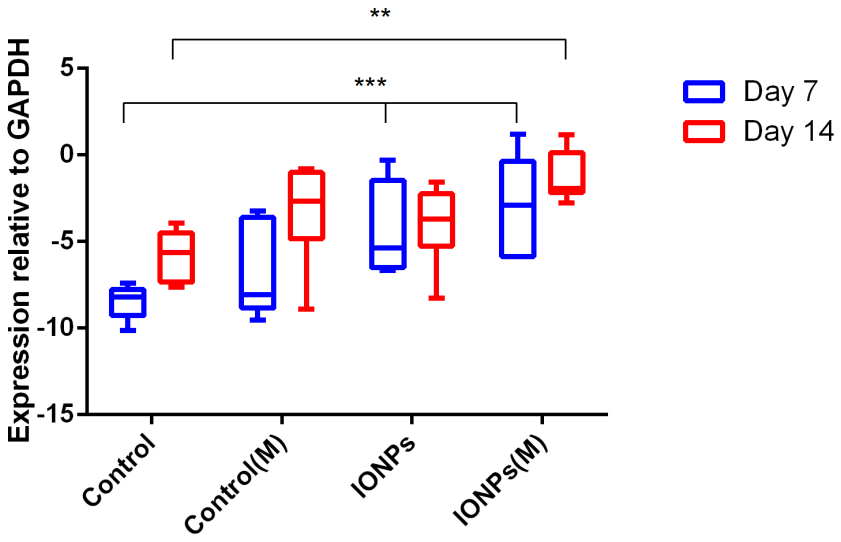

Figure 5.7: Relative expression of Runx2 normalised to GAPDH after 7 and 14 days of culture. Samples were cultured with(M)/without SMFs, and with/without the incorporation of IONPs (n=3, $*p<0.05$, $**p<0.01$, $***p<0.001$, $****p<0.0001$).

the control sample increased with increasing culture time. This demonstrates the collagen matrix can mediate the Runx-2 expression during osteogenesis. When compared to the controls, continuous treatment of both SMFs and IONPs enhanced the expression of Runx2, whereas this effect cannot be observed with IONPs or SMFs alone.

The expression of ON normalised to GAPDH is illustrated in Figure 5.8. As can be observed, after 7 days, the level of ON expression in the samples treated with IONPs, SMFs and both are higher than that in the control. Particularly, for the SMFs and IONPs combination treatment, the level of expression was the most enhanced. After 14 days, all samples treated with different conditions were increased to a similar level, and there were no significant differences between

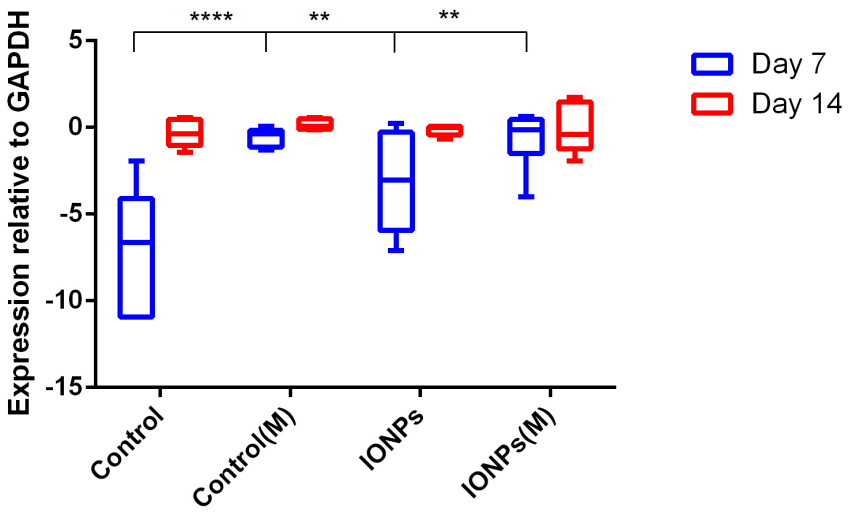

Figure 5.8: Relative expression of Osteonectin normalised to GAPDH after 7 and 14 days of culture. Samples were cultured with(M)/without SMFs, and with/without the incorporation of IONPs (n=3, $*p<0.05$, $**p<0.01$, $***p<0.001$, $****p<0.0001$).

samples. This shows that SMFs and IONPs can only enhance the expression of ON within a short time period, and have no significant influence for longer time periods.

Figure 5.9 and 5.10 represent the expression of BMP-2 and BMP-4, respectively. When cultured for 7 days, the expression of BMP-2 in collagen, treated with IONPs and SMFs alone, remained at a similar level to the control. However, when treated with both IONPs and SMFs, significant enhancement was observed when compared to the control. After 14 days, the expression of BMP-2 in the control sample did not increase with time, whereas the effect of the combination of IONPs and SMFs was significant. This shows the combination treatment can stimulate the expression of BMP-2 in collagen scaffolds. For BMP-4, the

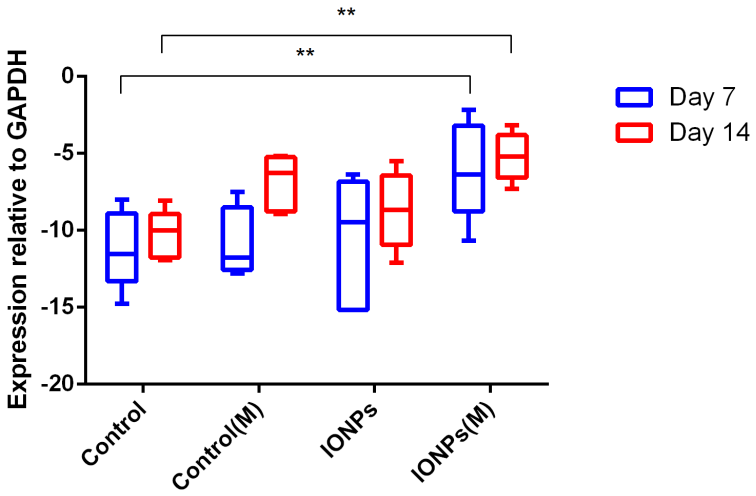

Figure 5.9: Relative expression of BMP-2 normalised to GAPDH after 7 and 14 days of culture. Samples were cultured with(M)/without SMFs, and with/without the incorporation of IONPs (n=3, $*p<0.05$, $**p<0.01$, $***p<0.001$, $****p<0.0001$).

treatment with SMFs did not affect the expression significantly, whereas the incorporation of IONPs, and further exposure to SMFs, the expression of BMP-4 increased significantly. The collagen scaffold itself may favour the production for a short period (7 days), while this effect was not observed for a longer time duration up to 14 days. The addition of IONPs or SMFs alone did not promote the expression any further, whereas when combined together, an enhancement can be observed up to 14 days. This demonstrates that the combination of IONPs and SMFs have a strong positive influence on BMP-4 expression. It is also of interest to note that the overall expression of BMP-4 was higher than that of BMP-2.

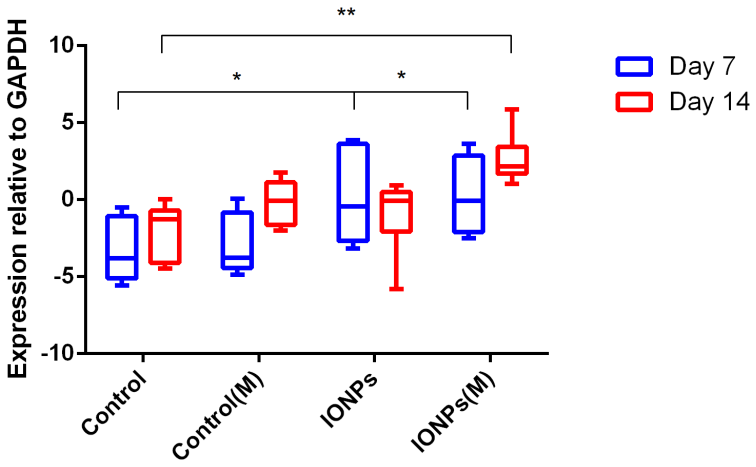

Figure 5.10: Relative expression of BMP-4 normalised to GAPDH after 7 and 14 days of culture. Samples were cultured with(M)/without SMFs, and with/without the incorporation of IONPs (n=3, ∗p<0.05, ∗∗p<0.01, ∗∗∗p<0.001, ∗ ∗ ∗∗p<0.0001).

5.7 Cellular Responses

In order to examine the cellular responses of the cells embedded in the 3D scaffolds, histology samples were prepared and stained with H & E. Three different sections were cut from each sample and examined with two magnifications (10X and 40X). The cell numbers in each image were counted and plotted with average number and standard deviation (n=3). Images were analysed by image analysis software (Image J) to quantify cell numbers. Cellular responses of compressed collagen gels seeded with MG-63 cell lines were obtained after 1, 3, 7 and 14 days of culture. As can be observed from Figures 5.11a, 5.11c, 5.11e and 5.11g, an increase in cell number was found over time, with fibrous collagen structure and healthy attached cells shown. As for the samples treated with SMFs, which are presented in Figures 5.11b, 5.11d, 5.11f and 5.11h, cells multiply over time. When further compared to the non-SMFs condition, a significant increase in cell

number can be observed after 3 days. This can be regarded as a validation of the cell proliferation measured by AB assay, that SMFs have a stimulating effect on the proliferation of MG-63 cell lines. The IONPs incorporated collagen scaffolds were then sectioned and stained. Figure 5.12a, 5.12c, 5.12e and 5.12g reveal the cross-section of the scaffolds cultured without the presence of SMFs, and Figure 5.12b, 5.12d, 5.12f and 5.12h represent the scaffolds cultured under SMFs. Cell number counted from these microscope images (shown in Figure 5.13) increased with increasing culture time, with higher counts shown under SMFs. This finding agrees with the AB assays that MG-63 cell lines were able to proliferate when in contact with IONPs and SMFs, indicating a stimulating effect.

5.8 Microstructure of the Cell-Seeded Magnetic Collagen Scaffolds

The microstructure of the cell loaded collagen scaffolds was examined after 1, 7 and 14 days under TEM. Figure 5.14a, 5.14b, 5.14c and 5.14d represent the results from day 1. As can be observed, when compared to the controls, there are no major changes in the cell shape or collagen structure with exposure to SMFs or incorporating IONPs. This could potentially be due to the early stage of treatment. Besides, the incorporation of IONPs can be identified, as being found inside the cell in either agglomerated or separated state, close to the cell membrane or inside the collagen fibrils (shown in Figure 5.15a, 5.15c, 5.15d and 5.15b).

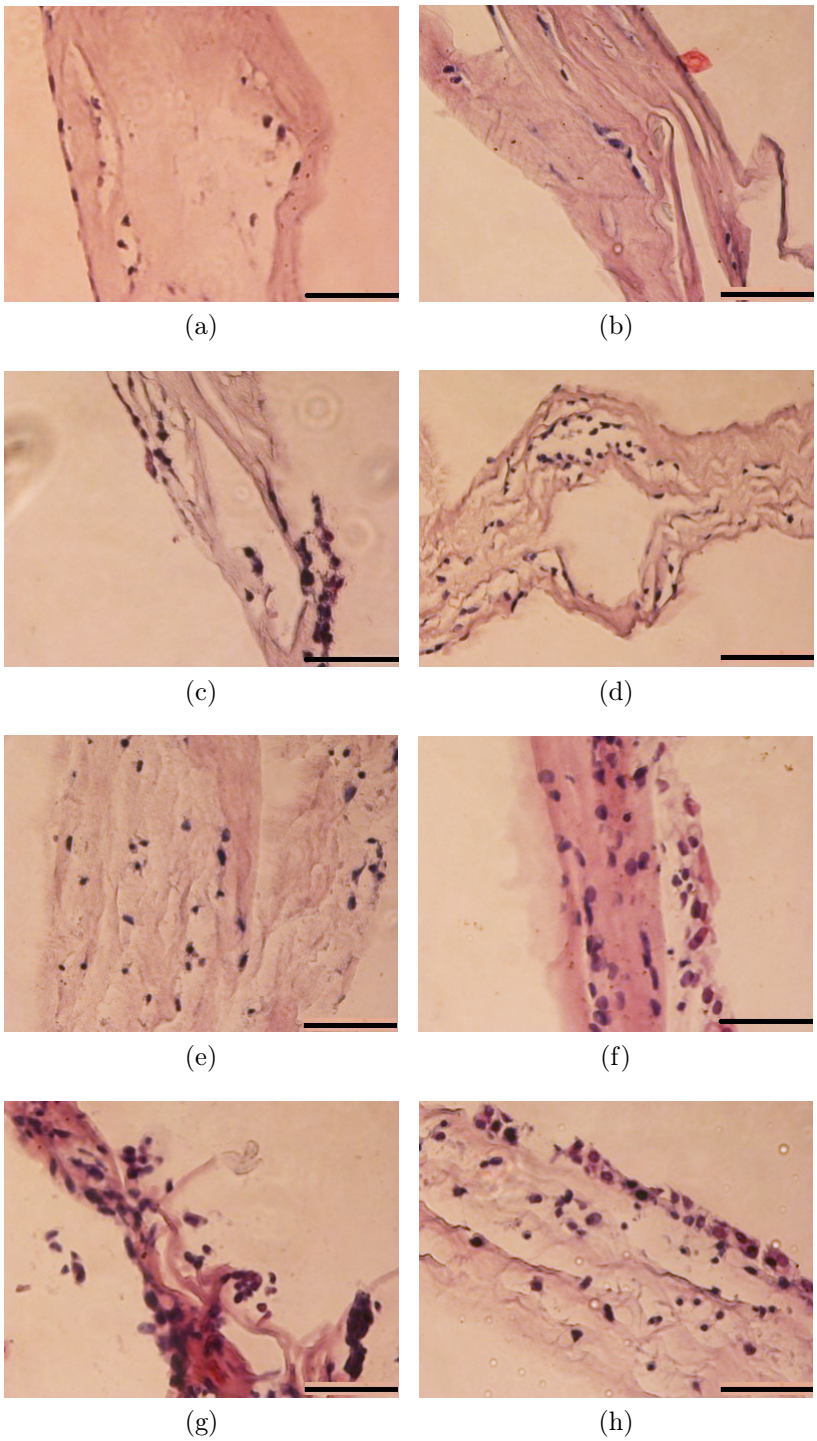

Figure 5.11: The effects of SMFs on cellular responses by histology at (a) (b) day 1, (c) (d) day 3, (e) (f) day 7 and (g) (h) day 14 without and with SMFs, respectively (n=3). Higher cell numbers were observed under SMFs, indicating a stimulating effect. Scale bar = 100 μm.

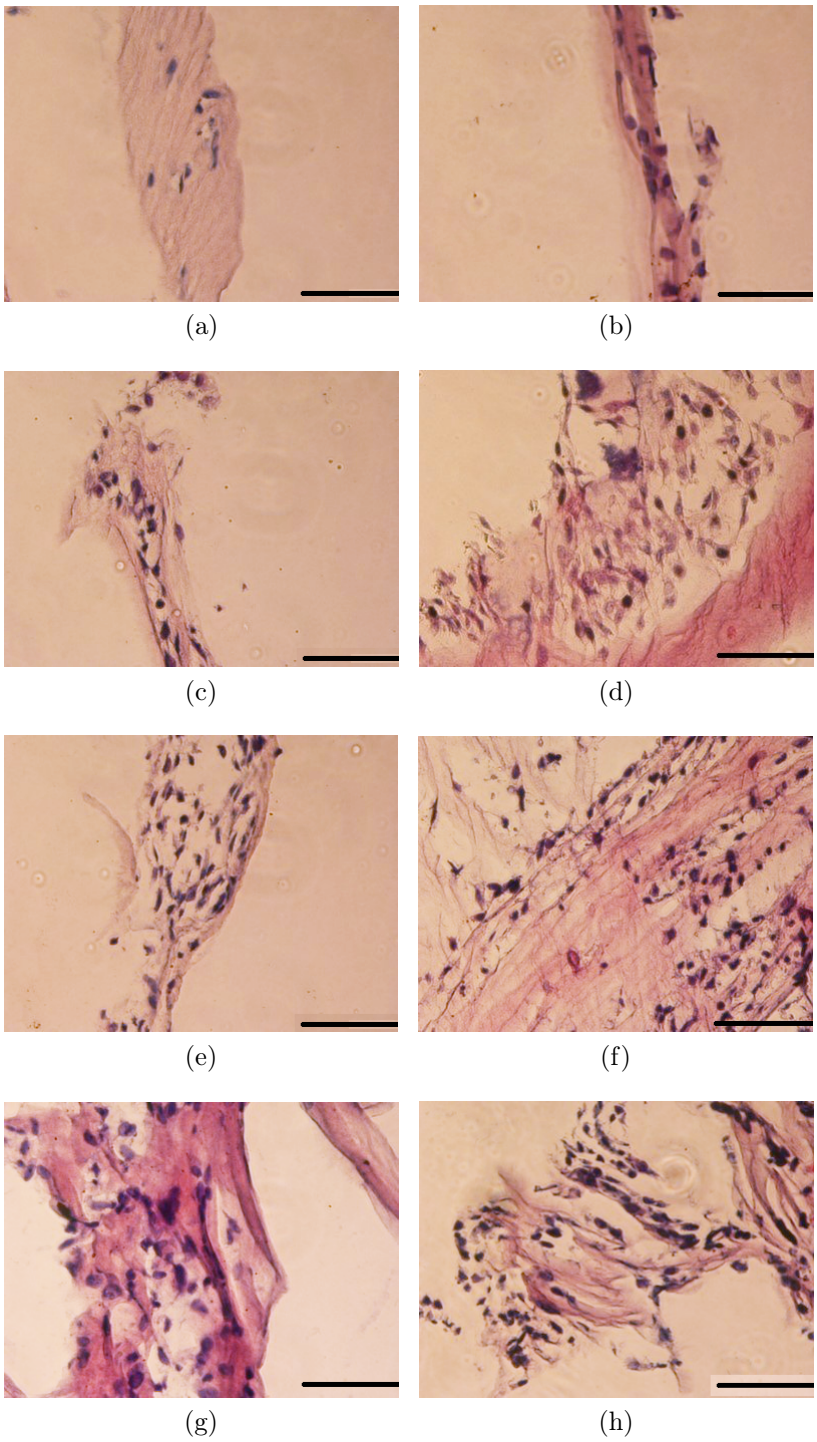

Figure 5.12: The effects of IONPs on cellular responses by histology at (a) (b) day 1, (c) (d) day 3, (e) (f) day 7 and (g) (h) day 14 without and with SMFs, respectively (n=3). Scale bar = 100 μm.

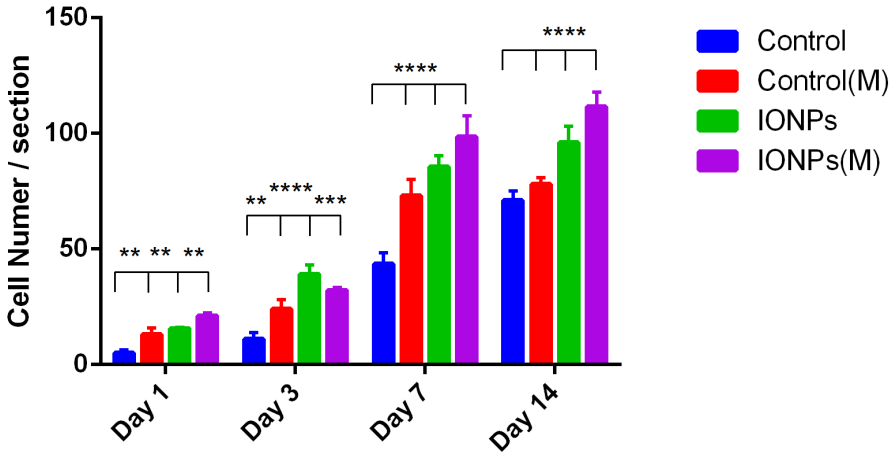

Figure 5.13: A comparison of cell number of MG-63 cell lines from histology for IONPs with and without SMFs. The cell number represents the average from three sections of one sample. By incorporating additional IONPs, the cell proliferation can be further enhanced (n=3, $*p<0.05$, $**p<0.01$, $***p<0.001$, $****p<0.0001$).

After 7 days, the change in cell/collagen matrix interactions can be observed, as shown in Figure 5.16a, 5.16b, 5.16c and 5.16d. Under the exposure by SMFs, the orientations of collagen fibres were affected. The fibres under SMFs show no preferred direction, some of the fibres remain in the same direction with the cells, whereas others tend to be perpendicular to the cells (indicated by red lines). This re-orientation could be caused by the SMFs. It is also worth noting that the incorporation of IONPs had a minimal effect on the re-orientation of the collagen fibres.

The microstructure of cell-seeded scaffolds after 14 days are presented in Figure 5.17a, 5.17c, 5.17b and 5.17d. For the scaffolds treated with SMFs, it can be observed that new matrices were built up around the cell membranes. Besides, a

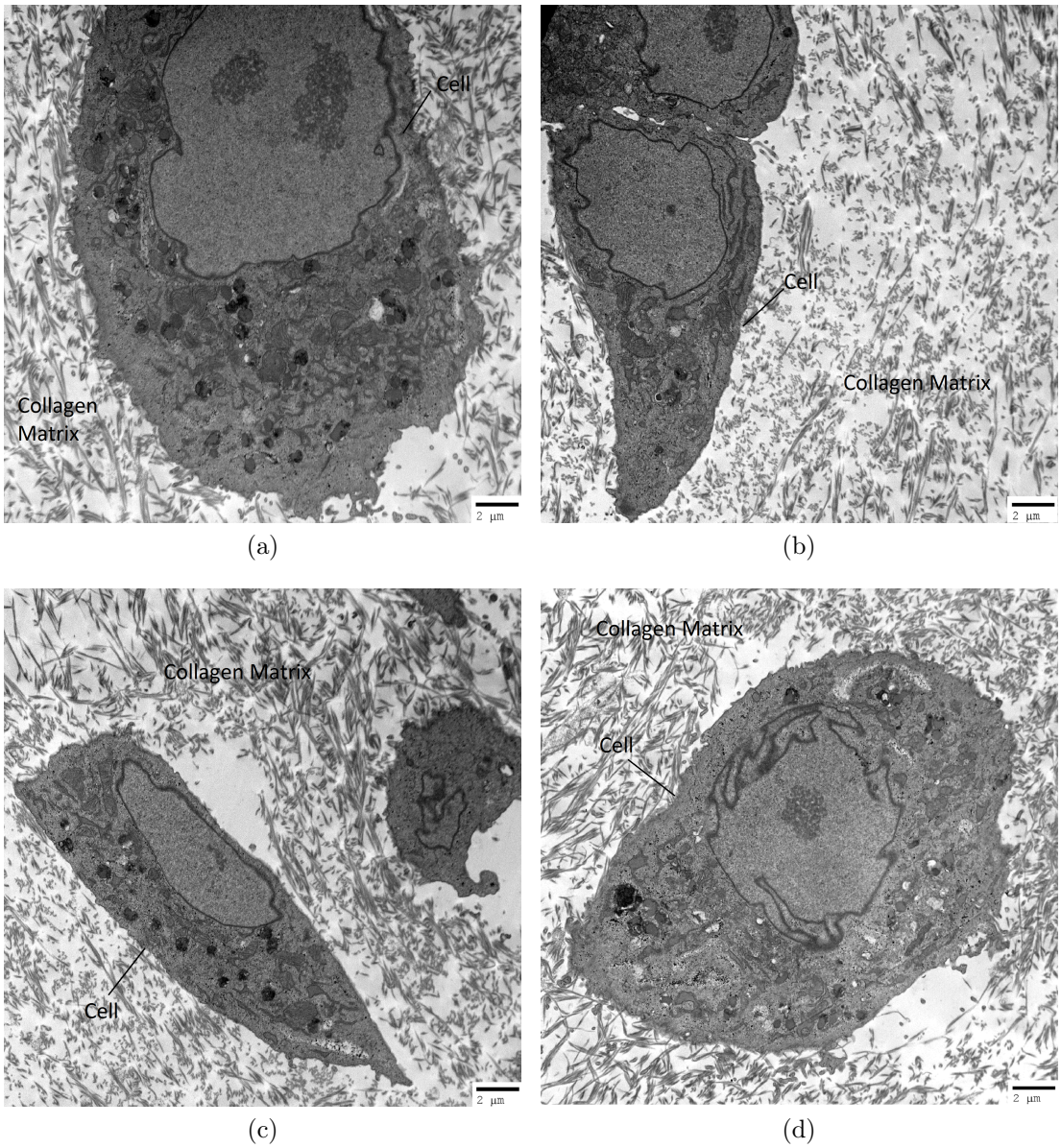

Figure 5.14: Microstructure of cell loaded collagen scaffolds examined under TEM at day 1. (a) collagen scaffolds without SMFs, (b) collagen scaffolds with SMFs, (c) collagen scaffolds incorporated with IONPs without SMFs and (d) collagen scaffolds incorporated with IONPs with SMFs. The incorporation of IONPs can be identified within the cell, at the edge of the cell membrane and inside the collagen fibrils.

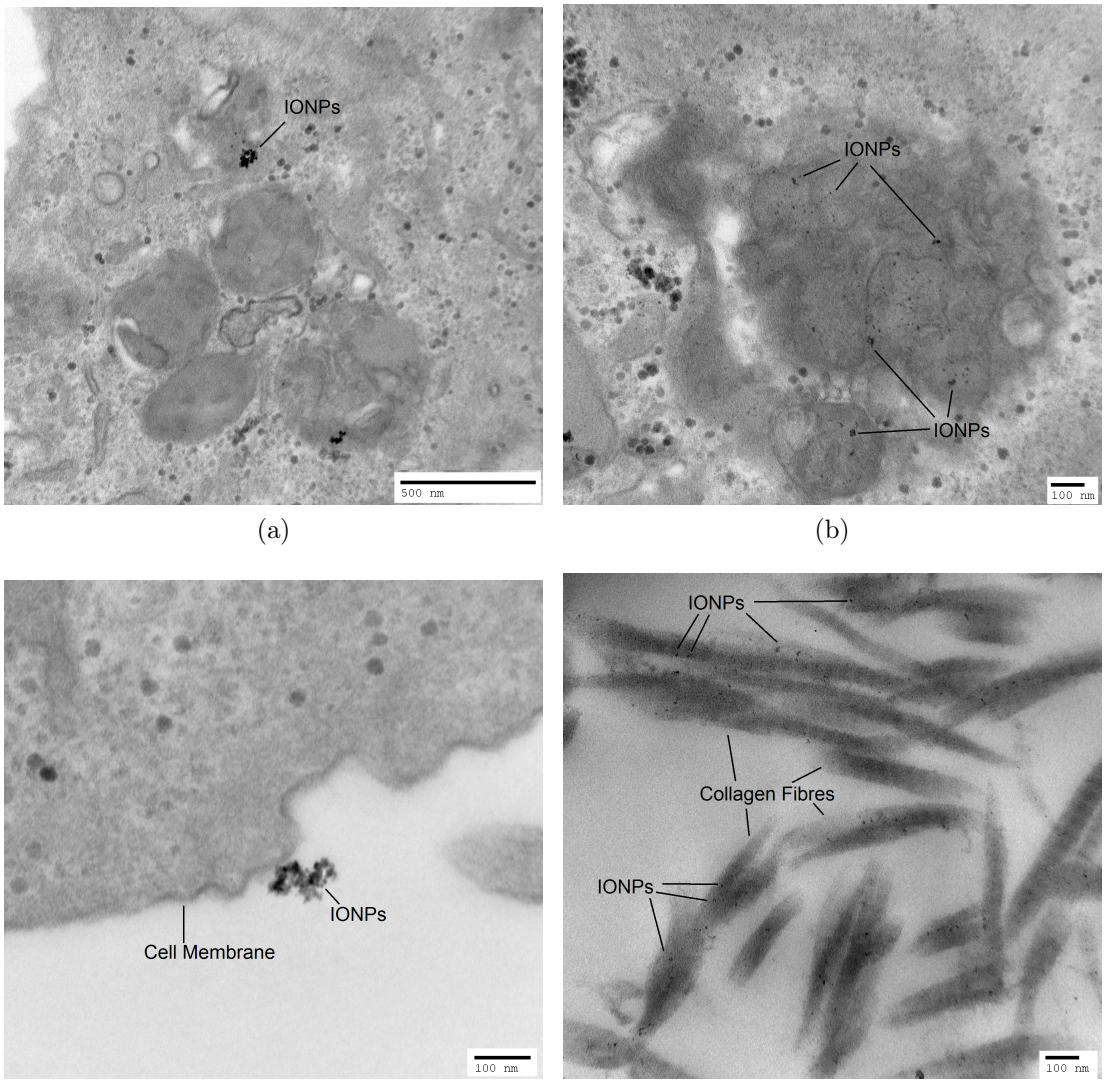

Figure 5.15: Microstructure of cell loaded collagen scaffolds examined under TEM at day 1. IONPs (a) agglomerate inside the cell, (b) spread out inside of the cell, (c) near the cell membrane and (d) trapped inside the collagen fibrils.

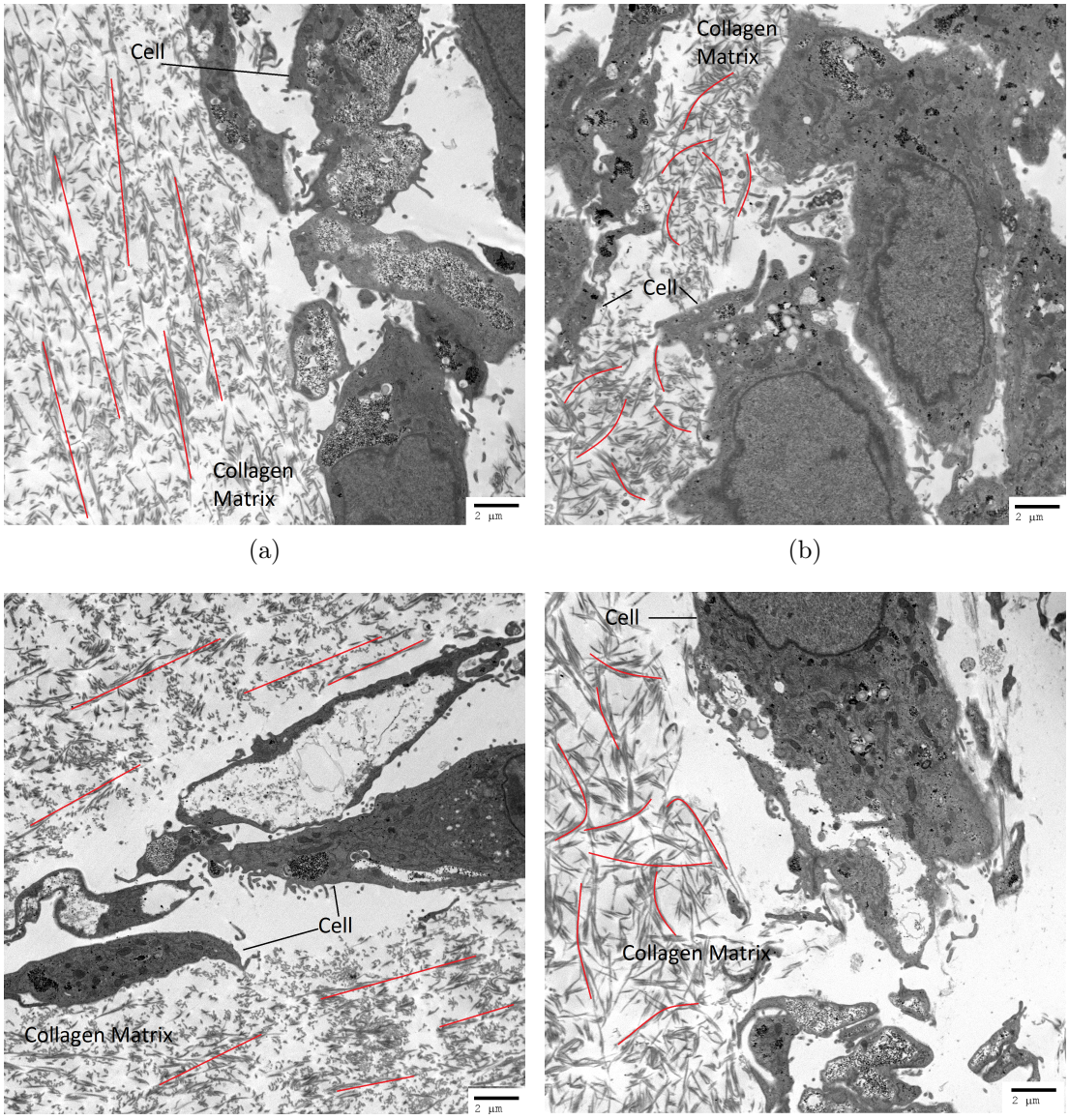

Figure 5.16: Microstructure of cell loaded collagen scaffolds examined under TEM at day 7 (a) collagen scaffolds without SMFs, (b) collagen scaffolds with SMFs, (c) collagen scaffolds incorporated with IONPs without SMFs and (d) collagen scaffolds incorporated with IONPs with SMFs. A change in the orientation of the collagen matrix can be observed.

more clear relationship between the collage orientation can be obtained (Figure 5.18a and 5.18b), that the reorientation of collagen fibrils were caused by SMFs. In order to identify whether this effect is directed by the direction of cells or vice versa, microstructural analysis of collagen gels without the incorporation of cells were investigated under SEM, as shown in Figure 5.19a and 5.19b. As can be observed (indicated by red lines), without the exposure of SMFs, the collagen fibrils experienced no preferred direction, but each of the fibre is straight and stretched. However, when exposed under SMFs, the orientation of the matrix was rotated, the fibres were in a relaxed format and tended to agglomerate into circles.This demonstrates that the re-orientation of the collagen fibres is due to the external SMFs, and not the cell regulation.

5.9 Discussion

5.9.1 Effects of SMFs on Cell Proliferation

The effects of SMFs, collagen matrix and the incorporation of IONPs on MG-63 cell behaviours were studied. By exposing with SMFs for 1, 3, 7 and 14 days, a stimulating effects of SMFs alone on cell proliferation can be observed for up to 7 days. Many studies demonstrated that the SMFs alone cannot promote MG-63 cell growth over longer culturing time, and even have an inhibitory effect. For example, Cai *et al.* [2015] observed increased cell proliferation of MC3T3-E1 cells when exposed under 100 mT SMFs between 4 hours and 7 days of culture. However, cell proliferation decreased afterwards. Cunha *et al.* [2012] indicated

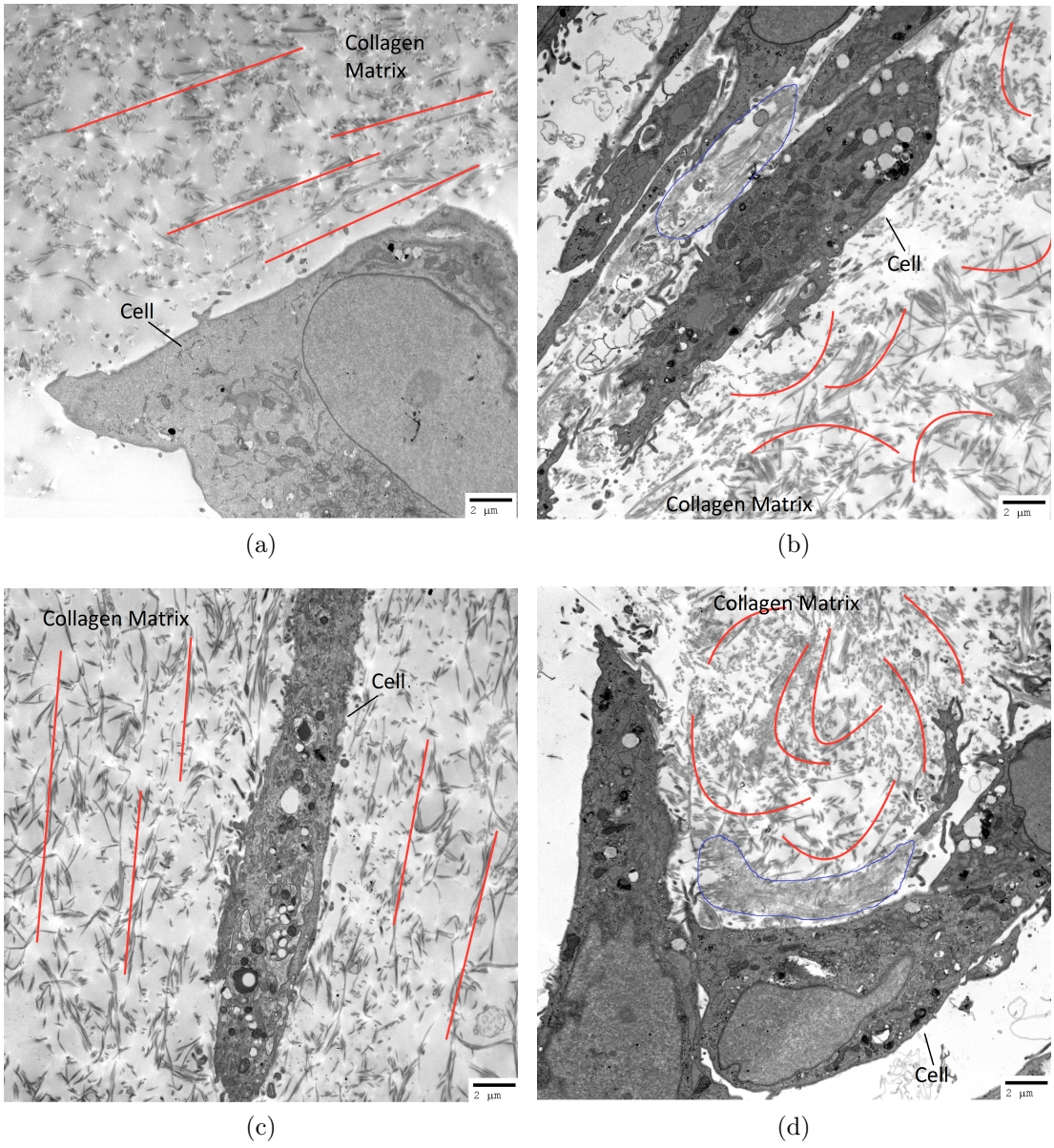

Figure 5.17: Microstructure of cell loaded collagen scaffolds examined under TEM at day 14. (a) collagen scaffolds without SMFs, (b) collagen scaffolds with SMFs, (c) collagen scaffolds incorporated with IONPs without SMFs and (d) collagen scaffolds incorporated with IONPs with SMFs. After 14 days, the changes in the collagen matrix continued (indicated by red lines), with new matrices built up around cell membranes when exposing under SMFs (circled with blue).

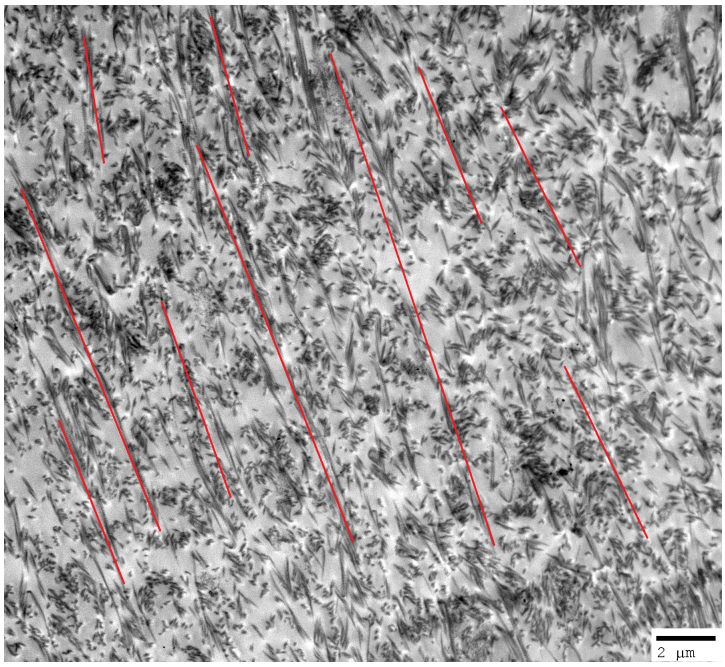

(a)

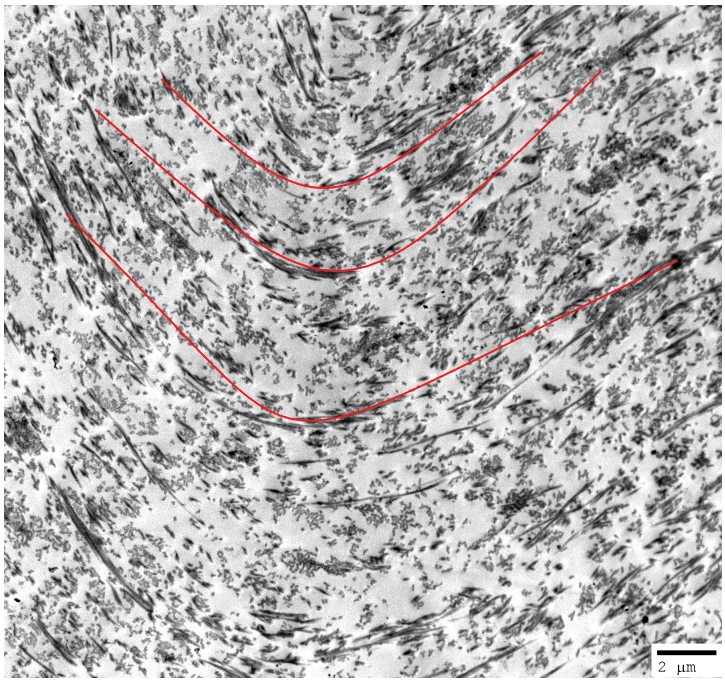

(b)

Figure 5.18: Microstructure of cell loaded collagen scaffolds examined under TEM at day 14. Collagen fibres (a) without SMFs and (b) with SMFs. The reorientation of collagen fibres are contributed from the SMFs not IONPs.

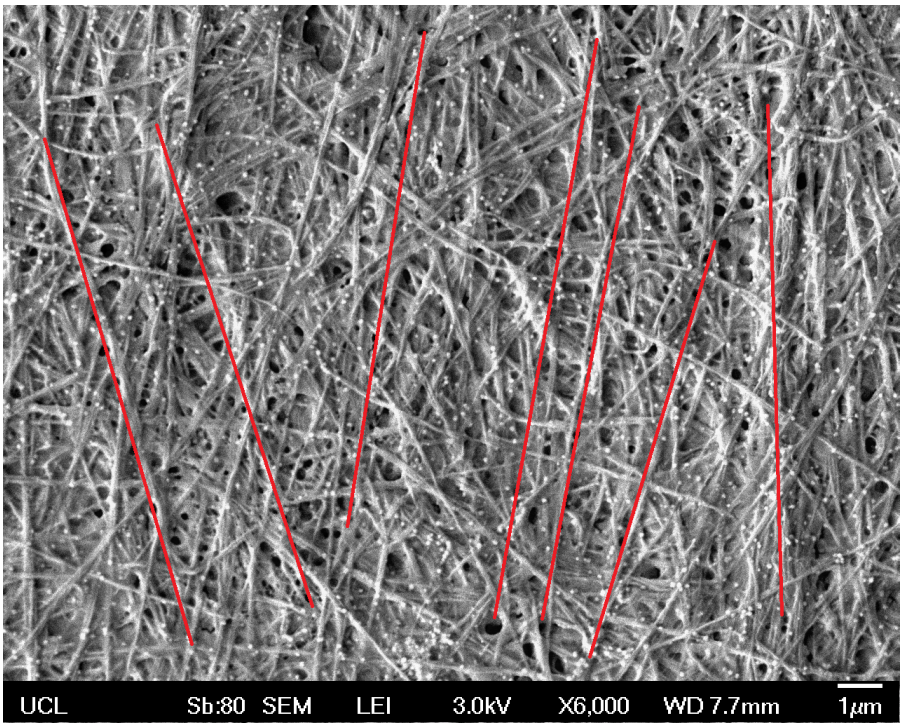

(a)

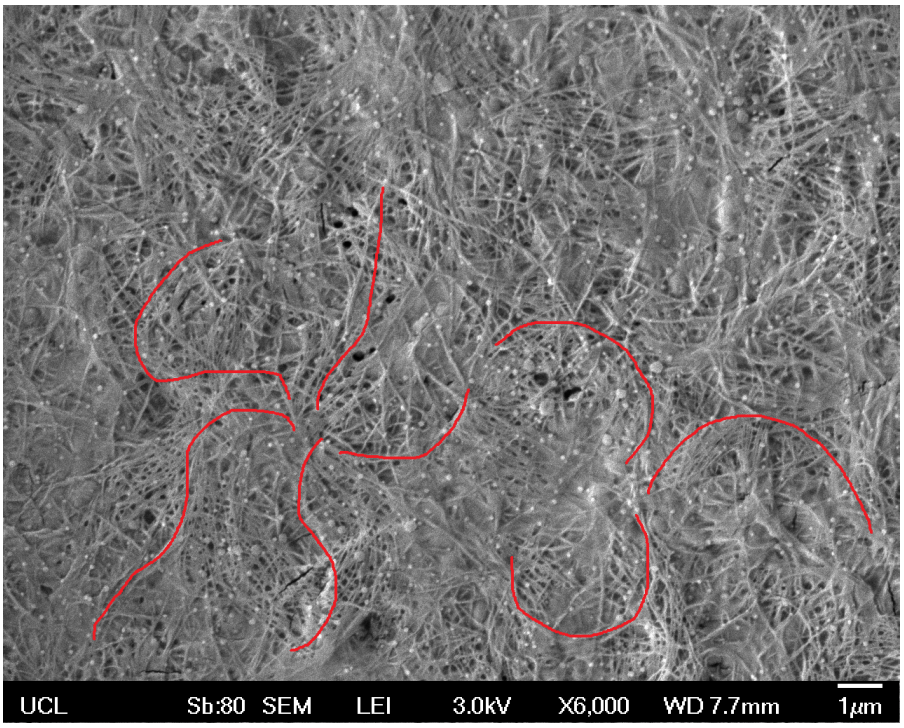

(b)

Figure 5.19: Microstructure of collagen fibres (a) without and (b) with SMFs.

a reduced number of MG-63 cells by SMFs (320 mT) after 7 days. Imaizumi *et al.* [2007] demonstrated that the proliferation of MC3T3-E1 was unchanged after 1 day but decreased by the exposure to SMFs (250 mT) after 4 and 7 days. It has been reported that bone and bone cells can only respond to SMFs for a short period, once bone cells get adapted to the static environment, they will not respond to the SMFs in terms of biological behaviour. The bone cells are more likely to grow in a dynamic environment.

However, when combining the effects of IONPs and SMFs together, the stimulating effect can be extended for a longer culture time (14 days). This can be attributed to the combined effects of SMFs, IONPs and the collagen matrix interactions. Meng *et al.* [2010] indicated that by introducing IONPs into polymer films under a 1 mT SMFs, the growth of bone cells can be enhanced. Similar observations have also been reported by Wei *et al.* [2011]. When incorporating IONPs into polymer nano-fibrous membranes, the MG-63 cell proliferation increased with increasing seeding time and IONPs loading. This can be caused by the interactions between magnetic fields and magnetic nanoparticles. Magnetic fields induce a high magnetic gradient, which causes displacement of the particles along the gradient vector, when the particles are in touch with cells, this leads to the production of compression and tensile forces on the cell membrane [Dobson, 2008], resulting in a range of cellular responses, including changes in intracellular calcium levels. Therefore the biological behaviours of cells can be modified.

Histology was employed to examine the cellular responses. By visualising the functional cells inside the collagen scaffolds, the effects of SMFs and IONPs on

cell proliferation examined by AB assay can be validated. Histology samples were prepared and examined under optical microscopy, and it was found when exposure to SMFs, the cell number increased after 3 days. The quantitative data obtained supported this finding, and this trend agrees with the AB assay results. By employing SMFs alone, increased cell activity can be observed from 3 days but falls slightly after 14 days. This suggests that the SMFs alone can influence cell growth over short time periods, while are not effective for long duration. The incorporation of IONPs can further the stimulation effects for 14 days. This suggests that by incorporating IONPs, the effect of SMFs can be prolonged.

5.9.2 Effects of SMFs on Cell Differentiation

Cell differentiation was also investigated. The exposure to SMFs promoted ALP production from MG-63 after 21 days, and the incorporation of IONPs further stimulated ALP production at a later stage. ALP is one of the key substances that indicate whether osteoblasts have entered the period of extracellular matrix development and maturation. When proliferation subsides, differentiation takes place, which explains why there is no significant increase in ALP level before 21 days. Previous studies have found that osteoblast-like cells expressed greater ALP levels after SMFs exposure [Cai *et al.*, 2015; Huang *et al.*, 2006; Kotani *et al.*, 2002; Meng *et al.*, 2010]. The effect of 400 mT SMFs on the expression of several genes in MG-63 cells has been studied, the data suggests that the local regulatory factors produced by SMFs treated cells, including collagen Type I, ALP and OP were greater than those of the untreated ones after only 3 days [Huang *et al.*,

2006]. The major effect of SMFs on osteoblasts differentiation can contribute to the reorientation and distortion of cell membranes and therefore modify the membrane properties, resulting in higher expression of growth factors associated with differentiation hence leading to higher levels of ALP production.

5.9.3 Effects of SMFs on Cell Mineralisation

SMFs, and the combination of SMFs and IONPs promoted mineralisation at an early stage (day 21) when compared to the control. This demonstrates that SMFs have a stimulating effect on cell mineralisation. After 6 weeks, all samples reached similar levels of mineralisation, indicating the completion of cell mineralisation, which is an essential process in osteogenesis. Mineralisation occurs extracellularly and involves the initial formation of apatite crystals in specific sites along collagen fibres followed by the replacement of much of the water in the tissue with mineral. Many theories have been advanced to explain the initiation of mineralisation, including local elevations of phosphate via hydrolysis of organic phosphates by alkaline phosphatase, enzymatic removal of inhibitors of mineral deposition and direct nucleation of hydroxyapatite or other calcium phosphate minerals onto the bone collagen fibres [Termine *et al.*, 1981]. The transition from proliferation stage to matrix maturation is suggested by the up regulation of genes associated with matrix development, such as collagen synthesis and ALP activity. Calcium accumulation starts at the matrix development stage and reaches its maximum during the mineralisation stage. The *in vitro* study from Hsu & Chang [2010] showed that SMFs (290 mT) combined with osteogenic induction

could enhance early extracellular calcium and bone mineralisation of dental pulp cells.

5.9.4 Effects of SMFs on Gene Expression

It was shown that the combination of SMFs and IONPs can induce ostogenesis in collagen scaffolds, however, the mechanisms at the molecular levels remain unclear. Osteogenesis is a complex process mediated by succession of gene activation and expression. Runx2, ON, BMP-2 and BMP-4 are important markers involved in this process (as detailed in Chapter 1).

Runx2 was up-modulated by the combination of IONPs and SMFs exposure after 7 to 14 days of culture. Similar findings have been demonstrated by Tsai *et al.* [2009]. By treating MSCs for 3, 7 and 10 days under a magnetic field, significant higher expression of Runx2 has been observed, accompanied with the up-regulation of ALP, collagen type I and OC [Yuge *et al.*, 2003]. Runx2 is the osteoblast-specific product of the Cbfa1 gene, and also a transcription factor that is essential for osteoblast differentiation and bone formation. The expression of Runx2 can also cause a stage dependent increase in the structural and functional proteins, for example, ALP, collagen type I, osteopontin, BSP and osteocalcin in osteoblasts. Many studies have demonstrated that Runx2 can induce *in vitro* osteoblast differentiation and mineralisation as well as *in vivo* bone formation [Selvamurugan *et al.*, 2007; Tsai *et al.*, 2009,?; Zhao *et al.*, 2005]. In accordance with the *in vivo* studies, *in vitro* studies have demonstrated that Runx2 is a pos-

itive regulator that can up-regulate the expression of bone matrix protein genes, allowing cells to acquire the osteoblastic phenotype while keeping the osteoblastic cells in an immature stage [Komori, 2010]. Taken together, the results presented in the current study suggest that SMFs exposure may induce an earlier osteogenic induction in MG-63 cell lines by modulating early osteoblastic gene expression of Runx2, hence accelerating the osteogenesis.

The expression of osteonectin was up regulated by the addition of IONPs under SMFs after 7 days. However, after 14 days, the level of ON production in the control group reached to a similar level to the other treated samples. One possible explanation could be that collagen itself has a significant influence on the expression of ON. ON is a glycoprotein in the bone that binds to both hydroxyapatite and collagen, therefore it plays a vital role in bone mineralisation, cell-matrix interactions, and extracellular matrix regulation. When ON is bound to insoluble type I collagen, the resultant complex binds synthetic apatite crystals and free calcium ions. One study suggested that ON is a tissue specific protein that exhibits several interesting activities, such as linking the bone mineral and collagen phases, perhaps initiating active mineralisation in normal skeletal tissue [Termine *et al.*, 1981]. The IONPs incorporated model under SMFs was shown to enhance the expression of ON over a 2 week period, which would explain the enhancement in the mineralisation level.

Findings from the current study indicate that the expression of BMP-2 and BMP-4 can be enhanced by the combination of SMFs and IONPs over 14 days of culture. Both BMPs and Runx2 are able to stimulate osteoblast differentiation

and bone formation and their interrelationships have also been examined. The BMPs provide signals that enhance Runx2 dependent transcription and at the same time, Runx2 provides information necessary for BMPs activity [Gersbach *et al.*, 2004]. It can be concluded that not only the transcriptional activity of Runx2 in osteogenic precusor cells requires BMP signalling but also the sensitivity of cells to BMPs is enhanced in the presence of Runx2. Therefore, the up-regulation of Runx2 and stimulation of the expression of BMPs, and the enhanced expression of BMPs can further promote the production of Runx2. Another interesting finding from this study is that, the expression of BMP-4 is higher than that in BMP-2. Bodamyali *et al.* [1998] studies the effects of magnetic field on the expression of several BMPs, including BMP-2 and BMP-4. They found that magnetic fields can up-regulate the expression of BMP-2, and the up-regulation of BMP-2 leading to an enhanced level of BMP-4. Taking all the effects together, the expression of BMP-2 can be enhanced by SMFs, IONPs and Runx2, whereas the expression of BMP-4 can be enhanced by the effects of SMFs, IONPs, Runx2 and also BMP-2. Therefore the expression of BMP-4 was comparably higher than that of BMP-2.

5.9.5 Effects of SMFs on Cell/matrix Interactions

The stimulatory effects of SMFs and IONPs on the osteogenesis process were evaluated, and this can contribute to the expression of several key genes at molecular level. However, the mechanism behind the up-regulation of the gene expression needs to be further understood. Therefore, the microstructure of cells embed-

ded in collagen scaffolds were examined. The cell/matrix interaction is a crucial factor which affects cell behaviour. Previous investigations tried to study the cellular responses of cells when seeded inside PC scaffolds, however, they have not focused on the microstructural analysis of the cell/matrix interactions yet.

When being exposed under SMFs for 7 days, the reorientation of the fibres can be observed, the fibres grow with no preferred direction, with some in line with the cells while others against the cells. When collagen fibres are affected by the SMFs, they move around their axis and produce friction forces. The collagen fibres which are located near the cell membranes will pass the friction to the cells, and this force could lead to changes in the cell membranes, such as to open up more calcium ion channels, hence modify the membrane properties. In order to determine whether this reorientation is caused by the SMFs or the cell regulation, microstructural analysis on the collagen gels without cells were examined. Without SMFs, the collagen fibres show no orientated directions, but with stretched and straight morphology. When subjected to SMFs, the collagen fibres tend to be re-orientated. With the effects of SMFs, some of the fibres tended to shift perpendicular to the direction of SMFs, however, the majority of the fibres were still randomly distributed.

From the microstructural analysis, what can be observed was that the direction of collagen fibres were changed under SMFs. Many studies have focused on exposing collagen solution to a strong static magnetic field with strength higher than 1T during gelation [Dubey *et al.*, 2001; Guido & Tranquillo, 1993; Kotani *et al.*, 2000; Torbet & Ronziere, 1984]. For example, Kotani *et al.* [2000] exposed

bone collagen matrix under a SMFs of 8T to evaluate the effects of strong SMFs on bone matrix. The collagen fibres oriented perpendicular to the direction of the magnetic field after 1 hour of exposure, while they normally randomly orientated without the exposure of SMFs. This can be explained by the liquid crystal property of collagen. Procollagen molecules have been shown to undergo liquid crystalline ordering in solution, prior to fibril assembly. This may provide an explanation for the liquid crystal-like architectures of different connective tissues [Hulmes, 2002]. One of the characteristic features of liquid crystals is that they can be ordered in electric and magnetic fields [Brown *et al.*, 1971]. Each collagen molecule has a small negative diamagnetic susceptibility [Pauling, 1979; Worcester, 1978]. The regular organisation of such molecules leads to a large enough negative diamagnetic susceptibility along the fibres to effect such alignment. The structural origins of diamagnetic anisotropy in proteins have been discussed in detail by Worcester [1978], in which peptide bonds and aromatic residues are the main potential sources of anisotropy. As there are relatively few aromatic groups in collagen, the anisotropy must be dominated by the peptide contribution [Torbet & Ronziere, 1984].

In the current study, the re-orientation of the collagen fibres can be observed, however, the alignment of the fibrils cannot be observed as described in other studies [Kotani *et al.*, 2000]. Several explanations can account for not observing the perpendicular alignment of the collagen fibres. First of all, the magnetic field intensity used here is relatively small when compared to other studies (72 - 144 mT when compared to 8T). The degree of orientation for a particle with diamagnetic anisotropy, $\Delta\chi$, in a magnetic field, H, is a function of the ratio:

$$\Delta\chi H^2 \quad / \quad 2kT \tag{5.1}$$

Where k is the Boltzmann constance and T is the absolute temperature [Torbet & Ronziere, 1984]. Therefore, given the same Boltzmann constance and absolute temperature, the degree of orientation of each collagen fibre is highly dependent upon the magnetic field strength. Smaller field strength induces smaller degree of orientation. Here, the diamagnetic anisotropy of a particle having an axis of rotational symmetry is the difference in magnetisation parallel/perpendicular to the axis of symmetry. Secondly, the compressed collagen gels used here are high in density when compare to other highly hydrated collagen gels, provide higher mechanical stability but less space of freedom. Therefore it may prevent some parts of the collagen fibres from rotating.

5.9.6 Effects of SMFs on Cell Membrane

Other explanations on the up-regulation of the Runx2, ON, BMP-2 and BMP-4 can be contributed on the modification of cell membranes. Bilayer membranes, which are composed of a number of protein and lipid molecules, possess anisotropic diamagnetism in nature [Yamagashi *et al.*, 1992]. Upon the exposure to SMFs, the phospholipid molecules of the membrane can be rotated by virtue of their collective diamagnetic properties. It also has been discovered that gradient magnetic field can unbalance the hydrostatic pressure across the bilayer lipid membrane [Suda & Ueno, 1997]. Both of these effects can possibly result in over

deformation of the cellular membrane, modification of the biological properties of embedded receptors in the membrane and, thereby altering the proliferation kinetics of the cells. Besides, it is generally known that morphological and structural changes to the plasma membrane interfere with many functional and structural features of the cells, leading, for example, to changes in cellular shape, cytoskeleton arrangement, ion flux, receptor distribution [Dini & Abbro, 2005]. To be more specific, the reorientation of the membrane matrix will influence the embedded ion channels, most likely by producing some degree of deformity of their intramembranous segment, hence leading to the activation of calcium channels [Rosen, 2003]. Increased concentration of Ca^{2+} can also promote the formation of micro-vesicles (MVs). MVs (100 - 1000 nm) are fragments of the plasma membrane, which play a role in inter-cellular communication and can transport mRNA, miRNA, and proteins between cells. MVs are able to enhance the regeneration of a number of tissues by exerting an effect on target cells or inducing neighbouring cells by the transfer of cytokines, such as transforming growth factor, hepatocyte growth factor, or vascular endothelial growth factor [Muralidharan-Chari *et al.*, 2010]. Influx and export of Ca^{2+} are the mechanisms that control the formation and secretion of MVs. The results presented by Stratton *et al.* [2013] suggested that the magnetic field accelerated cell membrane activity, allowing calcium influx, which in turn initiated the release of MVs from stimulated cells. In the study of Maredziak *et al.* [2015], they also demonstrated that magnetic fields can directly stimulate and promote the secretion of membrane-derived MVs in mesenchymal stem cells. The increase and mobilisation of Ca^{2+} during exposure of cells to SMFs can cause a cascade of microfilament and microtubular reorganisation, cell shape modifications, changes to surface carbohydrate residues [Bras *et al.*, 1998].

For example, as a result of SMFs of 0.4 T treatment, MG-63 cells became more stellar shapes with extensive processes and appeared to form multiple layers on the surface [Huang *et al.*, 2006]. Matrix vesicles released from the plasma membrane accumulated continuously around the SMFs exposed MG-63 cells have been observed by Chiu *et al.* [2007].

5.10 Summary

This chapter demonstrates that the combination of SMFs and IONPs can enhance several biological properties of MG-63 cells, including, proliferation, differentiation and mineralisation. The proliferation can be up-regulated up to a period of 14 days. When proliferation subsides, the ALP production level increased, and this can be further promoted when subjected under SMFs. Mineralisation normally happens at later stages of the cell cycle. Significant enhancement of the mineralisation level caused by SMFs can be observed at day 21. This indicates that SMFs and IONPs can lead to early mineralisation when compared to the control condition. Then after 6 weeks, all the scaffolds are fully mineralised, the effects of SMFs cannot be observed.

The effects of SMFs and IONPs at cellular and molecular level have then been examined. First of all, SMFs encouraged the expression of Runx2, ON, BMP-2 and BMP-4, which mediate the osteogenesis of the cell, including proliferation, differentiation and mineralisation process. Secondly, the cellular responses of cells embedded in collagen were investigated. Results demonstrated that SMFs

can stimulate cell growth within 7 days, while with the incorporation of IONPs; the stimulation effect can be expanded to 14 days. When further evaluating the influence of SMFs on the microstructure of cell/matrix, re-orientation of collagen fibres can be noticed. This can be considered as one of the reasons promotes biological behaviours. The interactions between the ECMs and the cells can potentially influence the membrane's phospholipid molecules; hence enhance the calcium ion flux. In summary, the SMFs and IONPs can affect osteogenesis in the following ways: The SMFs and the incorporation of IONPs can affect several cell membrane properties (due to the diamagnetic property of phospholipids) and the cell/matrix interactions (due to the the liquid crystal properties of the collagen matrix), which lead to the up-regulation of several key genes, such as Runx2, ON, BMP-2 and BMP-4, resultant in a stimulation effect of osteogenesis *in vitro*.

Chapter 6

Conclusions and Future work

6.1 General Discussion and Conclusion

The key findings of the this study are summarised as below:

1. A magnetic bio-reactor with desired strength was designed and used for *in vitro* studies. The magnetic field strength is dependent on the types and the relative position of the magnets. Neodymium magnets induced larger strength when compared to the samarium-cobalt magnets (given the same dimensions). When placing the magnetic poles facing to and close to each other, higher strength can be generated.

2. A 3D collagen based bone model was developed, which offers the possibility of incorporating various biofactors and supports cell growth. This includes the evaluation of using various cell lines, the comparison between 2D and

3D models, and the investigation of incorporating bio-factors. MG-63 cells have been affected by SMFs most significantly when compared to the other cell lines (MC3T3-E1 and UMR-106). When comparing the cell proliferation cultured on 2D surfaces and 3D PC collagen hydrogels, a stimulation effect can be observed for the 3D one. With the incorporation of IONPs, the cell proliferation can be further promoted, however, nHA and nZnO can not stimulate cell growth under SMFs.

3. With the incorporation of IONPs, the proliferation, differentiation and mineralisation of osteoblasts cultured in 3D collagen scaffolds have been stimulated under SMFs.

4. The SMFs and the incorporation of IONPs can affect several cell membrane properties (due to the diamagnetic property of phospholipids) and the cell/matrix interactions (due to the liquid crystal properties of the collagen matrix), which lead to the up-regulation of several key genes, such as Runx2, ON, BMP-2 and BMP-4, resulting in a stimulation effect of osteogenesis *in vitro*.

In vitro models provide a platform to investigate the cell behaviours under SMFs. Current tissue models exist in either 2D or 3D format. 2D models are simple to access and low in costs. However, 2D models cannot represent the real ECM structure in bone that is highly three dimensional. A desired model should be non-toxic to cells, have ECM-like structure, allow cells to attach and grow, and

have certain mechanical properties to maintain functionalities during the culture time. 3D natural tissue models have the advantage of suspending biomaterials in a tissue like matrix, and enable real time assessment of the accessible structure. Although there are limitations of using these models, such as the over-simplified system, they can still be useful to be employed as reliable *in vitro* testing platforms, for the understanding of the toxicity and cell responses. Among a wide range of natural materials, collagen type I is preferable as it is the main structure of extracellular matrix (ECM). Collagen hydrogels have been used as *in vitro* models for cell/matrix interactions, however, the conventional hydrogels are weak in mechanical stabilities. Plastic compression was used to increase the collagen hydrogel density, and therefore increase the physiology relevance of the hydrogel for local cells. In this study, gels were compressed into culture well-plate by the upward flow method, and were easily reproduced. Furthermore, the ability to incorporate cells and biofactors (growth factors, biocompatible materials) into compressed scaffolds makes the scaffolds more versatile and multifunctional.

In order to provide the cell/tissue model an *in vitro* SMFs environment, a magnetic bio-reactor was designed. To quantify the magnetic filed strength was the first step. The magnetic filed strength between two permanent magnets depends on the properties of the magnets (type, dimensions) and their relative positions of the magnetic poles (attraction or repulsion) and the separation distance. It was shown when the properties of the magnets have been fixed, placing the magnets face to face leads to a greater magnetic strength compared to the edge to edge position. Besides, a smaller gap between two magnets results in larger forces generated. The simulation and experimental results agreed with each other, how-

ever, there are always discrepancies between the values. This could be due to the experimental limitations or the effects of the magnetic field of the earth itself.

One of the hypotheses of this study is that the SMFs stimulate the fracture healing by influencing the osteogenesis process. SMFs with desired intensity have been shown to stimulate osteoblasts proliferation, differentiation and mineralisation *in vitro* [Cai *et al.*, 2015; Chiu *et al.*, 2007; Meng *et al.*, 2013; Rosen, 2003]. However, the results can be inconsistent due to the variations in the SMFs intensity, as well as the type of the cells seeded. In this study, three cell lines were tested under SMFs, including MG-63 (human, osteosarcoma), UMR-106 (rat, osteosarcoma) and MC3T3-E1 (mouse, non-transfomred). The results showed that all cells demonstrated an increased cell proliferation under the exposure of the SMFs. The highest stimulation effect was observed when cultured with MG-63 cells. When further introducing IONPs, nHA and nZnO into the cell seeded collagen scaffolds, a stimulating effect of IONPs incorporated scaffolds was observed under SMFs up to a concentration of 100 μg/ml. Higher dosages of IONPs was identified to be toxic to MG-63 cells *in vitro* both with and without SMFs. nHA encouraged the cell proliferation without the exposure of SMFs, with no significant improvements under SMFs. This demonstrated that nHA does not respond to the SMFs significantly. nZnO demonstrates the lowest stimulating effects on the cell proliferation, while being toxic to the cells at concentrations above 10 μg/ml.

The effects of SMFs and IONPs on other biological behaviours were then evaluated. When exposing under SMFs, or incorporated with IONPs alone, the

proliferation of MG-63 cells was only promoted up to 7 days. When further combining two together, the proliferation can be up-regulated up to 14 days. The short-time effect of SMFs on cell proliferation is not surprising, as it has been documented that osteoblasts respond to dynamic environment rather than static [Rubin & Lanyon, 1985]. By further incorporating IONPs, the particles were magnetised upon the exposure of SMFs, and hence were attracted to travel towards the magnetic poles. This caused a dynamic motion inside the scaffolds, effectively leaving the cells with a non-static environment. Therefore, the proliferation can be further enhanced. When proliferation subsides, the ALP production level is increased, and this can be further promoted by SMFs. The addition of IONPs also favour this process. Mineralisation normally happens at later stages of the cell cycle. Significant enhancement of the mineralisation level caused by SMFs can be observed at day 21. This indicates that SMFs and IONPs can lead to early mineralisation when compared to the control condition. However, after 6 weeks, all the scaffolds are fully mineralised, the effects of SMFs cannot be observed any more.

For the stimulating effects of SMFs on cell proliferation, differentiation and mineralisation, one hypothesis is that, SMFs stimulate the osteogenesis process by activating the calcium ion channels in the cell membrane, hence lead to the up-regulation of several key genes, such as Runx2, osteonectin and BMPs. By examining under TEM, reorientation of collagen fibres can be observed under SMFs treatment (potentially due to the liquid crystal-like property of collagen fibres). This reorientation caused changes in the cell/matrix interaction, which can potentially influence the phospholipid molecules of the cell membrane, and

hence enhance the calcium ion flux. Second, SMFs encouraged the expression of Runx2, ON, BMP-2 and BMP-4. Runx2 is a key transcription factor during cell cycle, the enhancement of Runx2 can lead to enhanced expression of ALP, collagen type I, osteocalcin, etc. Those genes are beneficial to the differentiation process of osteoblasts, as a result, a stimulation effect of SMFs on cell differentiation was observed. Besides, the expression of ON has been measured to demonstrate how SMFs influence cell mineralisation. ON is an important marker for early mineralisation, and the enhanced expression of ON by SMFs indicates the stimulation effects of SMFs on cell mineralisation. Many studies also demonstrated that SMFs can induce early osteoblasts mineralisation. In addition, the BMPs, especially BMP-2 and BMP-4 have been widely studied to enhance bone formations. Results from current study suggested that the combination of SMFs and IONPs can promote the expression of BMP-2 and BMP-4. The expression of BMP-4 were higher than that in BMP-2. One possible explanation is that, the expression of BMP-2 can be affected by SMFs, IONPs as well as Runx2, whereas BMP-4 can receive treatments from SMFs, IONPs, Runx2 and also BMP-2. To conclude, the cellular and molecular behaviours described above can contribute to the stimulating effects of osteoblasts by SMFs and IONPs.

In this study, plastic compression (PC) collagen hydrogels have been employed as a 3D bone model. Human osteosarcamo cell line, MG-63, has been selected as the cell model for human osteoblasts, and biocompatible iron oxide nanoparticles (IONPs) have been synthesised and incorporated within the model to further enhance the biological properties. A magnetic bio-reactor to support cell growth under SMFs has been designed and fabricated by 3D printing, and

used for *in vitro* studies. Results demonstrated that SMFs and IONPS can stimulate the proliferation, alkaline phosphatase production and level of mineralisation of MG-63 cells *in vitro*. The cellular interactions of the cell/matrix have also been examined under Transmission Electron Microscopy (TEM), where an reorientation of collagen fibres around cells have been observed. As for the molecular level, real-time polymerase chain reaction (PCR) has been conducted to determine the effects of SMFs on the expression of Runx2, Osteonectin, BMP-2 and BMP-4, in which stimulating effects have been identified with the combination of SMFs and IONPs. In conclusion, SMFs and IONPs altogether can enhance the proliferation, ALP production and mineralisation in the developed bone model *in vitro*, potentially by influencing the matrix/cell interactions, hence activating the calcium ion channels and encouraging the relative gene expressions. To this end, the system established in this thesis can be served as a novel bone model for *in vitro* evaluation of the effects of SMFs on osteoblasts, hence lead to a better understanding of the mechanisms behind.

6.2 Future Work

The 3D collagen model developed in this project has successfully served as an *in vitro* platform to evaluate the effects of SMFs on osteonegesis. In order to further develop the system for more complicate studies, several improvements can be attempted, as listed below.

First of all, the design of the magnetic bio-reactor can be improved. As the

current study only focused on one type of magnetic field, the effects of SMFs with varies strength are of interest to study. The effects of various intensity of SMFs on the biological behaviours of cells, as well as the effects on the collagen matrix orientation, can be further investigated. Besides, the magnetic bio-reactor developed here did not include auto media feeding system, the change of cell media was done manually. This increased the possibility of infections.

A tissue model normally consists three key components, the scaffolds, cells and biofactors. For the scaffolds fabrication, the current study was focused on the use of rat tail type I collagen. This type of collagen is isolated from rat tails, which is a different species other than human and may behave differently for *in vivo* use. Therefore, other types of collagen sources should be considered. Besides, in order to mimic the real bone structure, multilayers of the tissue model would be optimal. The current study only focused on a simple platform on which only single layer of collagen gel was employed.

As for the cell model, only one type of cell line, MG-63 was used to conduct biological testing. MG-63 cell line are cells derived from human osteosarcoma, they are not experiencing the same differentiation stages as human osteoblasts. Thus, mesenchymal stem cells (MSCs), from which osteoblasts are originated, can be suggested in the future studies.

As for the incorporation of biofactors, for example, IONPs, has only been employed at 4 different concentrations with a wide gap in between. IONPs with a concentration of 100 μg/ml showed a positive effect on the cell proliferative activ-

ity, whereas toxic effect was observed at concentrations of 1000 μg/ml. Therefore it is necessary to investigate the concentrations in between 100 and 1000 μg/ml to identify the threshold. In addition, although nHA and nZnO did not respond to SMFs significantly, they still possessed great capabilities for bone healing applications. A mixture of IONPs, nHA and nZnO can offer a tissue model with potential osteoconductive and antimicrobial properties.

Furthermore, more biological studies can be employed to investigate the effects of SMFs. For instance, the cell shape may have been influenced upon the exposure of SMFs, and hence cause the change in cell/matrix interactions and membrane properties. It is of interest to investigate whether the cells controlled the orientation of the collagen fibres or vice versa. Therefore, the change in cell morphology and cytoskeleton can be further studied.

Chapter 7

Appendix A: Characterisation of Iron Oxide Nanoparticles

The phase purity of IONPs was examined under X-Ray diffraction (XRD). Patterns revealed the presence of all the major peaks, 111, 220, 311, 400, 422, 511 and 440, with no secondary phases detected (Figure 7.1). The corresponding Bragg angles were 17.05, 30.25, 35.7, 43.4, 53.55, 57.2 and 63.05, respectively. The diffraction peaks corresponded well to magnetite Fe_3O_4 (JCPDS file, No. 00-011-0614), which suggests the particles are magnetite (Fe_3O_4) with a spinal structure [Liu *et al.*, 2006].

The microstructure of IONPs have been examined under Transmission Electron Microscopy (TEM) with results presented in Figure 7.2. The nanoparticles are spherical structured and have an average diameter of 13 $\pm$ 5 nm (n = 50).

The parameters of crystal structure can also be calculated according to the

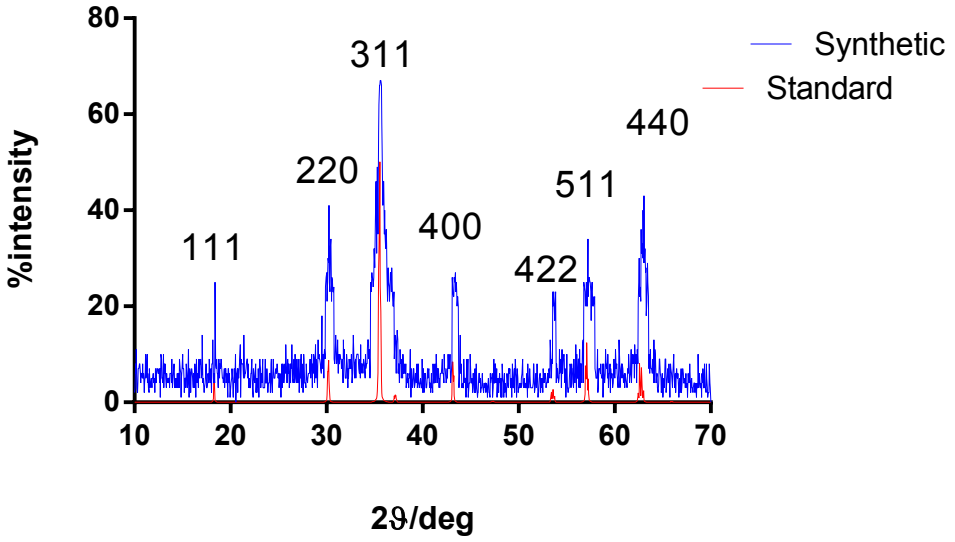

Figure 7.1: X-Ray Diffraction patterns of IONPs nanoparticles compares to the standard magnetite pattern (JCPDS file, No. 00-011-0614)

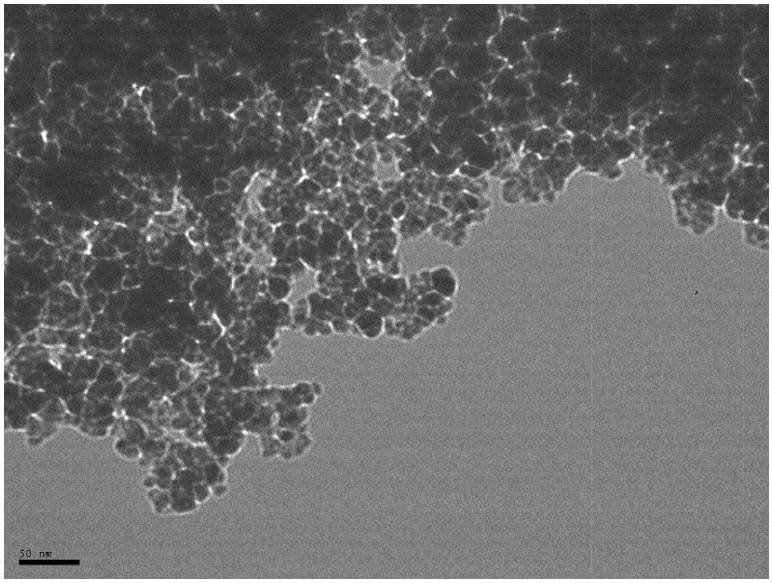

Figure 7.2: Microstructure of fabricated IONPs by co-precipitation method. The average size of the particles were measured as 13 ± 5 nm (n = 50).

wavelength and incidence angle of X-rays. This can be referred to as Bragg's equation:

$$n\lambda = 2d\sin\theta, \tag{7.1}$$

where n is an integer, d is the inter-atomic spacing and θ is the incident angle of the X-ray beam. In this study, λ is the X-ray wavelength (0.15406 nm), B is the full width at the half maximum (FWHM), θ is the corresponding Bragg angle and K is the shape parameter, which is 0.89 for magnetite. Taking the highest intensity peak, namely the (311) plane at $2\theta = 35.7$, and the half maximum intensity width of the peak after counting for instrument broadening, the calculated particle size was 11.5 nm.

References

Aaron, R.K., Ciombor, D.M. & Simon, B.J. (2004). Treatment of nonunions with electric and electromagnetic fields. *Clinical orthopaedics and related research*, **419**, 21–29. 2

Adems, J. & Hamblen, D.L. (1992). Outline of fractures. 40

Ahmed, T.A., Dare, E.V. & Hincke, M. (2008). Fibrin: a versatile scaffold for tissue engineering applications. *Tissue Engineering Part B: Reviews*, **14**, 199–215. 27

Aldinucci, C., Garcia, J.B., Palmi, M., Sgaragli, G., Benocci, A., Meini, A., Pessina, F., Rossi, C., Bonechi, C. & Pessina, G.P. (2003). The effect of exposure to high flux density static and pulsed magnetic fields on lymphocyte function. *Bioelectromagnetics*, **24**, 373–379. 55

Alekseeva, T., Jawad, H., Purser, M. & Brown, R. (2011). New improved technique of plastic compression of collagen using upward fluid flow. In *8th International Conference on Cell & Stem Cell Engineering (ICCE)*, 5–8, Springer. 79

Ardakani, A.G., Cheema, U., Brown, R.A. & Shipley, R.J. (2014). Quantifying the correlation between spatially defined oxygen gradients and cell fate in an engineered three-dimensional culture model. *Journal of The Royal Society Interface*, **11**, 20140501. 31

Askari, J. & Humphries, M. (2004). Cell–matrix interactions. *Encyclop Biol Chem*, **1**, 362–366. 21

Aubin, J.E. & Triffitt, J.T. (2002). Mesenchymal stem cells and osteoblast differentiation. *Principles of bone biology*, **1**, 59–81. 16

Aubin, J.E., Turksen, K. & Heersche, J.N. (1993). Osteoblastic cell lineage. *Cellular and molecular biology of bone*, 1–45. 19

Ba, X., Hadjiargyrou, M., DiMasi, E., Meng, Y., Simon, M., Tan, Z. & Rafailovich, M.H. (2011). The role of moderate static magnetic fields on biomineralization of osteoblasts on sulfonated polystyrene films. *Biomaterials*, **32**, 7831–7838. 56

Bai, W., Zhang, Z., Tian, W., He, X., Ma, Y., Zhao, Y. & Chai, Z. (2010). Toxicity of zinc oxide nanoparticles to zebrafish embryo: a physicochemical study of toxicity mechanism. *Journal of Nanoparticle Research*, **12**, 1645–1654. 130

Bard, D., Dickens, M., Smith, A.U. & Zarek, J. (1972). Isolation of living cells from mature mammalian bone. 18

Bell, E., Ivarsson, B. & Merrill, C. (1979). Production of a tissue-like structure by contraction of collagen lattices by human fibroblasts of different proliferative potential *in vivo*. *Proceedings of the National Academy of Sciences*, **76**, 1274–1278. 30

Belyaev, I.Y., Alipov, Y.D. & Harms-Ringdahl, M. (1997). Effects of zero magnetic field on the conformation of chromatin in human cells. *Biochimica et Biophysica Acta (BBA)-General Subjects*, **1336**, 465–473. 54

Benjamin, H., PAWLOWSKI, E. & BECKER, A.B. (1964). Collagen as temporary dressing and blood vessel replacement. *Archives of Surgery*, **88**, 725–727. 11

Berger, J., Reist, M., Mayer, J.M., Felt, O., Peppas, N. & Gurny, R. (2004). Structure and interactions in covalently and ionically crosslinked chitosan hydrogels for biomedical applications. *European Journal of Pharmaceutics and Biopharmaceutics*, **57**, 19–34. 27

Berry, C.C., Wells, S., Charles, S. & Curtis, A.S. (2003). Dextran and albumin derivatised iron oxide nanoparticles: influence on fibroblasts *in vivo*. *Biomaterials*, **24**, 4551–4557. 64

Bhattarai, N., Edmondson, D., Veiseh, O., Matsen, F.A. & Zhang, M. (2005). Electrospun chitosan-based nanofibers and their cellular compatibility. *Biomaterials*, **26**, 6176–6184. 26

Bikle, D.D. (2008). Integrins, insulin like growth factors, and the skeletal response to load. *Osteoporosis International*, **19**, 1237–1246. 45

Billiau, A., Edy, V., Heremans, H., Van Damme, J., Desmyter, J., Georgiades, J. & De Somer, P. (1977). Human interferon: mass production in a newly established cell line, MG-63. *Antimicrobial agents and chemotherapy*, **12**, 11–15. 19

Bitar, M., Brown, R.A., Salih, V., Kidane, A.G., Knowles, J.C. & Nazhat, S.N. (2007). Effect of cell density on osteoblastic differentiation and matrix degradation of biomimetic dense collagen scaffolds. *Biomacromolecules*, **9**, 129–135. 33, 36

Bodamyali, T., Bhatt, B., Hughes, F., Winrow, V., Kanczler, J., Simon, B., Abbott, J., Blake, D. & Stevens, C. (1998). Pulsed electromagnetic fields simultaneously induce osteogenesis and upregulate transcription of bone morphogenetic proteins 2 and 4 in rat osteoblasts *in vivo*. *Biochemical and biophysical research communications*, **250**, 458–461. 46, 51, 162

Bondemark, L., Kurol, J. & Wennberg, A. (1994). Orthodontic rare earth magnets - in vivo assessment of cytotoxicity. *British journal of orthodontics*, **21**, 335–341. 110

Bostrom, M.P., Lane, J.M., Berberian, W.S., Missri, A.A., Tomin, E., Weiland, A., Doty, S.B., Glaser, D. & Rosen, V.M. (1995). Immunolocalization and expression of bone morphogenetic proteins 2 and 4 in fracture healing. *Journal of orthopaedic research*, **13**, 357–367. 40

Bostrom, M.P., Saleh, K.J. & Einhorn, T.A. (1999). Osteoinductive growth factors in preclinical fracture and long bone defects models. *Orthopedic Clinics of North America*, **30**, 647–658. 44

Boyan, B.D., Schwartz, Z., Bonewald, L. & Swain, L. (1989). Localization of 1, 25-(OH) 2D3-responsive alkaline phosphatase in osteoblast-like cells (ROS 17/2.8, MG-63, and MC3T3-E1) and growth cartilage cells in culture. *Journal of Biological Chemistry*, **264**, 11879–11886. 20

Bras, W., Diakun, G.P., Diaz, J., Maret, G., Kramer, H., Bordas, J. & Medrano, F. (1998). The susceptibility of pure tubulin to high magnetic fields: a magnetic birefringence and x-ray fiber diffraction study. *Biophysical journal*, **74**, 1509–1521. 166

Brayner, R., Ferrari-Iliou, R., Brivois, N., Djediat, S., Benedetti, M.F. & Fiévet, F. (2006). Toxicological impact studies based on Escherichia coli bacteria in ultrafine ZnO nanoparticles colloidal medium. *Nano Letters*, **6**, 866–870. 48, 114

Brighton, C.T., Hozack, W.J., Brager, M.D., Windsor, R.E., Pollack, S.R., Vreslovic, E.J. & Kotwick, J.E. (1985). Fracture healing in the rabbit fibula when subjected to various capacitively coupled electrical fields. *Journal of orthopaedic research*, **3**, 331–340. 2

Brown, G.H., Neff, V.D. & Doane, J.W. (1971). A review of the structure and physical properties of liquid crystals. 11, 164

Brown, R.A. (2013). In the beginning there were soft collagen-cell gels: towards better 3D connective tissue models? *Experimental cell research*, **319**, 2460–2469. 29

Brown, R.A., Wiseman, M., Chuo, C.B., Cheema, U. & Nazhat, S.N. (2005). Ultrarapid engineering of biomimetic materials and tissues: Fabrication of nano-and microstructures by plastic compression. *Advanced Functional Materials*, **15**, 1762–1770. 3, 4, 29, 30, 31, 32, 33, 36, 37, 79

Brown, T.D. (2000). Techniques for mechanical stimulation of cells in vivo: a review. *Journal of biomechanics*, **33**, 3–14. 51

Browne, P.S. (1988). *Basic facts of fractures*. Blackwells. 40

Bucholz, R.W., Carlton, A. & Holmes, R. (1989). Interporous hydroxyapatite as a bone graft substitute in tibial plateau fractures. *Clinical orthopaedics and related research*, **240**, 53–62. 48

Busse, J.W., Bhandari, M., Kulkarni, A.V. & Tunks, E. (2002). The effect of low-intensity pulsed ultrasound therapy on time to fracture healing: a meta-analysis. *Canadian Medical Association Journal*, **166**, 437–441. 2

Buxton, P., Bitar, M., Gellynck, K., Parkar, M., Brown, R., Young, A., Knowles, J. & Nazhat, S. (2008). Dense collagen matrix accelerates osteogenic differentiation and rescues the apoptotic response to MMP inhibition. *Bone*, **43**, 377–385. 4, 30, 33, 34, 36

Cai, Q., Shi, Y., Shan, D., Jia, W., Duan, S., Deng, X. & Yang, X. (2015). Osteogenic differentiation of MC3T3-E1 cells on poly (L-lactide)/Fe_3O_4 nanofibers with static magnetic field exposure. *Materials Science and Engineering: C*. 2, 52, 55, 56, 58, 73, 109, 133, 153, 158, 172

Cen, L., Liu, W., Cui, L., Zhang, W. & Cao, Y. (2008). Collagen tissue engineering: development of novel biomaterials and applications. *Pediatric research*, **63**, 492–496. 6, 27, 28

Chakrapani, V.Y., Gnanamani, A., Giridev, V., Madhusoothanan, M. & Sekaran, G. (2012). Electrospinning of type I collagen and PCL nanofibers using acetic acid. *Journal of Applied Polymer Science*, **125**, 3221–3227. 25

Chao, E.Y., Inoue, N., Elias, J.J. & Aro, H. (1998). Enhancement of fracture healing by mechanical and surgical intervention. *Clinical orthopaedics and related research*, **355**, S163–S178. 2

Cheema, U., Ananta, M. & Mudera, V. (2011). *Collagen: applications of a natural polymer in regenerative medicine*. INTECH Open Access Publisher. 6, 37, 114

Chekina, N., Horák, D., Jendelová, P., Trchová, M., Beneš, M.J., Hrubỳ, M., Herynek, V., Turnovcová, K. & Syková, E. (2011). Fluorescent magnetic nanoparticles for biomedical applications. *Journal of Materials Chemistry*, **21**, 7630–7639. 63, 76

Chicatun, F., Pedraza, C.E., Ghezzi, C.E., Marelli, B., Kaartinen, M.T., McKee, M.D. & Nazhat, S.N. (2011). Osteoid-mimicking dense collagen/chitosan hybrid gels. *Biomacromolecules*, **12**, 2946–2956. 34

Chionna, A., Dwikat, M., Panzarini, E., Tenuzzo, B., Carla, E., Verri, T., Pagliara, P., Abbro, L. & Dini, L. (2003). Cell shape and plasma membrane alterations after static magnetic fields exposure. *European journal of histochemistry: EJH*, **47**, 299. 54, 55, 133

Chiu, K.H., Ou, K.L., Lee, S.Y., Lin, C.T., Chang, W.J., Chen, C.C. & Huang, H.M. (2007). Static magnetic fields promote osteoblast-like cells differentiation via increasing the membrane rigidity. *Annals of biomedical engineering*, **35**, 1932–1939. 2, 52, 54, 56, 58, 109, 133, 167, 172

Cho, T.J., Gerstenfeld, L.C. & Einhorn, T.A. (2002). Differential temporal expression of members of the transforming growth factor β superfamily during murine fracture healing. *Journal of Bone and Mineral Research*, **17**, 513–520. 45, 46

Claes, L.E., Heigele, C.A., Neidlinger-Wilke, C., Kaspar, D., Seidl, W., Margevicius, K.J. & Augat, P. (1998). Effects of mechanical factors on the fracture healing process. *Clinical orthopaedics and related research*, **355**, S132–S147. 2

Clover, J. & Gowen, M. (1994). Are MG-63 and HOS TE85 human osteosarcoma cell lines representative models of the osteoblastic phenotype? *Bone*, **15**, 585–591. 20

Cornell, R.M. & Schwertmann, U. (2003). *The iron oxides: structure, properties, reactions, occurrences and uses*. John Wiley & Sons. 62, 128

Cowin, S.C. (1986). Wolff's law of trabecular architecture at remodeling equilibrium. *Journal of biomechanical engineering*, **108**, 83–88. 49, 132

Cunha, C., Panseri, S., Marcacci, M. & Tampieri, A. (2012). Evaluation of the effects of a moderate intensity static magnetic field application on human osteoblast-like cells. *American Journal of Biomedical Engineering*, **2**, 263–268. 54, 58, 133, 153

Czekanska, E., Stoddart, M., Richards, R. & Hayes, J. (2012). In search of an osteoblast cell model for *in vivo* research. *Eur Cell Mater*, **24**, 1–17. 126, 131

Czekanska, E.M., Stoddart, M.J., Ralphs, J.R., Richards, R. & Hayes, J. (2014). A phenotypic comparison of osteoblast cell lines versus human primary osteoblasts for biomaterials testing. *Journal of biomedical materials research Part A*, **102**, 2636–2643. 125

Darendeliler, M.A., Sinclair, P.M. & Kusy, R.P. (1995). The effects of samarium-cobalt magnets and pulsed electromagnetic fields on tooth movement. *American Journal of Orthodontics and Dentofacial Orthopedics*, **107**, 578–588. 110

De, M., Chou, S.S., Joshi, H.M. & Dravid, V.P. (2011). Hybrid magnetic nanostructures (MNS) for magnetic resonance imaging applications. *Advanced drug delivery reviews*, **63**, 1282–1299. 61

De Mattei, M., Caruso, A., Traina, G.C., Pezzetti, F., Baroni, T. & Sollazzo, V. (1999). Correlation between pulsed electromagnetic fields exposure time and cell proliferation increase in human osteosarcoma cell lines and human normal osteoblast cells *in vivo*. *Bioelectromagnetics*, **20**, 177–182. 51

Degen, I. & Stetsula, V. (1971). Consolidation of bone fragments in a constant magnetic field. *Ortopediia travmatologiia i protezirovanie*, **32**, 45–48. 109

Dini, L. & Abbro, L. (2005). Bioeffects of moderate-intensity static magnetic fields on cell cultures. *Micron*, **36**, 195–217. 53, 166

Dobson, J. (2008). Remote control of cellular behaviour with magnetic nanoparticles. *Nature nanotechnology*, **3**, 139–143. 157

Dobson, J., Cartmell, S.H., Keramane, A. & El Haj, A.J. (2006). Principles and design of a novel magnetic force mechanical conditioning bioreactor for tissue engineering, stem cell

conditioning, and dynamic *in vivo* screening. *IEEE transactions on nanobioscience*, **5**, 173–177. 52

Domb, A.J. & Kumar, N. (2011). *Biodegradable polymers in clinical use and clinical development*. John Wiley & Sons. 6

Driessens, F., Verbeeck, R. & Kiekens, P. (1983). Mechanism of substitution in carbonated apatites. *Zeitschrift für anorganische und allgemeine Chemie*, **504**, 195–200. 47

Drury, J.L. & Mooney, D.J. (2003). Hydrogels for tissue engineering: scaffold design variables and applications. *Biomaterials*, **24**, 4337–4351. 27

Duarte, L. (1983). The stimulation of bone growth by ultrasound. *Archives of orthopaedic and traumatic surgery*, **101**, 153–159. 2

Dubey, N., Letourneau, P. & Tranquillo, R. (2001). Neuronal contact guidance in magnetically aligned fibrin gels: effect of variation in gel mechano-structural properties. *Biomaterials*, **22**, 1065–1075. 11, 163

Duncan, R. & Turner, C. (1995). Mechanotransduction and the functional response of bone to mechanical strain. *Calcified tissue international*, **57**, 344–358. 49, 50, 51

Dutta, R.C. & Dutta, A.K. (2009). Cell-interactive 3D-scaffold; advances and applications. *Biotechnology advances*, **27**, 334–339. 29, 127

Dvir, T., Timko, B.P., Kohane, D.S. & Langer, R. (2011). Nanotechnological strategies for engineering complex tissues. *Nature nanotechnology*, **6**, 13–22. 26

Einhorn, T.A. (1995). Current concepts review. enhancement of fracture-healing. *The Journal of Bone and Joint Surgery-american Volume*, **77**, 940–956. 41, 47

Epstein, F.H., Manolagas, S.C. & Jilka, R.L. (1995). Bone marrow, cytokines, and bone remodeling-emerging insights into the pathophysiology of osteoporosis. *New England journal of medicine*, **332**, 305–311. 15

Feng, S.W., Lo, Y.J., Chang, W.J., Lin, C.T., Lee, S.Y., Abiko, Y. & Huang, H.M. (2010). Static magnetic field exposure promotes differentiation of osteoblastic cells grown on the surface of a poly-l-lactide substrate. *Medical & biological engineering & computing*, **48**, 793–798. 56, 58

Fitzsimmons, R., Ryaby, J., Magee, F. & Baylink, D. (1994). Combined magnetic fields increased net calcium flux in bone cells. *Calcified tissue international*, **55**, 376–380. 51

Franceschi, R., Romano, P. & Park, K. (1988). Regulation of type I collagen synthesis by 1, 25-dihydroxyvitamin D3 in human osteosarcoma cells. *Journal of Biological Chemistry*, **263**, 18938–18945. 20

Franceschi, R.T., James, W.M. & Zerlauth, G. (1985). 1α, 25-Dihydroxyvitamin D3 specific regulation of growth, morphology, and fibronectin in a human osteosarcoma cell line. *Journal of cellular physiology*, **123**, 401–409. 20

Frost, H.M. (2003). Bone's mechanostat: a 2003 update. *The Anatomical Record Part A: Discoveries in Molecular, Cellular, and Evolutionary Biology*, **275**, 1081–1101. 50

Gartzke, J. & Lange, K. (2002). Cellular target of weak magnetic fields: ionic conduction along actin filaments of microvilli. *American Journal of Physiology-Cell Physiology*, **283**, C1333–C1346. 53

Ge, Y., Zhang, Y., He, S., Nie, F., Teng, G. & Gu, N. (2009). Fluorescence modified chitosan-coated magnetic nanoparticles for high-efficient cellular imaging. *Nanoscale research letters*, **4**, 287. 64

Gersbach, C.A., Byers, B.A., Pavlath, G.K. & García, A.J. (2004). Runx2/cbfa1 stimulates transdifferentiation of primary skeletal myoblasts into a mineralizing osteoblastic phenotype. *Experimental cell research*, **300**, 406–417. 162

Ghezzi, C.E., Marelli, B., Muja, N., Hirota, N., Martin, J.G., Barralet, J.E., Alessandrino, A., Freddi, G. & Nazhat, S.N. (2011a). Mesenchymal stem cell-seeded

multilayered dense collagen-silk fibroin hybrid for tissue engineering applications. *Biotechnology journal*, **6**, 1198–1207. 35

Ghezzi, C.E., Muja, N., Marelli, B. & Nazhat, S.N. (2011b). Real time responses of fibroblasts to plastically compressed fibrillar collagen hydrogels. *Biomaterials*, **32**, 4761–4772. 4, 33, 36

Glickstein, H., El, R.B., Link, G., Breuer, W., Konijn, A.M., Hershko, C., Nick, H. & Cabantchik, Z.I. (2006). Action of chelators in iron-loaded cardiac cells: accessibility to intracellular labile iron and functional consequences. *Blood*, **108**, 3195–3203. 62

Goh, Y.F., Shakir, I. & Hussain, R. (2013). Electrospun fibers for tissue engineering, drug delivery, and wound dressing. *Journal of Materials Science*, **48**, 3027–3054. 26

Gordon, M.K. & Hahn, R.A. (2010). Collagens. *Cell and tissue research*, **339**, 247. 6

Grant, S.F. & Ralston, S.H. (1997). Genes and osteoporosis. *Trends in Endocrinology & Metabolism*, **8**, 232–236. 16

Gray, H., Williams, P. & Bannister, L. (1995). Gray's anatomy: the anatomical basis of medicine and surgery. 38th. *New York: Churchill Livingstone*. 39

Guido, S. & Tranquillo, R.T. (1993). A methodology for the systematic and quantitative study of cell contact guidance in oriented collagen gels. correlation of fibroblast orientation and gel birefringence. *Journal of Cell Science*, **105**, 317–331. 11, 163

Gupta, A.K. & Wells, S. (2004). Surface-modified superparamagnetic nanoparticles for drug delivery: preparation, characterization, and cytotoxicity studies. *IEEE transactions on nanobioscience*, **3**, 66–73. 63, 64

Gurski, L.A., Jha, A.K., Zhang, C., Jia, X. & Farach-Carson, M.C. (2009). Hyaluronic acid-based hydrogels as 3D matrices for in vivo evaluation of chemotherapeutic drugs using poorly adherent prostate cancer cells. *Biomaterials*, **30**, 6076–6085. 27

Haddad, J.B., Obolensky, A.G. & Shinnick, P. (2007). The biologic effects and the therapeutic mechanism of action of electric and electromagnetic field stimulation on bone and cartilage: new findings and a review of earlier work. *The Journal of Alternative and Complementary Medicine*, **13**, 485–490. 2

Hadjipanayi, E., Mudera, V. & Brown, R. (2009a). Close dependence of fibroblast proliferation on collagen scaffold matrix stiffness. *Journal of tissue engineering and regenerative medicine*, **3**, 77. 33, 36

Hadjipanayi, E., Mudera, V. & Brown, R.A. (2009b). Guiding cell migration in 3D: a collagen matrix with graded directional stiffness. *Cytoskeleton*, **66**, 121–128. 31

Hadjipanayi, E., Cheema, U., Mudera, V., Deng, D., Liu, W. & Brown, R. (2011). First implantable device for hypoxia-mediated angiogenic induction. *Journal of controlled release*, **153**, 217–224. 36

Harris, H. (1990). The human alkaline phosphatases: what we know and what we don't know. *Clinica Chimica Acta*, **186**, 133–150. 17

Harris, J.R. & Reiber, A. (2007). Influence of saline and pH on collagen type I fibrillogenesis *in vivo*: fibril polymorphism and colloidal gold labelling. *Micron*, **38**, 513–521. 78

Heermeier, K., Spanner, M., Träger, J., Gradinger, R., Strauss, P., Kraus, W. & Schmidt, J. (1998). Effects of extremely low frequency electromagnetic field (EMF) on collagen type I mRNA expression and extracellular matrix synthesis of human osteoblastic cells. *Bioelectromagnetics*, **19**, 222–231. 51

Heino, J., Ignotz, R.A., Hemler, M.E., Crouse, C. & Massague, J. (1989). Regulation of cell adhesion receptors by transforming growth factor-beta. concomitant regulation of integrins that share a common beta 1 subunit. *Journal of Biological Chemistry*, **264**, 380–388. 19

Heng, B.C., Zhao, X., Xiong, S., Ng, K.W., Boey, F.Y.C. & Loo, J.S.C. (2010). Toxicity of zinc oxide (ZnO) nanoparticles on human bronchial epithelial cells (BEAS-2B) is accentuated by oxidative stress. *Food and Chemical Toxicology*, **48**, 1762–1766. 130

Heremans, H., Billiau, A., Cassiman, J.J., Mulier, J. & De Somer, P. (1978). *In vitro* cultivation of human tumor tissues ii. morphological and virological characterization of three cell lines. *Oncology*, **35**, 246–252. 19

Hernandez-Gil, I.F.T., Gracia, M.A., del Canto Pingarrn, M. & Jerez, L.B. (2006). Physiological bases of bone regeneration i. histology and physiology of bone tissue. *Med Oral*, **11**, E47–51. 13, 14, 44

Hirose, H., Nakahara, T. & Miyakoshi, J. (2003). Orientation of human glioblastoma cells embedded in type I collagen, caused by exposure to a 10 T static magnetic field. *Neuroscience letters*, **338**, 88–90. 57

Hodge, A.J. & Petruska, J.A. (1963). Recent studies with the electron microscope on ordered aggregates of the tropocollagen molecule. *Aspects of protein structure*, 289–300. 8

Hollinger, J. & Wong, M.E. (1996). The integrated processes of hard tissue regeneration with special emphasis on fracture healing. *Oral Surgery, Oral Medicine, Oral Pathology, Oral Radiology, and Endodontology*, **82**, 594–606. 2

Hong, F.T. (1995). Magnetic field effects on biomolecules, cells, and living organisms. *Biosystems*, **36**, 187–229. 53

Hsu, S.h. & Chang, J.C. (2010). The static magnetic field accelerates the osteogenic differentiation and mineralization of dental pulp cells. *Cytotechnology*, **62**, 143–155. 55, 58, 159

Hu, K., Shi, H., Zhu, J., Deng, D., Zhou, G., Zhang, W., Cao, Y. & Liu, W. (2010). Compressed collagen gel as the scaffold for skin engineering. *Biomedical microdevices*, **12**, 627–635. 30

Huang, C., Soenen, S.J., Rejman, J., Trekker, J., Chengxun, L., Lagae, L., Ceelen, W., Wilhelm, C., Demeester, J. & De Smedt, S.C. (2012). Magnetic electrospun fibers for cancer therapy. *Advanced Functional Materials*, **22**, 2479–2486. 25, 62

Huang, H.M., Lee, S.Y., Yao, W.C., Lin, C.T. & Yeh, C.Y. (2006). Static magnetic fields up-regulate osteoblast maturity by affecting local differentiation factors. *Clinical orthopaedics and related research*, **447**, 201–208. 56, 58, 158, 167

Huang, J., Best, S., Bonfield, W., Brooks, R., Rushton, N., Jayasinghe, S. & Edirisinghe, M. (2004). In vitro assessment of the biological response to nano-sized hydroxyapatite. *Journal of Materials Science: Materials in Medicine*, **15**, 441–445. 48

Huang, J., Lin, Y.W., Fu, X.W., Best, S.M., Brooks, R.A., Rushton, N. & Bonfield, W. (2007). Development of nano-sized hydroxyapatite reinforced composites for tissue engineering scaffolds. *Journal of Materials Science: Materials in Medicine*, **18**, 2151–2157. 77

Huang, Z.M., Zhang, Y.Z., Kotaki, M. & Ramakrishna, S. (2003). A review on polymer nanofibers by electrospinning and their applications in nanocomposites. *Composites science and technology*, **63**, 2223–2253. 25

Hulmes, D.J. (2002). Building collagen molecules, fibrils, and suprafibrillar structures. *Journal of structural biology*, **137**, 2–10. 8, 11, 164

Hunter, G.K. & Goldberg, H.A. (1993). Nucleation of hydroxyapatite by bone sialoprotein. *Proceedings of the National Academy of Sciences*, **90**, 8562–8565. 17

Hussain, S., Hess, K., Gearhart, J., Geiss, K. & Schlager, J. (2005). *In vitro* toxicity of nanoparticles in BRL 3A rat liver cells. *Toxicology* in vivo, **19**, 975–983. 64

Imaizumi, Y., Ozawa, S., Hirukawa, K., Togari, A. & Tanaka, Y. (2007). Effects of a static magnetic field on mineralization of MC3T3-E1 cells. *Prosthodontic Research & Practice*, **6**, 87–92. 36, 54, 56, 58, 109, 133, 157

Jahn, K., Richards, R., Archer, C.W. & Stoddart, M. (2010). Pellet culture model for human primary osteoblasts. *Eur Cell Mater*, **20**, 149. 24

Jiang, X., Cao, H.Q., Shi, L.Y., Ng, S.Y., Stanton, L.W. & Chew, S.Y. (2012). Nanofiber topography and sustained biochemical signaling enhance human mesenchymal stem cell neural commitment. *Acta biomaterialia*, **8**, 1290–1302. 25

Jones, D., Nolte, H., Scholübbers, J., Turner, E. & Veltel, D. (1991). Biochemical signal transduction of mechanical strain in osteoblast-like cells. *Biomaterials*, **12**, 101–110. 51

Jones, J.R., Ehrenfried, L.M. & Hench, L.L. (2006). Optimising bioactive glass scaffolds for bone tissue engineering. *Biomaterials*, **27**, 964–973. 2

Jones, S., Boyde, A. & Pawley, J. (1975). Osteoblasts and collagen orientation. *Cell and tissue research*, **159**, 73–80. 9

Jonsson, K.B., Frost, A., Nilsson, O., Ljunghall, S. & Ljunggren, Ö. (1999). Three isolation techniques for primary culture of human osteoblast-like cells: a comparison. *Acta orthopaedica Scandinavica*, **70**, 365–373. 19

Jouni, F.J., Abdolmaleki, P. & Movahedin, M. (2013). Investigation on the effect of static magnetic field up to 15 mT on the viability and proliferation rate of rat bone marrow stem cells. In vitro *Cellular & Developmental Biology-Animal*, **49**, 212–219. 55, 58

Kadler, K.E., Hill, A. & Canty-Laird, E.G. (2008). Collagen fibrillogenesis: fibronectin, integrins, and minor collagens as organizers and nucleators. *Current opinion in cell biology*, **20**, 495–501. 9

Kale, S., Biermann, S., Edwards, C., Tarnowski, C., Morris, M. & Long, M.W. (2000). Three-dimensional cellular development is essential for ex vivo formation of human bone. *Nature biotechnology*, **18**, 954–958. 24

Kar, K., Amin, P., Bryan, M.A., Persikov, A.V., Mohs, A., Wang, Y.H. & Brodsky, B. (2006). Self-association of collagen triple helic peptides into higher order structures. *Journal of Biological Chemistry*, **281**, 33283–33290. 8

Karlsson, H.L., Cronholm, P., Gustafsson, J. & Moller, L. (2008). Copper oxide nanoparticles are highly toxic: a comparison between metal oxide nanoparticles and carbon nanotubes. *Chemical research in toxicology*, **21**, 1726–1732. 62, 64

Kartsogiannis, V. & Ng, K.W. (2004). Cell lines and primary cell cultures in the study of bone cell biology. *Molecular and cellular endocrinology*, **228**, 79–102. 125

Katti, D.S., Robinson, K.W., Ko, F.K. & Laurencin, C.T. (2004). Bioresorbable nanofiber-based systems for wound healing and drug delivery: Optimization of fabrication parameters. *Journal of Biomedical Materials Research Part B: Applied Biomaterials*, **70**, 286–296. 26

Kavaliers, M. & Ossenkopp, K.P. (1994). Effects of magnetic and electric. *Biological effects of electric and magnetic fields: Sources and mechanisms*, **1**, 205. 53

Kenwright, J. & Goodship, A.E. (1989). Controlled mechanical stimulation in the treatment of tibial fractures. *Clinical orthopaedics and related research*, **241**, 36–47. 2

Kielty, C.M. & Grant, M.E. (2003). The collagen family: structure, assembly, and organization in the extracellular matrix. *Connective Tissue and Its Heritable Disorders: Molecular, Genetic, and Medical Aspects, Second Edition*, 159–221. 8

Kievit, F.M., Veiseh, O., Bhattarai, N., Fang, C., Gunn, J.W., Lee, D., Ellenbogen, R.G., Olson, J.M. & Zhang, M. (2009). PEI–PEG–chitosan-copolymer-coated iron oxide nanoparticles for safe gene delivery: synthesis, complexation, and transfection. *Advanced functional materials*, **19**, 2244–2251. 63

Kim, H.J., Chang, I.T., Heo, S.J., Koak, J.Y., Kim, S.K. & Jang, J.H. (2005). Effect of magnetic field on the fibronectin adsorption, cell attachment and proliferation on titanium surface. *Clinical Oral Implants Research*, **16**, 557–562. 73, 109

Kim, J.S., Yoon, T.J., Yu, K.N., Kim, B.G., Park, S.J., Kim, H.W., Lee, K.H., Park, S.B., Lee, J.K. & Cho, M.H. (2006). Toxicity and tissue distribution of magnetic nanoparticles in mice. *Toxicological Sciences*, **89**, 338–347. 63, 64

Kini, U. & Nandeesh, B. (2012). Physiology of bone formation, remodeling, and metabolism. In *Radionuclide and hybrid bone imaging*, 29–57, Springer. 9, 13

Kirkwood, J.E. & Fuller, G.G. (2009). Liquid crystalline collagen: a self-assembled morphology for the orientation of mammalian cells. *Langmuir*, **25**, 3200–3206. 8, 11

Knighton, D.R. & Fiegel, V.D. (1989). Macrophage-derived growth factors in wound healing: regulation of growth factor production by the oxygen microenvironment. *Am Rev Respir Dis*, **140**, 1108–1111. 39

Komori, T. (2010). Regulation of bone development and extracellular matrix protein genes by Runx2. *Cell and tissue research*, **339**, 189–195. 161

Kotani, H., Iwasaka, M., Ueno, S. & Curtis, A. (2000). Magnetic orientation of collagen and bone mixture. *Journal of Applied Physics*, **87**, 6191–6193. 11, 12, 163, 164

Kotani, H., Kawaguchi, H., Shimoaka, T., Iwasaka, M., Ueno, S., Ozawa, H., Nakamura, K. & Hoshi, K. (2002). Strong static magnetic field stimulates bone formation to a definite orientation *in vitro* and *in vivo*. *Journal of Bone and Mineral Research*, **17**, 1814–1821. 50, 57, 158

Kumar, S. (2003). Selective laser sintering: a qualitative and objective approach. *JOM Journal of the Minerals, Metals and Materials Society*, **55**, 43–47. 74

Kwong, F.N. & Harris, M.B. (2008). Recent developments in the biology of fracture repair. *Journal of the American Academy of Orthopaedic Surgeons*, **16**, 619–625. 1, 43

Lajeunesse, D., Frondoza, C., Schoffield, B. & Sacktor, B. (1990). Osteocalcin secretion by the human osteosarcoma cell line MG-63. *Journal of Bone and Mineral Research*, **5**, 915–922. 20

Landry, P.S., Sadasivan, K.K., Marino, A.A. & Albright, J.A. (1997). Electromagnetic fields can affect osteogenesis by increasing the rate of differentiation. *Clinical orthopaedics and related research*, **338**, 262–270. 51

Lanyon, L. (1984). Functional strain as a determinant for bone remodeling. *Calcified tissue international*, **36**, S56–S61. 51

Lednev, V. (1996). Bioeffects of weak static and alternating magnetic fields. *Biofizika*, **41**, 224–232. 54

Lian, J.B. & Stein, G.S. (1992). Concepts of osteoblast growth and differentiation: basis for modulation of bone cell development and tissue formation. *Critical Reviews in Oral Biology & Medicine*, **3**, 269–305. 15, 16

Lind, M. (1998). Growth factor stimulation of bone healing. effects on osteoblasts, osteomies, and implants fixation. *Acta orthopaedica Scandinavica. Supplementum*, **283**, 2–37. 2

Lind, M., Schumacker, B., Søballe, K., Keller, J., Melsen, F. & Bünger, C. (1993). Transforming growth factor-β enhances fracture healing in rabbit tibiae. *Acta Orthopaedica Scandinavica*, **64**, 553–556. 45

Liu, X., Kaminski, M.D., Guan, Y., Chen, H., Liu, H. & Rosengart, A.J. (2006). Preparation and characterization of hydrophobic superparamagnetic magnetite gel. *Journal of Magnetism and Magnetic Materials*, **306**, 248–253. 178

Lu, A.H., Salabas, E.e. & Schüth, F. (2007). Magnetic nanoparticles: synthesis, protection, functionalization, and application. *Angewandte Chemie International Edition*, **46**, 1222–1244. 74

Lu, J.W., Zhu, Y.L., Guo, Z.X., Hu, P. & Yu, J. (2006). Electrospinning of sodium alginate with poly (ethylene oxide). *Polymer*, **47**, 8026–8031. 25

Lu, X., Niu, M., Qiao, R. & Gao, M. (2008). Superdispersible PVP-Coated Fe3O4 Nanocrystals Prepared by a One-Pot Reaction. *The Journal of Physical Chemistry B*, **112**, 14390–14394. 74

Lübbe, A.S., Alexiou, C. & Bergemann, C. (2001). Clinical applications of magnetic drug targeting. *Journal of Surgical Research*, **95**, 200–206. 61

Ma, H.l., Qi, X.r., Maitani, Y. & Nagai, T. (2007). Preparation and characterization of superparamagnetic iron oxide nanoparticles stabilized by alginate. *International journal of pharmaceutics*, **333**, 177–186. 63

Mahmoudi, M., Simchi, A., Imani, M., Shokrgozar, M.A., Milani, A.S., Häfeli, U.O. & Stroeve, P. (2010). A new approach for the *in vivo* identification of the cytotoxicity of superparamagnetic iron oxide nanoparticles. *Colloids and Surfaces B: Biointerfaces*, **75**, 300–309. 128, 129

Malakhov, S., Khomenko, A.Y., Belousov, S., Prazdnichnyi, A., Chvalun, S., Shepelev, A. & Budyka, A. (2009). Method of manufacturing nonwovens by electrospinning from polymer melts. *Fibre chemistry*, **41**, 355–359. 26

Maredziak, M., Marycz, K., Lewandowski, D., Siudzinska, A. & Smieszek, A. (2015). Static magnetic field enhances synthesis and secretion of membrane-derived microvesicles (MVs) rich in VEGF and BMP-2 in equine adipose-derived stromal cells (EqASCs)?a new approach in veterinary regenerative medicine. In vitro *Cellular & Developmental Biology-Animal*, **51**, 230–240. 166

Marelli, B., Ghezzi, C.E., Barralet, J.E., Boccaccini, A.R. & Nazhat, S.N. (2010). Three-dimensional mineralization of dense nanofibrillar collagen- bioglass hybrid scaffolds. *Biomacromolecules*, **11**, 1470–1479. 35

Marelli, B., Ghezzi, C.E., Barralet, J.E. & Nazhat, S.N. (2011). Collagen gel fibrillar density dictates the extent of mineralization *in vivo*. *Soft Matter*, **7**, 9898–9907. 4, 34, 36

Marelli, B., Ghezzi, C., Alessandrino, A., Freddi, G. & Nazhat, S. (2014). Anionic fibroin-derived polypeptides accelerate msc osteoblastic differentiation in a three-dimensional osteoid-like dense collagen niche. *Journal of Materials Chemistry B*, **2**, 5339–5343. 35

Markland, P., Zhang, Y., Amidon, G.L. & Yang, V.C. (1999). A pH-and ionic strength-responsive polypeptide hydrogel: synthesis, characterization, and preliminary protein release studies. 27

Markov, M., Wang, S. & Pilla, A. (1993). Effects of weak low frequency sinusoidal and dc magnetic fields on myosin phosphorylation in a cell-free preparation. *Bioelectrochemistry and Bioenergetics*, **30**, 119–125. 54

Martinez, M., Del Campo, M., Medina, S., Sanchez, M., Sanchez-Cabezudo, M., Esbrit, P., Martinez, P., Moreno, I., Rodrigo, A., Garces, M. *et al.* (1999). Influence of skeletal site of origin and donor age on osteoblastic cell growth and differentiation. *Calcified tissue international*, **64**, 280–286. 9

Maruyama, Z., Yoshida, C.A., Furuichi, T., Amizuka, N., Ito, M., Fukuyama, R., Miyazaki, T., Kitaura, H., Nakamura, K., Fujita, T. *et al.* (2007). Runx2 determines bone maturity and turnover rate in postnatal bone development and is involved in bone loss in estrogen deficiency. *Developmental dynamics*, **236**, 1876–1890. 16

Mascolo, M.C., Pei, Y. & Ring, T.A. (2013). Room temperature co-precipitation synthesis of magnetite nanoparticles in a large ph window with different bases. *Materials*, **6**, 5549–5567. 74

Mason, B.N., Califano, J.P. & Reinhart-King, C.A. (2012). Matrix stiffness: A regulator of cellular behavior and tissue formation. In *Engineering Biomaterials for Regenerative Medicine*, 19–37, Springer. 21

Matthews, J.A., Wnek, G.E., Simpson, D.G. & Bowlin, G.L. (2002). Electrospinning of collagen nanofibers. *Biomacromolecules*, **3**, 232–238. 26

Memarzadeh, K., Sharili, A.S., Huang, J., Rawlinson, S.C. & Allaker, R.P. (2015). Nanoparticulate zinc oxide as a coating material for orthopedic and dental implants. *Journal of Biomedical Materials Research Part A*, **103**, 981–989. 48, 130

Meng, J., Zhang, Y., Qi, X., Kong, H., Wang, C., Xu, Z., Xie, S., Gu, N. & Xu, H. (2010). Paramagnetic nanofibrous composite films enhance the osteogenic responses of pre-osteoblast cells. *Nanoscale*, **2**, 2565–2569. 56, 157, 158

Meng, J., Xiao, B., Zhang, Y., Liu, J., Xue, H., Lei, J., Kong, H., Huang, Y., Jin, Z., Gu, N. *et al.* (2013). Super-paramagnetic responsive nanofibrous scaffolds under static magnetic field enhance osteogenesis for bone repair *in vivo*. *Scientific reports*, **3**, 2655. 2, 52, 133, 172

Mi, S., Chen, B., Wright, B. & Connon, C.J. (2010). Ex vivo construction of an artificial ocular surface by combination of corneal limbal epithelial cells and a compressed collagen scaffold containing keratocytes. *Tissue Engineering Part A*, **16**, 2091–2100. 30

Mills, L.A. & Simpson, A.H.R. (2013). The relative incidence of fracture non-union in the scottish population (5.17 million): a 5-year epidemiological study. *BMJ open*, **3**, e002276. 1

Miltenyi, S., Muller, W., Weichel, W. & Radbruch, A. (1990). High gradient magnetic cell separation with macs. *Cytometry*, **11**, 231–238. 59

Mo, X., Iwata, H., Matsuda, S. & Ikada, Y. (2000). Soft tissue adhesive composed of modified gelatin and polysaccharides. *Journal of Biomaterials Science, Polymer Edition*, **11**, 341–351. 26

Moalli, M.R., Caldwell, N.J., Patil, P.V. & Goldstein, S.A. (2000). An *in vivo* model for investigations of mechanical signal transduction in trabecular bone. *Journal of Bone and Mineral Research*, **15**, 1346–1353. 50

Mollon, B., da Silva, V., Busse, J.W., Einhorn, T.A. & Bhandari, M. (2008). Electrical stimulation for long-bone fracture-healing: a meta-analysis of randomized controlled trials. *J Bone Joint Surg Am*, **90**, 2322–2330. 2

Morshed, S. (2014). Current options for determining fracture union. *Advances in medicine*, **2014**. 41

Mudera, V., Morgan, M., Cheema, U., Nazhat, S. & Brown, R. (2007). Ultra-rapid engineered collagen constructs tested in an *in vivo* nursery site. *Journal of tissue engineering and regenerative medicine*, **1**, 192–198. 31

Muralidharan-Chari, V., Clancy, J.W., Sedgwick, A. & D'Souza-Schorey, C. (2010). Microvesicles: mediators of extracellular communication during cancer progression. *Journal of cell science*, **123**, 1603–1611. 166

Murugan, R. & Ramakrishna, S. (2005). Development of nanocomposites for bone grafting. *Composites Science and Technology*, **65**, 2385–2406. 48

Muthusubramaniam, L., Peng, L., Zaitseva, T., Paukshto, M., Martin, G.R. & Desai, T.A. (2012). Collagen fibril diameter and alignment promote the quiescent keratocyte phenotype. *Journal of Biomedical Materials Research Part A*, **100**, 613–621. 21

Naqvi, S., Samim, M., Abdin, M., Ahmed, F.J., Maitra, A., Prashant, C. & Dinda, A.K. (2010). Concentration-dependent toxicity of iron oxide nanoparticles mediated by increased oxidative stress. *International journal of nanomedicine*, **5**, 983. 62, 64, 128

Nazhat, S.N., Abou Neel, E.A., Kidane, A., Ahmed, I., Hope, C., Kershaw, M., Lee, P.D., Stride, E., Saffari, N., Knowles, J.C. *et al.* (2007). Controlled microchannelling in dense collagen scaffolds by soluble phosphate glass fibers. *Biomacromolecules*, **8**, 543–551. 37

Neel, E.A.A., Cheema, U., Knowles, J.C., Brown, R.A. & Nazhat, S.N. (2006). Use of multiple unconfined compression for control of collagen gel scaffold density and mechanical properties. *Soft Matter*, **2**, 986–992. 37

Nisbet, D., Forsythe, J.S., Shen, W., Finkelstein, D. & Horne, M.K. (2008). Review paper: a review of the cellular response on electrospun nanofibers for tissue engineering. *Journal of biomaterials applications*. 24, 26

Ohgushi, H., Okumura, M., Yoshikawa, T., Inboue, K., Senpuku, N., Tamai, S. & Shors, E.C. (1992). Bone formation processin porous calcium carbonate and hydroxyapatite. *Journal of biomedical materials research*, **26**, 885–895. 2

Oryan, A., Alidadi, S. & Moshiri, A. (2013). Current concerns regarding healing of bone defects. *Hard tissue*, **2**, 1–12. 42

Ottaviani, E., Malagoli, D., Ferrari, A., Tagliazucchi, D., Conte, A. & Gobba, F. (2002). 50 Hz magnetic fields of varying flux intensity affect cell shape changes in invertebrate immunocytes: The role of potassium ion channels. *Bioelectromagnetics*, **23**, 292–297. 54

Owen, T.A., Aronow, M., Shalhoub, V., Barone, L.M., Wilming, L., Tassinari, M.S., Kennedy, M.B., Pockwinse, S., Lian, J.B. & Stein, G.S. (1990). Progressive development of the rat osteoblast phenotype *in vivo*: reciprocal relationships in expression of genes associated with osteoblast proliferation and differentiation during formation of the bone extracellular matrix. *Journal of cellular physiology*, **143**, 420–430. 18

Pankhurst, Q.A., Connolly, J., Jones, S. & Dobson, J. (2003). Applications of magnetic nanoparticles in biomedicine. *Journal of physics D: Applied physics*, **36**, R167. 60

Papachroni, K.K., Karatzas, D.N., Papavassiliou, K.A., Basdra, E.K. & Papavassiliou, A.G. (2009). Mechanotransduction in osteoblast regulation and bone disease. *Trends in molecular medicine*, **15**, 208–216. 45, 50

Paradisi, S., Donelli, G., Santini, M.T., Straface, E. & Malorni, W. (1993). A 50-Hz magnetic field induces structural and biophysical changes in membranes. *Bioelectromagnetics*, **14**, 247–255. 54, 55

Park, J.E. & Barbul, A. (2004). Understanding the role of immune regulation in wound healing. *The American Journal of Surgery*, **187**, S11–S16. 39

Patel, V.R. & Amiji, M.M. (1996). Preparation and characterization of freeze-dried chitosan-poly (ethylene oxide) hydrogels for site-specific antibiotic delivery in the stomach. *Pharmaceutical research*, **13**, 588–593. 27

Pauling, L. (1979). Diamagnetic anisotropy of the peptide group. *Proceedings of the National Academy of Sciences*, **76**, 2293–2294. 11, 164

Pautke, C., SCHIEKER, M., TISCHER, T., KOLK, A., NETH, P., MUTSCHLER, W. & MILZ, S. (2004). Characterization of osteosarcoma cell lines MG-63, Saos-2 and U-2 OS in comparison to human osteoblasts. *Anticancer research*, **24**, 3743–3748. 123, 125

Pavlin, D., Zadro, R. & Gluhak-Heinrich, J. (2001). Temporal pattern of stimulation of osteoblast-associated genes during mechanically-induced osteogenesis *in vivo*: early responses of osteocalcin and type I collagen. *Connective tissue research*, **42**, 135–148. 50

Phillips, J.B., Bunting, S.C., Hall, S.M. & Brown, R.A. (2005). Neural tissue engineering: a self-organizing collagen guidance conduit. *Tissue engineering*, **11**, 1611–1617. 29

Phimphilai, M., Zhao, Z., Boules, H., Roca, H. & Franceschi, R.T. (2006). BMP signaling is required for Runx2-dependent induction of the osteoblast phenotype. *Journal of Bone and Mineral Research*, **21**, 637–646. 46

Pierschbacher, M., Dedhar, S., Ruoslahti, E., Argraves, S. & Suzuki, S. (1988). An adhesion variant of the MIG-63 osteosarcoma cell line displays an osteoblast-like phenotype. *Cell and molecular biology of vertebrate hard tissues*, **136**, 131–141. 20

Posner, A. (1978). " the chemistry of bone mineral". *Bulletin of the Hospital for Joint Diseases*, **39**, 126–144. 47

Pritchard, J. (1972). General histology of bone. *The biochemistry and physiology of bone*, **1**. 13, 14

Quarles, L.D., Yohay, D.A., Lever, L.W., Caton, R. & Wenstrup, R.J. (1992). Distinct proliferative and differentiated stages of murine MC3T3-E1 cells in culture: an *in vitro* model of osteoblast development. *Journal of Bone and Mineral Research*, **7**, 683–692. 20

Reijnders, C.M., Bravenboer, N., Tromp, A.M., Blankenstein, M.A. & Lips, P. (2007). Effect of mechanical loading on insulin-like growth factor-I gene expression in rat tibia. *Journal of Endocrinology*, **192**, 131–140. 45

Reiter, R.J. (1993). A review of neuroendocrine and neurochemical changes associated with static and extremely low frequency electromagnetic field exposure. *Integrative Physiological and Behavioral Science*, **28**, 57–75. 54

Revell, P.A. (2012). *Pathology of bone*. Springer Science & Business Media. 14, 38

Riley, M.A., Walmsley, A.D. & Harris, I.R. (2001). Magnets in prosthetic dentistry. *The Journal of prosthetic dentistry*, **86**, 137–142. 73

Ritchie, R.O., Kinney, J.H., Kruzic, J.J. & Nalla, R.K. (2005). A fracture mechanics and mechanistic approach to the failure of cortical bone. *Fatigue & Fracture of Engineering Materials & Structures*, **28**, 345–371. 7

Roach, H. (1994). Why does bone matrix contain non-collagenous proteins? the possible roles of osteocalcin, osteonectin, osteopontin and bone sialoprotein in bone mineralisation and resorption. *Cell biology international*, **18**, 617–628. 17, 18

Robling, A.G., Burr, D.B. & Turner, C.H. (2000). Partitioning a daily mechanical stimulus into discrete loading bouts improves the osteogenic response to loading. *Journal of Bone and Mineral Research*, **15**, 1596–1602. 50

Rosen, A.D. (1996). Inhibition of calcium channel activation in GH3 cells by static magnetic fields. *Biochimica et Biophysica Acta (BBA)-Biomembranes*, **1282**, 149–155. 54

Rosen, A.D. (2003). Mechanism of action of moderate-intensity static magnetic fields on biological systems. *Cell biochemistry and biophysics*, **39**, 163–173. 2, 52, 53, 57, 133, 166, 172

Ross, S.M., Ferrier, J.M. & Aubin, J.E. (1989). Studies on the alignment of fibroblasts in uniform applied electrical fields. *Bioelectromagnetics*, **10**, 371–384. 54

Rowley, J.A., Madlambayan, G. & Mooney, D.J. (1999). Alginate hydrogels as synthetic extracellular matrix materials. *Biomaterials*, **20**, 45–53. 27

Rubin, C.T. & Lanyon, L.E. (1985). Regulation of bone mass by mechanical strain magnitude. *Calcified tissue international*, **37**, 411–417. 2, 51, 53, 133, 173

Ryaby, J.T. (1998). Clinical effects of electromagnetic and electric fields on fracture healing. *Clinical orthopaedics and related research*, **355**, S205–S215. 2

San Thian, E., Ahmad, Z., Huang, J., Edirisinghe, M.J., Jayasinghe, S.N., Ireland, D.C., Brooks, R.A., Rushton, N., Bonfield, W. & Best, S.M. (2008). The role of electrosprayed apatite nanocrystals in guiding osteoblast behaviour. *Biomaterials*, **29**, 1833–1843. 129

Sapir, Y., Polyak, B. & Cohen, S. (2014). Cardiac tissue engineering in magnetically actuated scaffolds. *Nanotechnology*, **25**, 014009. 60

Sathyendra, V. & Darowish, M. (2013). Basic science of bone healing. *Hand clinics*, **29**, 473–481. 44, 50

Sato, M., Ochi, T., Nakase, T., Hirota, S., Kitamura, Y., Nomura, S. & Yasui, N. (1999). Mechanical Tension-Stress Induces Expression of Bone Morphogenetic Protein (BMP)-2 and BMP-4, but Not BMP-6, BMP-7, and GDF-5 mRNA, During Distraction Osteogenesis. *Journal of Bone and Mineral Research*, **14**, 1084–1095. 46

Schmitt, J.M., Hwang, K., Winn, S.R. & Hollinger, J.O. (1999). Bone morphogenetic proteins: an update on basic biology and clinical relevance. *Journal of orthopaedic research*, **17**, 269–278. 46

Schriefer, J.L., Warden, S.J., Saxon, L.K., Robling, A.G. & Turner, C.H. (2005). Cellular accommodation and the response of bone to mechanical loading. *Journal of biomechanics*, **38**, 1838–1845. 50

Selvamurugan, N., Kwok, S., Vasilov, A., Jefcoat, S.C. & Partridge, N.C. (2007). Effects of BMP-2 and pulsed electromagnetic field (PEMF) on rat primary osteoblastic cell proliferation and gene expression. *Journal of orthopaedic research*, **25**, 1213–1220. 160

Shupak, N.M., Prato, F.S. & Thomas, A.W. (2003). Therapeutic uses of pulsed magnetic-field exposure: a review. *Radio Sci Bull*, **307**, 9À30. 52

Skomski, R. (2008). *Simple models of magnetism*. Oxford University Press on Demand. 59

Stern, P.H. & Krieger, N.S. (1983). Comparison of fetal rat limb bones and neonatal mouse calvaria: effects of parathyroid hormone and 1, 25-dihydroxyvitamin d 3. *Calcified tissue international*, **35**, 172–176. 19

Stevens, M.M. (2008). Biomaterials for bone tissue engineering. *Materials today*, **11**, 18–25. 25

Stratton, D., Lange, S. & Inal, J.M. (2013). Pulsed extremely low-frequency magnetic fields stimulate microvesicle release from human monocytic leukaemia cells. *Biochemical and biophysical research communications*, **430**, 470–475. 166

Suda, T. & Ueno, S. (1997). Effect of strong magnetic fields on the characteristics of bilayer lipid membranes. *Journal of applied physics*, **81**, 4318–4320. 165

Sudo, H., Kodama, H.A., Amagai, Y., Yamamoto, S. & Kasai, S. (1983). *In vitro* differentiation and calcification in a new clonal osteogenic cell line derived from newborn mouse calvaria. *J Cell Biol*, **96**, 191–198. 20

Sun, S., Murray, C., Weller, D., Folks, L. & Moser, A. (2000). Monodisperse fept nanoparticles and ferromagnetic fept nanocrystal superlattices. *Science*, **287**, 1989–1992. 61

Tabata, Y., Miyao, M., Ozeki, M. & Ikada, Y. (2000). Controlled release of vascular endothelial growth factor by use of collagen hydrogels. *Journal of Biomaterials Science, Polymer Edition*, **11**, 915–930. 113

Teja, A.S. & Koh, P.Y. (2009). Synthesis, properties, and applications of magnetic iron oxide nanoparticles. *Progress in crystal growth and characterization of materials*, **55**, 22–45. 62, 74

Termine, J.D., Kleinman, H.K., Whitson, S.W., Conn, K.M., McGarvey, M.L. & Martin, G.R. (1981). Osteonectin, a bone-specific protein linking mineral to collagen. *Cell*, **26**, 99–105. 159, 161

Tomasek, J.J., Gabbiani, G., Hinz, B., Chaponnier, C. & Brown, R.A. (2002). Myofibroblasts and mechano-regulation of connective tissue remodelling. *Nature reviews Molecular cell biology*, **3**, 349–363. 29

Tonna, E.A. & Cronkite, E.P. (1961). Cellular response to fracture studied with tritiated thymidine. *J Bone Joint Surg Am*, **43**, 352–362. 39

Torbet, J. & Ronziere, M.C. (1984). Magnetic alignment of collagen during self-assembly. *Biochemical journal*, **219**, 1057–1059. 11, 163, 164, 165

Trock, D.H. (2000). Electromagnetic fields and magnets: investigational treatment for musculoskeletal disorders. *Rheumatic Disease Clinics of North America*, **26**, 51–62. 2

Tsai, M.T., Li, W.J., Tuan, R.S. & Chang, W.H. (2009). Modulation of osteogenesis in human mesenchymal stem cells by specific pulsed electromagnetic field stimulation. *Journal of Orthopaedic Research*, **27**, 1169–1174. 160

Urist, M.R. (1965). Bone: formation by autoinduction. *Science*, **150**, 893–899. 46

van der Rijt, J.A., van der Werf, K.O., Bennink, M.L., Dijkstra, P.J. & Feijen, J. (2006). Micromechanical testing of individual collagen fibrils. *Macromolecular bioscience*, **6**, 697–702. 37

Vaughan, J.M. (1970). The physiology of bone. 10

Victoria, G., Petrisor, B., Drew, B. & Dick, D. (2009). Bone stimulation for fracture healing: What's all the fuss? *Indian journal of orthopaedics*, **43**, 117. 41

Viguet-Carrin, S., Garnero, P. & Delmas, P. (2006). The role of collagen in bone strength. *Osteoporosis international*, **17**, 319–336. 8

Voegele, T.J., Voegele-Kadletz, M., Esposito, V., Macfelda, K., Oberndorfer, U., Vecsei, V. & Schabus, R. (1999). The effect of different isolation techniques on human osteoblast-like cell growth. *Anticancer research*, **20**, 3575–3581. 19

Wallace, A., Draper, E., Strachan, R., McCarthy, I. & Hughes, S. (1994). The vascular response to fracture micromovement. *Clinical orthopaedics and related research*, **301**, 281–290. 51

Wang, D., Christensen, K., Chawla, K., Xiao, G., Krebsbach, P.H. & Franceschi, R.T. (1999). Isolation and characterization of MC3T3-E1 preosteoblast subclones with distinct *in vitro* and *in vivo* differentiation/mineralization potential. *Journal of Bone and Mineral Research*, **14**, 893–903. 20

Wang, M., Singh, H., Hatton, T. & Rutledge, G. (2004). Field-responsive superparamagnetic composite nanofibers by electrospinning. *Polymer*, **45**, 5505–5514. 25

Webster, T.J. *et al.* (2007). *Nanotechnology for the regeneration of hard and soft tissues*. World Scientific. 15

Wei, G. & Ma, P.X. (2004). Structure and properties of nano-hydroxyapatite/polymer composite scaffolds for bone tissue engineering. *Biomaterials*, **25**, 4749–4757. 48

Wei, Y., Zhang, X., Song, Y., Han, B., Hu, X., Wang, X., Lin, Y. & Deng, X. (2011). Magnetic biodegradable Fe_3O_4/CS/PVA nanofibrous membranes for bone regeneration. *Biomedical Materials*, **6**, 055008. 157

White, D.J., Puranen, S., Johnson, M.S. & Heino, J. (2004). The collagen receptor subfamily of the integrins. *The international journal of biochemistry & cell biology*, **36**, 1405–1410. 21

Worcester, D. (1978). Structural origins of diamagnetic anisotropy in proteins. *Proceedings of the National Academy of Sciences*, **75**, 5475–5477. 11, 164

Xia, T., Kovochich, M., Liong, M., Madler, L., Gilbert, B., Shi, H., Yeh, J.I., Zink, J.I. & Nel, A.E. (2008). Comparison of the mechanism of toxicity of zinc oxide and cerium oxide nanoparticles based on dissolution and oxidative stress properties. *ACS nano*, **2**, 2121–2134. 130

Xiao, G., Wang, D., Benson, M.D., Karsenty, G. & Franceschi, R.T. (1998). Role of the α2-integrin in osteoblast-specific gene expression and activation of the Osf2 transcription factor. *Journal of Biological Chemistry*, **273**, 32988–32994. 17

Xiao, N., Wen, Q., Liu, Q., Yang, Q. & Li, Y. (2014). Electrospinning preparation of β-cyclodextrin/glutaraldehyde crosslinked PVP nanofibrous membranes to adsorb dye in aqueous solution. *Chemical Research in Chinese Universities*, **30**, 1057–1062. 25

Yamagashi, A., Takeuchi, T., Hagashi, T. & Date, M. (1992). Diamagnetic orientation of blood cells in high magnetic field. *Physica B: Condensed Matter*, **177**, 523–526. 165

Yamaguchi, A., Komori, T. & Suda, T. (2000). Regulation of osteoblast differentiation mediated by bone morphogenetic proteins, hedgehogs, and Cbfa1. *Endocrine reviews*, **21**, 393–411. 46

Yamamoto, M., Ikada, Y. & Tabata, Y. (2001). Controlled release of growth factors based on biodegradation of gelatin hydrogel. *Journal of Biomaterials Science, Polymer Edition*, **12**, 77–88. 27

Yamamoto, Y., Ohsaki, Y., Goto, T., Nakasima, A. & Iijima, T. (2003). Effects of static magnetic fields on bone formation in rat osteoblast cultures. *Journal of dental research*, **82**, 962–966. 55, 56, 58, 109

Yin, Z., Chen, X., Chen, J.L., Shen, W.L., Nguyen, T.M.H., Gao, L. & Ouyang, H.W. (2010). The regulation of tendon stem cell differentiation by the alignment of nanofibers. *Biomaterials*, **31**, 2163–2175. 25

Yoshii, F., Zhanshan, Y., Isobe, K., Shinozaki, K. & Makuuchi, K. (1999). Electron beam crosslinked PEO and PEO/PVA hydrogels for wound dressing. *Radiation Physics and Chemistry*, **55**, 133–138. 27

Yoshimoto, H., Shin, Y., Terai, H. & Vacanti, J. (2003). A biodegradable nanofiber scaffold by electrospinning and its potential for bone tissue engineering. *Biomaterials*, **24**, 2077–2082. 25

Yoshizawa, H., Tsuchiya, T., Mizoe, H., Ozeki, H., Kanao, S., Yomori, H., Sakane, C., Hasebe, S., Motomura, T., Yamakawa, T. *et al.* (2002). No effect of extremely low-frequency magnetic field observed on cell growth or initial response of cell proliferation in human cancer cell lines. *Bioelectromagnetics*, **23**, 355–368. 55

Yu, Y.Y., Lieu, S., Lu, C., Miclau, T., Marcucio, R.S. & Colnot, C. (2010). Immunolocalization of BMPs, BMP antagonists, receptors, and effectors during fracture repair. *Bone*, **46**, 841–851. 40

Yuan, L. & Veis, A. (1973). The self-assembly of collagen molecules. *Biopolymers*, **12**, 1437–1444. 28

Yuge, L., Okubo, A., Miyashita, T., Kumagai, T., Nikawa, T., Takeda, S., Kanno, M., Urabe, Y., Sugiyama, M. & Kataoka, K. (2003). Physical stress by magnetic force accelerates differentiation of human osteoblasts. *Biochemical and biophysical research communications*, **311**, 32–38. 160

Zeng, X.B., Hu, H., Xie, L.Q., Lan, F., Jiang, W., Wu, Y. & Gu, Z.W. (2012). Magnetic responsive hydroxyapatite composite scaffolds construction for bone defect reparation. *Int. J. Nanomed*, **7**, 3365–3378. 129

Zhao, Z., Zhao, M., Xiao, G. & Franceschi, R.T. (2005). Gene transfer of the Runx2 transcription factor enhances osteogenic activity of bone marrow stromal cells *in vitro* and *in vivo*. *Molecular Therapy*, **12**, 247–253. 160